

University of Massachusetts Medical School

eScholarship@UMMS

GSBS Dissertations and Theses

Graduate School of Biomedical Sciences

2016-09-01

Overcoming Toxicity from Transgene Overexpression Through Vector Design in AAV Gene Therapy for GM2 Gangliosidoses

Diane L. Golebiowski

University of Massachusetts Medical School

Let us know how access to this document benefits you.

Follow this and additional works at: https://escholarship.umassmed.edu/gsbs_diss



Part of the [Disease Modeling Commons](#), [Enzymes and Coenzymes Commons](#), [Molecular Biology Commons](#), [Nervous System Diseases Commons](#), [Other Neuroscience and Neurobiology Commons](#), [Pharmacology Commons](#), [Toxicology Commons](#), and the [Translational Medical Research Commons](#)

Repository Citation

Golebiowski DL. (2016). Overcoming Toxicity from Transgene Overexpression Through Vector Design in AAV Gene Therapy for GM2 Gangliosidoses. GSBS Dissertations and Theses. <https://doi.org/10.13028/M22C8K>. Retrieved from https://escholarship.umassmed.edu/gsbs_diss/895

This material is brought to you by eScholarship@UMMS. It has been accepted for inclusion in GSBS Dissertations and Theses by an authorized administrator of eScholarship@UMMS. For more information, please contact Lisa.Palmer@umassmed.edu.

OVERCOMING TOXICITY FROM TRANSGENE OVEREXPRESSION
THROUGH VECTOR DESIGN IN AAV GENE THERAPY FOR GM2
GANGLIOSIDOSES

A Dissertation Presented

By

DIANE LYNN GOLEBIOWSKI

Submitted to the Faculty of the
University of Massachusetts Graduate School of Biomedical Sciences, Worcester

in partial fulfillment of the requirements for the degree of

DOCTOR OF PHILOSOPHY

SEPTEMBER 1, 2016

INTERDISCIPLINARY GRADUATE PROGRAM

OVERCOMING TOXICITY FROM TRANSGENE OVEREXPRESSION
THROUGH VECTOR DESIGN IN AAV GENE THERAPY FOR GM2
GANGLIOSIDOSES

A Dissertation Presented
By

DIANE LYNN GOLEBIOWSKI

Dissertation Defense Committee GSBS Members

Neil Aronin, M.D.

Neuroscience Program

David Weaver, Ph.D.

Neuroscience Program

Mai ElMallah, M.D.

Interdisciplinary Graduate Program

Chair of the Dissertation Committee

Guangping Gao, Ph.D.

Interdisciplinary Graduate Program

External Dissertation Committee Member

Alessandra Biffi, M.D.

Associate Professor of Pediatrics, Harvard Medical School

Thesis Advisor

Miguel Sena-Esteves, Ph.D.

Interdisciplinary Graduate Program

Student Program

Interdisciplinary Graduate Program

September 1, 2016

DEDICATION

I would like to dedicate this dissertation to the patients, parents, and families of The Cure Tay-Sachs Foundation (CTSF) and The National Tay-Sachs & Allied Diseases Association (NTSAD).

ACKNOWLEDGEMENTS

I would like to thank my thesis advisor, Dr. Miguel Sena-Esteves for giving me the opportunity to work in his lab on such an important project. I have learned so much from his expertise and mentorship and it has positively influenced my scientific thinking and career. His optimism and persistence helped me to not give up on this project when faced with its many challenges.

I would like to thank my Thesis Research Advisory Committee members, Dr. Guangping Gao, Dr. David Weaver, Dr. Claudio Punzo, and Dr. Daryl Bosco for their thoughtful input and encouragement throughout my PhD studies.

I would like to thank my Dissertation Exam Committee members, Dr. Guangping Gao, Dr. Neil Aronin, Dr. David Weaver, Dr. Mai ElMallah, and Dr. Alessandra Biffi for their thoughtful input and for helping me transition to the next phase of my career.

I would like to thank the many collaborators mentioned in the preface for their work and expertise, without which this work would not have been possible.

I would like to thank Dr. Richard P. Moser for the use of his MRI compatible stereotaxic frame. This work would also not have been possible without the financial support of the Cure Tay-Sachs Foundation, National Tay-Sachs and Allied Diseases Association, and a Public Health Service grant from the National Institutes of Health (U01NS064096).

I would like to thank all the current and past lab members of the Sena-Esteves lab for taking a sincere interest in both my scientific and personal lives

as well as for their friendship, especially Dr. Lorelei Stoica, Dr. Allison Keeler-Klunk, Dr. Rita Batista, Jennifer Ferreira, Dr. Sourav Roy Choudhury, Dr. Dwijit GuhaSarkar, Dr. Cara Weismann, and Stacy Maitland.

I would like to thank the members of Gene Therapy Center at the University of Massachusetts Medical School for creating such a wonderful and collaborative environment to work in everyday. Thank you Qin Su for always squeezing me into the Vector Core queue. Thank you to Denise Maclachlan, Chloe Hinrichs, Margaret Humphries, and Dr. Terrence Flotte for their support.

I would like to thank the undergraduate and high school students that I had the opportunity to mentor, Justin Ungerleider, Amanda Curtis, and Brian D'Amore, you have taught me how to be a mentor while making significant contributions to research.

I would like to thank Dr. Vicki Cameron, my research mentor at Ithaca College, as well as Dr. Shwetal Mehta, Dr. John Alberta, and Dr. Charles Stiles, my supervisors at Dana-Farber Cancer Institute, for inspiring me to pursue a career in science and teaching me the experimental skills that allowed me to excel technically.

Finally, I would like to thank my many friends and family for their love and support. Thank you to my parents, Reginald and Michelle Duby, who worked hard so that I could have an exceptional education and instilled in me sound morals and a strong work ethic. They taught me how to face life's personal and professional challenges with grace. A special thank you to my husband,

Christopher Golebiowski, who inspires me to work hard, for his love, support, and patience throughout my graduate education.

ABSTRACT

GM2 gangliosidoses are a family of lysosomal storage disorders that include both Tay-Sachs and Sandhoff diseases. These disorders result from deficiencies in the lysosomal enzyme β -N-acetylhexosaminidase (HexA). Impairment of HexA leads to accumulation of its substrate, GM2 ganglioside, in cells resulting in cellular dysfunction and death. There is currently no treatment for GM2 gangliosidoses. Patients primarily present with neurological dysfunction and degeneration. Here we developed a central nervous system gene therapy through direct injection that leads to long-term survival in the Sandhoff disease mouse model. We deliver an equal mixture of AAVrh8 vectors that encode for the two subunits (α and β) of HexA into the thalami and lateral ventricle. This strategy has also been shown to be safe and effective in treating the cat model of Sandhoff disease. We tested the feasibility and safety of this therapy in non-human primates, which unexpectedly lead to neurotoxicity in the thalami. We hypothesized that toxicity was due to high overexpression of HexA, which dose reduction of vector could not compensate for. In order to maintain AAV dose, and therefore widespread HexA distribution in the brain, six new vector designs were screened for toxicity in nude mice. The top three vectors that showed reduction of HexA expression with low toxicity were chosen and tested for safety in non-human primates. A final formulation was chosen from the primate screen that showed overexpression of HexA with minimal to no toxicity. Therapeutic efficacy studies were performed in Sandhoff disease mice to define the minimum effective dose.

TABLE OF CONTENTS

REVIEWER PAGE	ii
DEDICATION	iii
ACKNOWLEDGEMENTS	iv
ABSTRACT	vii
LIST OF TABLES	x
LIST OF FIGURES	xi
PREFACE	xiii
CHAPTER I – INTRODUCTION	1
<hr/>	
Lysosomal storage disorders	1
GM2 gangliosidoses	2
<i>Animal models of GM2 gangliosidoses</i>	5
Treatment for Lysosomal Storage Disorders	6
Adeno-associated viral vector	8
AAV-mediated gene therapy for Lysosomal storage disorders	13
<i>Intraparenchymal delivery</i>	14
<i>CSF delivery</i>	15
<i>Intravenous (IV) delivery</i>	16
Previous and ongoing treatment strategies for GM2 gangliosidoses	19
<i>Substrate reduction therapy (SRT)</i>	19
<i>Stem cell transplantation</i>	20
<i>Bone marrow transplantation (BMT)</i>	21
<i>Novel isozymes that mimic HexA</i>	22
<i>AAV mediated gene therapy for GM2 gangliosidoses</i>	23
Preclinical studies in non-human primates	24
CHAPTER II - LONG-TERM CORRECTION OF SANDHOFF DISEASE BY AAVrh8-MEDIATED GENE TRANSFER OF MOUSE β-N-ACETYLHEXOSAMINIDASE	26
<hr/>	
Materials & Methods	26
Results	31
<i>Intracranial delivery of AAVrh8-mHexa/β vector extends lifespan and improves motor performance of Sandhoff disease mice</i>	31
<i>Dose-dependent extension in lifespan with prolonged motor performance in Sandhoff Disease mice with AAVrh8-mHexa/β treatment</i>	33
<i>Behavioral evaluation of AAVrh8 treated normal mice</i>	36
<i>Widespread CNS expression of Hexosaminidase and reduction of GM2 ganglioside storage in AAVrh8 treated SD mice</i>	37

CHAPTER III - DIRECT INTRACRANIAL INJECTION OF AAVrH8 ENCODING MONKEY β-N-ACETYLHEXOSAMINIDASE CAUSES NEUROTOXICITY IN PRIMATE BRAIN	39
Materials & Methods	39
Results	48
<i>Experimental Design</i>	48
<i>Clinical Observations</i>	49
<i>Pathology</i>	51
<i>Hexosaminidase expression and localization</i>	54
CHAPTER IV - OPTIMIZATION OF AAV VECTOR DESIGN FOR SAFE EXPRESSION OF β -N-ACETYLHEXOSAMINIDASE IN THE BRAIN FOR GM2 GANGLIOSIDOSES GENE THERAPY	58
Materials & Methods	58
Results	64
<i>Experimental Design</i>	64
<i>Hexosaminidase activity and expression in nude mouse brain</i>	65
<i>Neuropathology in nude mouse brain</i>	70
<i>Lower Hexosaminidase overexpression results in less gliosis</i>	71
<i>Testing new vector designs in primates for Hexosaminidase expression and safety</i>	73
<i>Clinical outcomes in primates</i>	73
<i>Hexosaminidase activity in primate brain</i>	74
<i>Neuropathology in primate brain</i>	75
<i>Testing therapeutic efficacy and defining a new minimal effective dose of AAVrh8-CB-CI-mHexa/β in Sandhoff disease mouse model</i>	77
CHAPTER V - DISCUSSION	82
APPENDIX A - SEQUENCES OF PROMOTERS AND OTHER TRANSCRIPTIONAL ELEMENTS	94
APPENDIX B - HISTOPATHOLOGIC CHANGES SEEN IN SHORT TERM PRE-CLINICAL SAFETY FOR GENE THERAPY FOR TAY-SACHS AND SANDHOFF DISEASE	95
BIBLIOGRAPHY	97

LIST OF TABLES

Table 1.1	Clinical trials for AAV gene therapy for CNS diseases.	12
Table 1.2	Preclinical AAV gene therapy studies for lysosomal storage diseases.	18
Table 3.1	Summary of neurological symptoms observed in study animals.	50
Table 3.2	Serum titers against recombinant human Hex α -subunit and AAVrh8 capsid.	52
Table 4.1	Experimental groups and relative hexosaminidase activity in the injected coronal brain block.	69
Table 4.2	Increase in hexosaminidase activity in the thalamus of AAVrh8 injected non-human primates.	75
Table 4.3	Dosing scale from mouse to monkey to human.	81

LIST OF FIGURES

Figure 1.1	Genetics of GM2 Gangliosidoses.	4
Figure 1.2	Genomic organization of recombinant adeno-associated viral vectors.	8
Figure 2.1	Intracranial AAVrh8-mHex α / β treatment increases lifespan of Sandhoff disease mice and results in retained motor performance.	32
Figure 2.2	Intracranial AAVrh8-mHex α / β treatment in Sandhoff disease mice provides a dose-dependent extension in lifespan and prolongs motor performance.	35
Figure 2.3	Intracranial delivery of AAVrh8-mHex α / β has minimal impact on motor performance of normal mice.	37
Figure 2.4	Intracranial AAVrh8-mHex α / β treatment reduces GM2 ganglioside storage and results in widespread Hexosaminidase expression in the central nervous system of Sandhoff disease mice.	38
Figure 3.1	Characterization of AAVrh8 vectors.	49
Figure 3.2	Corresponding coronal sections of brain T2-weighted MRI at pre-surgery and pre-necropsy indicating signal alterations at endpoint in treated animal.	51
Figure 3.3	Neuropathology.	53
Figure 3.4	Immunological profile of perivascular cuffs in AAVrh8-cmHex α / β injected monkey thalamus.	54
Figure 3.5	Increased Hex expression and activity in the CNS.	55
Figure 3.6	Hex α - or Hex β -subunit localization in monkey thalamus.	57
Figure 4.1	Panel of new AAV vectors with an expected gradient of HexA expression levels.	65

Figure 4.2	Total hexosaminidase isozyme activity in athymic nude mouse brain after intracranial delivery of AAVrh8 vectors encoding cynomolgus Hex α and Hex β .	67
Figure 4.3	HexA and HexS isozyme activity in athymic nude mouse brain after intracranial delivery of AAVrh8 vectors encoding cynomolgus Hex α and Hex β .	68
Figure 4.4	NHP hexosaminidase expression in athymic nude mouse brain varies among AAVrh8 vectors.	69
Figure 4.5	Mouse brains expressing highest levels of NHP hexosaminidase protein contain eosinophilic neurons.	70
Figure 4.6	Absence of microglial activation in brains injected with AAVrh8 vectors expressing lower levels of NHP hexosaminidase.	71
Figure 4.7	Absence of astrocyte activation in brains injected with AAVrh8 vectors expressing lower levels of NHP hexosaminidase.	72
Figure 4.8	New AAVrh8 vectors selected for further testing in non-human primates.	73
Figure 4.9	T2- and T1-weighted brain MRI sections of AAVrh8 injected non-human primates over time.	74
Figure 4.10	Neuropathological findings in the thalamus of AAVrh8 injected non-human primates.	77
Figure 4.11	Intracranial injection of AAVrh8-CB-CI-mHex α / β vector reduces GM2 ganglioside storage in CNS with a concomitant increase in hexosaminidase activity leads to improved survival of Sandhoff disease mice.	79
Figure 4.12	Increasing doses of CSF delivered AAVrh8-CB-CI-mHex α / β vector further reduce GM2 ganglioside storage in spinal cord and cerebellum.	80
Figure 5.1	β -N-acetylhexosaminidase α -subunit amino acid sequences.	93
Figure 5.2	β -N-acetylhexosaminidase β -subunit amino acid sequences.	93

PREFACE

Most of the work presented here was completed in Dr. Miguel Sena-Esteves' Laboratory at the University of Massachusetts Medical School under his supervision. In addition, Dr. Douglas R. Martin at Auburn University was a consultant on this project.

Chapter I

Some parts of the Introduction are based on a book chapter that I wrote and was published in *Gene Delivery and Therapy for Neurological Disorders*.¹

Chapter II

The Sandhoff disease (SD) mice in Chapter II were housed at Boston College and surgeries and tissue collection were performed there. Hannah Rockwell, in the Laboratory of Thomas Seyfried at Boston College, was responsible for maintaining the SD mouse colony, experimental animals, and their behavioral testing. I performed all surgeries with the assistance of Miguel Sena-Esteves. I performed all necropsies, tissue, and data analysis. Stanley Leroy created and packaged the AAVrh8-mHex α/β vectors in the Laboratory of Miguel Sena-Esteves. The University of Massachusetts Medical School Vector Core packaged the AAV8-TBG-mHex β vector that I cloned. I extracted all tissue and prepared samples for LC-MS/MS analysis of GM2 ganglioside content. Samples were run at the University of Massachusetts Medical School Proteomics

and Mass Spectrometry Facility and analyzed by myself.

Chapter III

Chapter III has been submitted to Human Gene Therapy and is currently under review. I am the first author on this article, and completed the first stage of manuscript composition. Dr. Sena-Esteves and co-authors edited the manuscript into its final form. Dr. Sena-Esteves is the corresponding author. Dwijit GuhaSarkar originally cloned the cynomolgus macaque *HEXA* and *HEXB* cDNA. Stacy Maitland packaged the final AAVrh8-CBA-Hex α/β -WPRE^{mut6 Δ ATG} vectors and measured their endotoxin levels. The Core Electron Microscopy Facility at the University of Massachusetts Medical School analyzed vectors for empty capsids with electron microscopy. The University of Massachusetts Medical School Vector Core screened primates for neutralizing antibodies against AAVrh8. Drs. Wael Asaad and Churl-Su Kwon performed primate surgeries at the New England Center for Stroke Research in the University of Massachusetts Medical School. Drs. Imramshah M.J. van der Bom and Anna Luisa Kühn also performed imaging there under the supervision of Dr. Matthew Gounis. Nina Bishop from Animal Medicine at the University of Massachusetts Medical School assisted with primate surgeries and neurological monitoring. Elizabeth Curran and Nilisa Silva performed monkey necropsies at the New England Primate Research Center (NEPRC). Neuropathology (H&E, CD68, CD3, CD20) was stained at NEPRC and assessed by Drs. Andrew Miller and Keiko Petrosky

under the supervision of Dr. Susan Westmoreland. Dr. Allison Bradbury, in the Laboratory of Dr. Douglas R. Martin at Auburn University, measured serum antibody titers towards AAVrh8 and human Hex α (Figure 3.2). I diluted vector for injection, performed neurological assessments, and all other tissue and data analysis.

Chapter IV

The AAVrh8-cmHex α/β vectors in Chapter IV were cloned with the assistance of Stacy Maitland and purified by myself. Elena Balkanska-Sinclair assisted me with nude mouse surgeries and tissue collection and also performed *in vitro* enzymatic assays on CNS tissue (Figures 4.2 & 4.3). Nude mouse tissue embedding, H&E, Iba-1, and GFAP staining was performed by the University of Massachusetts Medical School Morphology Core Facility. Drs. Wael Asaad, Julie Pilitsis, and Miguel Sena-Esteves performed primate surgeries at the New England Center for Stroke Research in the University of Massachusetts Medical School. Dr. Kajo Van der Marel performed imaging there under the supervision of Dr. Matthew Gounis. Nina Bishop and Dr. Rosemary Santos from Animal Medicine at the University of Massachusetts Medical School assisted with primate surgeries and neurological monitoring. Elizabeth Curran performed monkey necropsies at NEPRC. Neuropathology of monkey thalamus (H&E) was stained by the University of Massachusetts Medical School Morphology Core Facility and assessed by Drs. Keiko Petrosky and Elizabeth Hutto under the

supervision of Dr. Sheila M. Cummings Macri at NEPRC. Jennifer Ferreira, in the Laboratory of Dr. Miguel Sena-Esteves, assisted me with tissue biopsy collection for *in vitro* enzymatic assays in Table 4.2. AAVrh8-CB-CI-mHex α/β vectors were cloned and packaged by myself and I performed all experiments, tissue, and data analysis using this vector on SD mice. I extracted all tissue and prepared samples for LC-MS/MS analysis of GM2 ganglioside content. Samples were run at the University of Massachusetts Medical School Proteomics and Mass Spectrometry Facility and analyzed by myself. I performed all other experiments and/or tissue and data analysis as well as manuscript preparations.

CHAPTER I – INTRODUCTION

Lysosomal storage disorders

Lysosomal storage disorders (LSDs) are caused by a defective enzyme or cofactor that performs its function ultimately in the lysosome. Over 40 lysosomal enzymes work in tandem to break specific covalent bonds sequentially and degrade cellular metabolites to their basic components (amino acids, lipids, and sugars). A lysosomal enzyme defect blocks one or multiple metabolic pathways, leading to accumulation of specific substrates such as glycogen, mucopolysaccharides (MPS), glycoproteins, and sphingolipids.² Cellular dysfunction and death result from different molecular mechanisms such as direct toxicity of a substrate or dysregulation of intracellular calcium homeostasis (e.g., GM1-gangliosidosis and psychosine in Krabbe disease).³⁻⁵ Most of the monogenic LSDs are inherited in an autosomal recessive manner, though notable exceptions include X-linked disorders such as Hunter syndrome (MPS II), Danon disease, and Fabry disease. There are at least 50 LSDs, most often caused by a deficiency or complete loss of a soluble lysosomal enzyme.⁶ Less commonly, LSDs may be caused by defective accessory or lysosomal membrane proteins. For example, the AB variant of GM2 gangliosidosis is due to the loss of the GM2 activator protein, which is necessary for β -hexosaminidase to break down GM2 ganglioside.^{2, 7} Niemann-Pick disease type C (NPC) is caused by mutations in the NPC1 gene, which encodes a lysosomal membrane transporter.

Dysfunction of the transport system leads to storage of free cholesterol and other glycolipids in lysosomes.^{3, 4, 8}

Taken together, the incidence of all LSDs is estimated to be 1 in 8,000 live births. Though infants and children are most commonly and severely affected, later-onset forms of LSDs have a milder phenotype with a spectrum of symptoms.^{6, 9} This is thought to result from mutations where enzymes retain some residual activity, unlike in the infantile associated mutations where there is no residual activity. Due to universal necessity of functional lysosomes, LSDs present clinically with multiple organ pathology, though severe neurological symptoms often overshadow peripheral disease manifestations.^{2, 6} Recent studies have now documented mild neurological disease in many LSDs once thought to be non-neuropathic, such as Pompe disease.¹⁰

GM2 gangliosidoses

Tay-Sachs Disease (TSD) and Sandhoff Disease (SD) belong to a family of lysosomal storage disorders (LSDs) known as GM2 gangliosidoses. The incidences of Tay-Sachs disease is 1 in 222,000 live births while Sandhoff disease is 1 in 422,000 live births. The carrier frequency for Tay-Sachs disease is 1 in 224 while Sandhoff disease is 1 in 310 people.⁹ The carrier frequency and incidence of Tay-Sachs disease is about one hundred times higher in the Ashkenazi Jewish population.¹¹ Both TSD and SD result from a deficiency in the lysosomal enzyme β -N-acetylhexosaminidase (Hex, hexosaminidase, EC

3.2.1.52), which breaks down the cellular metabolite GM2 ganglioside into GM3 ganglioside by hydrolyzing the terminal N-acetyl galactosamine residue in the lysosome. HexA is a heterodimer of α - and β -subunits, which are encoded by the *HEXA* and *HEXB* genes, respectively. TSD results from mutations in *HEXA* (Chr 15q23-24) while SD results from mutations in *HEXB* (Chr 5q13). Other isozymes of Hex include HexB, a β/β dimer, and HexS, a α/α dimer, neither of which can cleave GM2 ganglioside in humans.¹² However, HexB participates in the catabolic pathway in other species, notably mice.¹³ As with most lysosomal glycosidases, Hex isozymes can cleave a broad spectrum of substrates with the terminal non-reducing sugars, GlcNAc or GalNAc, in β -linkage.¹² The GM2 activator protein, encoded by the *GM2AP* gene, is also required to transfer GM2 ganglioside to HexA for cleavage. Mutations in *GM2AP* (Chr 5q32-33), although rare, lead to the AB variant of GM2 gangliosidosis (Figure 1.1). HexA deficiency leads to accumulation of GM2 ganglioside in the lysosome causing dysfunction and eventual cell death. GM2 gangliosidosis primarily affect the central nervous system (CNS) leading to progressive neuronal degeneration.¹² Other peripheral pathology has been unveiled after correction of the CNS phenotype, such as distension of the urinary bladder and fecal impaction in Sandhoff disease cats and mice.^{14, 15} In addition, two brothers with late-onset Sandhoff disease also presented with dysautonomic achalasia.¹⁶

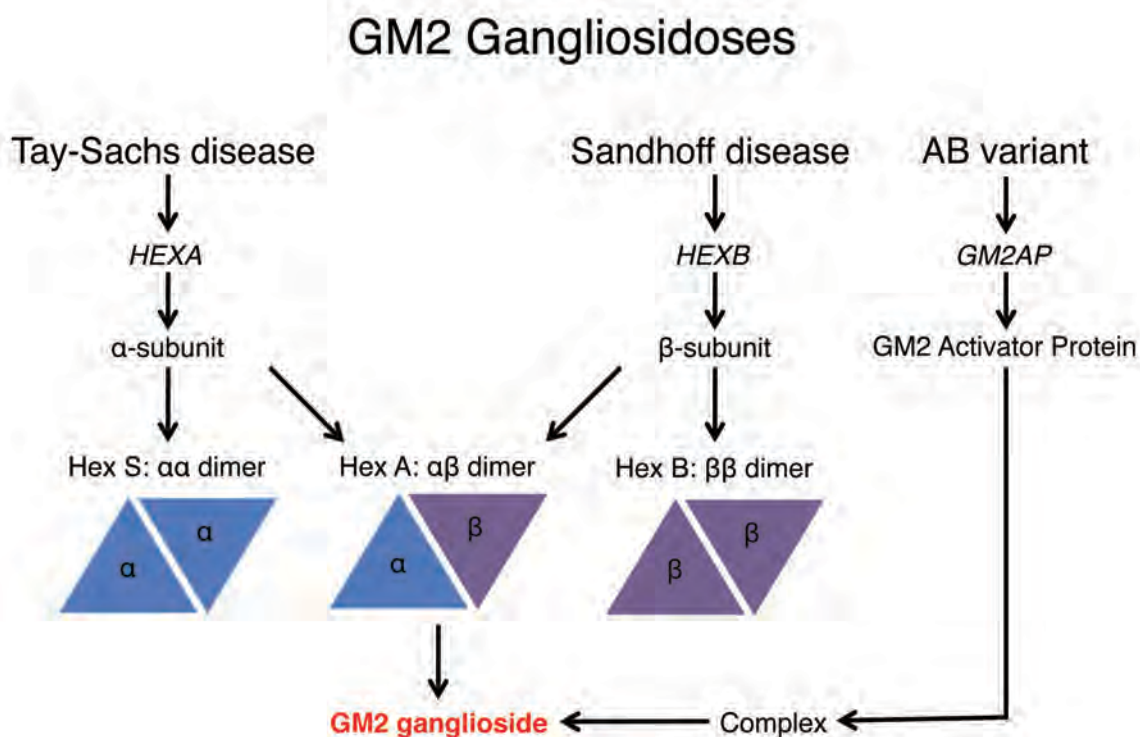


Figure 1.1 Genetics of GM2 Gangliosidoses. Hex A is a dimer of two protein subunits, α , encoded by *HEXA* gene and β , encoded by *HEXB* gene. Hex A is the only isozyme of Hex able to cleave GM2 ganglioside in humans. The GM2 activator protein, encoded by the *GM2AP* gene is also required for GM2 ganglioside cleavage. Mutations in *GM2AP* result in the AB variant of GM2 Gangliosidoses. Defects in HexA lead to GM2 accumulation and cellular toxicity.

The three clinical forms of GM2 gangliosidoses are infantile, juvenile, and late-onset, classified by their age of onset and disease severity. The most severe infantile form is characterized by onset at approximately six months of age and premature death within the first five years of life. Infantile forms result from mutations that result in little to no HexA activity. Infants develop normally for the first 6 months and patients are usually diagnosed at approximately one year of age due to regression of, or failure to reach, developmental milestones. Symptoms include seizures, deficits in motor function, and dysphagia. Patients

eventually decline to a vegetative state before succumbing to the disease. Presently the care for these patients consists of palliative measures because there is no effective treatment.¹⁷ Juvenile and late-onset forms present heterogeneously with progressive manifestations of symptoms such as psychosis, dystonia, and ataxia.¹²

Animal models of GM2 gangliosidosis

SD mice and cats, and TSD sheep are the three available animal models of GM2 gangliosidosis whose phenotypes mimic the symptoms seen in human patients. A SD mouse model was created which is a knock-out of *Hexb* gene. SD mice accumulate GM2 ganglioside in the brain, show neurological deficits such as ataxia, tremors, and loss of motor function, and have a lifespan of only around 120 days. Interestingly, when this strategy was employed to create a TSD mouse, targeting *Hexa*, GM2 ganglioside storage was milder due to an alternate metabolic pathway present in mice where HexB can participate in GM2 catabolism with sialidase. TSD mice do not have a neurological phenotype.¹⁸ Both the SD cat and TSD Jacob sheep are naturally occurring large animal models used to study GM2 gangliosidosis that also accumulate GM2 ganglioside, both models show a reduction in lifespan, with SD cats living 4.5 ± 0.5 months and TSD sheep 8-10 months, as well as neurological and motor dysfunction^{14, 19-21}. Since their identification almost 40 years ago, SD cats have been characterized in great detail.²²⁻²⁸

Treatment for Lysosomal Storage Disorders

A portion of lysosomal enzymes produced by mammalian cells are secreted, especially when expressed at supraphysiological levels, and can be taken up by the mannose-6-phosphate (M6P) receptor for delivery to the lysosomal compartment.²⁹ Termed “cross-correction,” this mechanism is exploited by both enzyme replacement therapy (ERT) and gene therapy to restore functional enzyme to diseased cells. In the case of gene therapy, only a fraction of an organ, tissue, or cell type need to be genetically engineered to become an endogenous factory for producing and secreting normal enzyme, which is then available to unmodified cells.^{30, 31}

The current standard of care for LSDs is ERT, in which patients are regularly administered recombinant enzyme parenterally.³² ERT is ineffective in treating the neurological components of LSDs because of the blood–brain barrier (BBB). The structure and physiology of the BBB prevents most high-molecular-weight substances, including proteins, from entering the CNS. Cell surface receptors exist on brain endothelial cells to mediate transport of macromolecules into the brain and thus play a fundamental role in homeostasis of the CNS microenvironment. Unfortunately, no such mechanism exists to transport circulating recombinant lysosomal enzymes across the BBB even when high levels are present in the circulation.^{33, 34} In order to circumvent the BBB, many have successfully treated both small and large LSD animal models by injecting recombinant lysosomal enzymes directly into cerebrospinal fluid (CSF) via

intracisternal, intrathecal, or intracerebroventricular (ICV) administration and this approach is also being tested clinically.³⁵⁻⁴³

Another approach that is currently the subject of intense interest is to target lysosomal enzymes to the brain via fusion/conjugation with protein domains/peptides derived from proteins that are naturally transported across the BBB.⁴⁴⁻⁵⁰

Allogenic stem cell transplantation has been used to treat a variety of LSDs, using both hematopoietic stem cells (HSCs) and neural stem cells (NSCs). These strategies have been widely improved upon by the use of gene therapy and viral vectors, such as lentivirus, to overexpress lysosomal enzymes in these cells and by using autologous cell transplantation.⁵¹ NSCs derived from patient iPS cells have been engineered to overexpress arylsulfatase A (ARSA) and treat the metachromatic leukodystrophy (MLD) mouse model.⁵² Additionally, lentiviral-mediated *ex vivo* gene transfer of arylsulfatase A into a patient's own hematopoietic stem cells followed by intravenous reinfusion has been shown to attenuate CNS disease progression in an ongoing clinical trial (NCT01560182) for MLD.^{53, 54}

Direct injection of lentiviral vectors encoding for appropriate lysosomal enzymes into the brain for MPS VII and MLD have shown improvement in disease pathology.^{55, 56} Similarly, feline immunodeficiency virus-based vectors (FIVs) encoding β -glucuronidase were injected into the striatum of MPS VII mice and resulted in cognitive improvement.⁵⁷

Adeno-associated viral vector

Adeno-associated virus (AAV) is a replication-deficient parvovirus. The single-stranded 4.7 kb DNA genome is composed of the *rep* and *cap* genes flanked by inverted terminal repeats (ITR). The AAV virion is a non-enveloped 20 nm capsid composed of three viral proteins (VP) VP1, VP2, and VP3 at a 1:1:18 ratio (60 capsomeres total).⁵⁸ Wild type AAV is prevalent in humans, and had not been linked to any disease until a recent publication reported wild type AAV2 sequences inserted into oncogenes of 6% of examined hepatocellular carcinomas (HCC.)⁵⁹ However, recombinant AAV vectors (rAAV) have very different properties than wild type AAV and to date over 100 clinical trials using rAAV have never reported HCC development. Still, the long-term safety of most rAAV therapies remains to be examined.^{60, 61} Recombinant AAV vectors are devoid of viral coding sequences and carry an ITR-flanked transcription cassette consisting of a promoter driving expression of a gene of interest and a polyadenylation signal (Figure 1.2). The ITR elements are necessary for vector genome replication and packaging during production and postinfection processing to generate stable, transcriptionally active genomes in target cells.



Figure 1.2 Genomic organization of recombinant adeno-associated viral vectors. Recombinant adeno-associated viral vectors contain two inverted terminal repeats, which are non-coding and the only viral elements contained in the vector.

Recombinant AAV has become the platform of choice for in vivo gene delivery to CNS for a number of reasons including its ability to transduce dividing and non-dividing cells at high efficiency, mediate long-term gene expression, and maintain an excellent safety profile both in animal models and human clinical trials. However, the immunology of rAAV-encoded transgenes after gene transfer to CNS is an evolving field, and it appears that new more powerful capsids, such as AAV9, are also more likely to trigger immune responses than less robust AAV serotypes, such as AAV2, when encoding either non mammalian transgenes, such as green fluorescent protein (GFP) or species mismatched therapeutic genes.⁶² Most experiments in mouse models of LSDs have been conducted with rAAV vectors encoding human enzymes. In some animal models, the therapeutic efficacy appears to be compromised by the immune system,^{63, 64} and it is unclear whether this is due to an immune response to a species mismatched enzyme or because of the knockout nature of most mouse models in which no protein is detectable. This aspect should be considered carefully in the planning of preclinical efficacy and safety experiments in large animal models as the use of rAAV vectors encoding human enzymes can confound the interpretation of outcomes.¹⁴ Although the degree of homology between human and other mammalian enzymes (especially monkey) is very high, there may be sufficient amino acid differences to generate new epitopes that may trigger an immune response. The approach that is often employed to test rAAV vectors encoding human enzymes in large animals is to use immunosuppression.⁶⁵⁻⁶⁷ For obvious

reasons, this can blunt or mask responses that would otherwise become apparent and possibly limiting to the implementation of a particular vector design and/or delivery route. Finally, the amino acid differences between enzymes from different species could alter protein–protein interactions in subtle ways and influence both therapeutic outcomes and toxicological profiles. For these reasons, we use rAAV vectors encoding species-specific enzymes in our preclinical efficacy and safety studies.

The most commonly used promoters to drive gene expression in rAAV vectors are ubiquitous strong promoters such as CBA (also known by the designations of CAG or CB), in which the chicken beta-actin promoter is fused to the human cytomegalovirus (CMV) immediate early gene enhancer with a chimeric intron⁶⁸.

For applications in CNS where neuronal restricted expression is desired, the human synapsin-1 promoter appears to be quite effective.⁶⁹ Despite its large size (1.7–1.8 kb), the promoter for glial fibrillary acidic protein (GFAP) can be used to restrict expression to astrocytes. Additionally, a smaller version, gfaABC₁D, which is only 681 base pairs has been developed.⁷⁰ Eighteen MiniPromoters compatible with AAV have been developed with targeted CNS delivery.⁷¹ Furthermore, The ITR elements of AAV have been shown to act as promoters in the brain.^{72, 73} Other transcriptional elements, such as woodchuck hepatitis virus posttranscriptional regulatory element (WPRE) or chimeric introns, can be added to increase transgene expression.^{74, 75} Though the majority of AAV

capsids display a high degree of neurotropism in rodent brain, a few serotypes such as AAV5 transduce astrocytes and neurons equally well.⁷⁶⁻⁷⁸ The vast majority of rAAV vectors carry ITR elements from AAV2, but nonetheless they can be packaged at high efficiency in a variety of AAV capsids.⁷⁹ Many types of AAV have been identified that efficiently transduce the CNS such as AAV2, AAV1, AAV5, AAV8, AAV9, AAVrh8, and AAVrh10.^{76, 80-88} Additionally, many naturally occurring AAV capsids, such as AAV9 and AAVrh10, as well as novel engineered capsids transduce cells in the CNS after intravenous delivery in adult mice.⁸⁹⁻⁹² However, the choice of promoter to drive transgene expression influences our perception of tropism, as the two are intimately associated.

AAV mediated gene therapy has been applied to treat many other neurodegenerative diseases other than LSDs, including Alzheimer's disease, Parkinson's disease, Huntington's disease, amyotrophic lateral sclerosis, and spinal muscular atrophy (SMA). Therapy for some of these use gene therapy to silence gene expression in dominantly inherited diseases by RNA interference.⁹³ Therapeutic responses have been reported in many of these animal models and clinical trials have been started or will be started very soon (TABLE 1.1).⁹³ Unfortunately, production of humoral immunity and the cross reactivity of antibodies towards AAV capsids currently prevents successful readministration of these therapies, if necessary. However, much work is being done in modulating immune responses and identifying novel capsids that would thwart pre-existing or acquired immunity towards AAV.⁹⁴

Injection site	# of injections	Disease	rAAV Serotype	Transgene	Promoter	Dose (vg)	Volume (µL)	Identifier	Status
<i>Intracerebral</i>									
white matter	6	Canavan	2	ASP	NSE	9x10 ¹¹	900		completed
white matter	12	Neuronal ceroid lipofuscinosis (CLN2)	2	CLN2	CAG	1.8x10 ¹² -3.2x10 ¹²	600	NCT00151216	completed
white matter	12	Neuronal ceroid lipofuscinosis (CLN2)	rh10	CLN2	CAG	2.85x10 ¹¹ -9x10 ¹¹	1800	NCT01414985	ongoing
white matter	12	Mucopolysaccharidosis IIIA	rh10	SGSH	PGK	7.2x10 ¹¹	720	NCT01474343	completed
white matter, cerebellum	12, 4	Mucopolysaccharidosis IIIB	5	NAGLU	PGK	4x10 ¹²	960	ISRCTN19653672	ongoing
white matter	12	Metachromatic leukodystrophy	rh10	ARSA	CAG	1x10 ¹² -4x10 ¹²	not available	NCT01801709	ongoing
substantia nigra	2	Parkinson	2	GAD	CAG	2x10 ¹²	70	NCT00643880	completed
putamen	4	Parkinson	2	AADC	CMV	9x10 ¹⁰ -3x10 ¹¹	200	NCT00229736	completed
putamen	8	Parkinson	2	NTN (CERE-120)	CAG	1.3x10 ¹¹ -5.4x10 ¹¹	80	NCT00252850, NCT00400634	completed
substantia nigra	6, 4	Parkinson	2	NTN (CERE-120)	CAG	9.4 x 10 ¹¹ -2.4 x 10 ¹²	360	NCT00985517	ongoing
striatum	2	Parkinson	2	GDNF	CMV	9x10 ¹⁰ -3x10 ¹²	not available	NCT01621581	ongoing
striatum	2	Parkinson	2	AADC	not available	7.5x10 ¹¹ -1.5x10 ¹²	not available	NCT01973543	ongoing
putamen	4	Parkinson	not available	AADC	not available	3x10 ¹¹ -9x10 ¹¹	200, 600	NCT02418898	ongoing
putamen	2	Parkinson	2	AADC	not available	not available	not available	NCT01395641	ongoing
nucleus basalis of meynert	4 or 6	Alzheimer	2	NGF (CERE-120)	CAG	1.2x10 ¹⁰ -1.2x10 ¹¹	40, 80	NCT00087789	completed
not available		Alzheimer	2	NGF (CERE-120)	CAG	2x10 ¹¹	not available	NCT00876863	not available
<i>Intrathecal</i>									
not available		Giant axonal neuropathy	9	GAN	JeT	not available	not available	NCT02362438	ongoing
lumbar		Neuronal ceroid lipofuscinosis (CLN6)	9	CLN6	CAG	1.5x10 ¹³ vg/kg	not available	NCT02725580	ongoing
<i>Intravenous</i>									
peripheral vein		Spinal muscular atrophy type I	9	SMN	CAG	6.7x10 ¹³ -3.3x10 ¹⁴ vg/kg	not available	NCT02122952	ongoing
peripheral vein			9	SGSH	U1a	5x10 ¹² -1x10 ¹³ vg/kg	not available	NCT02716246	ongoing

Table 1.1 Clinical trials for AAV gene therapy for CNS diseases. Modified from Hocquemiller, 2016.⁹³

AAV-mediated gene therapy for Lysosomal storage disorders

LSDs are good candidates for AAV mediated gene therapy since most of them are caused by mutations in a single gene and it would provide a permanent one-time treatment. It is also known that correction or improvement of disease burden can be seen with only 10-15% normal enzyme activity.⁹⁵ As stated earlier, similarly to ERT, cross-correction would allow a relatively small number of endogenous cells genetically modified to overexpress a lysosomal enzyme to supply it to a much larger population of cells that could be in a single organ or the entire body.⁹³ Distribution of lysosomal enzymes from vector-transduced cells in the brain occurs by simple diffusion, as well as retrograde and anterograde axonal transport to distant, interconnected structures.⁹⁶⁻¹⁰¹ In addition, CSF flow in the perivascular space of Virchow-Robin also appears to contribute to the widespread distribution of lysosomal enzymes in the brain.¹⁰² By utilizing the innate properties of lysosomal enzymes and the brain itself, global therapy throughout the CNS may be achieved from focal gene delivery. Finally, since axonal transport is known to distribute the AAV vector itself, remote foci of enzyme-producing cells may be established from a single injection into strategic brain structures.^{76, 101, 103, 104} AAV vectors that can cross the BBB have also opened the possibility for intravenous AAV delivery of vectors encoding lysosomal enzymes.^{83, 87}

Intraparenchymal delivery

Gene therapy by direct intracranial injections is an attractive method for the treatment of LSDs with CNS involvement because it bypasses the BBB, requires smaller vector doses than intravenous or CSF delivery, and is targeted to the brain more specifically.⁹³ Previous studies have targeted highly interconnected structures in the CNS, such as the striatum,¹⁰⁵⁻¹⁰⁷ deep cerebellar nuclei (DCN),¹⁰⁸ ventral tegmental area (VTA),¹⁰³ or thalamus,¹⁰⁹ relying heavily on axonal transport of enzymes and possibly also on interstitial fluid flow.^{76, 101, 103, 104, 110} A complete list of preclinical studies in small and large animal models for LSDs that target the CNS with intraparenchymal injection of rAAVs is summarized in Table 1.2. Ten patients with Late infantile neuronal ceroid lipofuscinosis (LINCL) were treated in a phase I clinical trial (NCT00151216) using AAV2 with 12 injections into the white matter. Overall the therapy was deemed safe and showed a slower rate of decline in patients.¹¹¹ A phase I/II clinical trial (NCT01414985) for LINCL is ongoing with a new generation of AAVrh10 based vectors that have improved enzyme distribution and better immunogenicity profile than AAV2. Intracranial injection into the white matter for children with MPS type IIIA using AAVrh10 encoding sulfoglucosamine sulfohydrolase and sulfatase-modifying enzyme factor 1 (SGSH and SUMF1) has also been tested in a phase I/II clinical trial (NCT01474343) with reported safety and disease stability after one year, and in one patient improvement was observed.¹¹² Injections into the white matter with AAV5 and AAV10 for MPS type

IIIB and MLD respectively are also currently being tested in phase I/II trials (ISRCTN19853672, NCT01801709) (Table 1.1).

Our work has focused on targeting AAVrh8 vectors to the thalamus for the widespread distribution of lysosomal enzymes in the mammalian brain. The thalamus receives afferent input from many structures throughout the CNS and relays the information to the cerebral cortex, from which it also receives reciprocal input. Therefore, the thalamus can be viewed as the central node of a “built-in” network for the dissemination of lysosomal enzymes throughout the CNS via axonal transport. Though AAV gene delivery to the thalamus can supply therapeutic levels of a lysosomal enzyme to the cerebrum, it is not sufficient to treat the cerebellum and spinal cord.^{109, 113} Therefore, we explored additional targets to supply these structures with therapeutic levels of enzyme by combining bilateral thalamic infusion with bilateral injections into DCN or delivery into CSF via the cerebral lateral ventricles.

CSF delivery

Another strategy to treat the CNS has been to deliver AAV vectors through CSF infusion, similarly to infusion of recombinant enzymes. CSF infusion has been tested with many AAV serotypes (1,2,4,5,8,9, rh8, and rh10) and through many routes including intraventricular and intrathecal administration, as well as into the cisterna magna in small and large animal models for LSDs with therapeutic success. Intracisternal delivery is easy to achieve in animal models,

however, translating this delivery modality to humans may be challenging. An alternative approach is to target ependymal cells in the ventricular system allowing secretion of enzyme into CSF for subsequent distribution.^{102, 114} CSF delivery can also lead to benefit to non-CNS organs in the absence of serum antibodies against the AAV capsid.¹¹⁵ A complete list of preclinical studies in small and large animal models for LSDs that target the CSF with rAAVs is summarized in Table 1.2. A phase I/II clinical trial (NCT02725580) for Batten (CLN6) disease has begun using AAV9 delivered intrathecally by lumbar puncture (Table 1).⁹³ The combination of cisterna magna infusion while the patient is held in the Trendelenburg position, i.e. head lower than the feet with an inclination of about 30°, has improved single injection CSF delivery for SMA.¹¹⁶

Intravenous (IV) delivery

Whole body, or systemic, treatment for LSDs is an attractive prospect given that all cells in the body require lysosomal enzymes despite the CNS being most susceptible to disease pathology in most LSDs. Once patients no longer succumb to these diseases due to CNS manifestations other peripheral clinical pathologies will likely be uncovered. AAV capsids, such as AAV9 and AAVrh10 have the ability to cross the BBB after IV delivery in adult mice and transduce cells in the CNS.^{83, 87} The efficiency and cell-type transduction pattern in the CNS in larger animal models, especially for LSDs, has yet to be completely elucidated. Reduced transduction, as compared to rodents, was seen with IV delivery of

AAV9 to non-human primates.^{83, 87} Additionally the accumulation of sialic acid, a known inhibitor of AAV9, in the CNS of MPS VIII mice prevented CNS benefit when delivered IV.¹¹⁷ Adult animals have been successfully treated with IV AAV delivery for LSDs, however, intervention at an earlier age is most beneficial. A complete list of preclinical studies with IV delivery of rAAV in mouse models for LSDs is summarized in Table 1.2. A phase I/II clinical trial using IV delivery of AAV9 for SMA (NCT02122952) and MPS IIIA (NCT02716246) have begun (Table 1). IV delivery in humans requires very large doses of vector, up to $\sim 3 \times 10^{14}$ vg/kg.⁹³

	Model	Disease	rAAV Serotype		Model	Disease	rAAV Serotype		Model	Disease	rAAV Serotype
Intracerebral	Mice	GM1 gangliosidosis	1	CSF	Mice	MPS I	8	Intravenous	Mouse	GM1 gangliosidosis	9
		GM2 gangliosidoses	2			MPS I	2			GM2 gangliosidoses	9
		GCL	2/5			MPS IIIA	9			GCL	rh10
		INCL	5			MPS IIIA	5			GCL	2/5
		JNCL	rh10			MPS IIIB	9			MLD	9
		LINCL	2 or 5			MPS IIIB	2			MSD	4 or 9
		MPS I	2 or 5			MPS VII	2			MPS II	5
		MPS IIIA	rh10			MPS VII	4			MPS II	8
		MPS IIIB	2 or 5			MPS VII	1; 2 or 5			MPS IIIA	rh74
		MPS IIIB	5			GCL	1			MPS IIIA	9
	MPS VII	5	GM1 gangliosidosis	1	MPS IIIB	9					
	MLD	1; 9 or rh10	MLD	9 or 1	MPS IIIB	2					
	NPD	2	MLD	1	MPS VII	9					
	Cat	GM1 gangliosidosis	1 or rh8	Cat	AMD	1 or 9	IP & CSF	Cat	MPS I	8	
		GM2 gangliosidoses	1 or rh8		MPS I	9			MPS VII	9 or rh10	
	Dog	MPS I	5	Dog	MPS I	9	Intravenous & CSF	Cat	GM2 gangliosidoses	rh8	
MPS IIIB		5	MPS IIIA*		9	MSD			4 or 9		
NHP*	MLD	5	Dog	MPS IIIA*	9	Mice	Mice	MPS IIIB	2		
	MLD	rh10		MPS IIIB*	9			MPS VII	2		
	LINCL	rh10		MPS VII	9 or rh10			Dog	MPS VII	9 or rh10	
	MPS I	1; 2 or 5		LINCL	1; 2; 4; 5; 8 or 9						
NHP*	MPS I	9	NHP*	MPS I	9						

Table 1.2 Preclinical AAV gene therapy studies for lysosomal storage diseases. * indicates wild type animals, AMD, a-mannosidosis, GCL, globoid cell leukodystrophy, INCL, infantile neuronal ceroid lipofuscinosis, JNCL, juvenile neuronal ceroid lipofuscinosis, LINCL, late infantile neuronal ceroid lipofuscinosis, MLD, metachromatic leukodystrophy, MPS, mucopolysaccharidosis, MSD, multiple sulfatase deficiency, NPD, Niemann-Pick disease. Modified from Hocquemiller, 2016.⁹³

Previous and ongoing treatment strategies for GM2 gangliosidosis

Substrate reduction therapy (SRT)

N-butyldeoxynojirimycin (NB-DNJ, Miglustat, Zavesca) is a small molecule oral drug, originally developed as an anti-viral drug for treating HIV.^{118, 119} It has been shown to cross the BBB and impair glycosphingolipid formation through inhibition of glucosylceramide synthase, which is required for glycosphingolipid synthesis. Thus NB-DNJ began to be tested as a substrate reduction therapy for LSDs. The drug was shown to reduce storage in TSD, SD, as well as in the closely related LSD, GM1 gangliosidosis mice. Extension of lifespan (42% increase in SD mice) was seen in both SD and GM1 gangliosidosis mice.¹²⁰⁻¹²⁴ NB-DNJ has been shown to benefit both Gaucher and NPC patients.¹²⁵⁻¹²⁷ Unfortunately, no measured benefit to late-onset TSD or juvenile GM2 gangliosidosis patients was seen in clinical studies.^{128, 129} Slight improvement was reported in individual patients.¹³⁰⁻¹³²

Another compound which inhibits glucosylceramide synthase, N-(5-adamantane-1-yl-methoxy)pentyl)-deoxynojirimycin (AMP-DMP, Genz-529468), was administered orally to SD mice beginning at 25 days of age and resulted in an increase in lifespan (34%, $p < 0.0001$) with reduction in GM2 ganglioside storage in the brain. Interestingly, treated mice showed an increase in brain glycosphingolipids despite improved motor function. Therefore benefits seen in the SD phenotype could be due to off-target effects of AMP-DMP.¹³³ Additionally, ethylenedioxy PIP2 oxalate (3h), an inhibitor of ceramide glucosyltransferase in

the glycosphingolipid synthesis pathway and has recently been shown to reduce GM2 ganglioside storage in the liver and brain when delivered postnatally to SD mice.¹³⁴

Stem cell transplantation

Intracranial transplantation of mouse neural stem cells (mNSCs) into the forebrain and cerebellum of newborn SD mice resulted in a 70% extension in lifespan. Results were similar when human derived NSCs were used. Combination therapy of mNSC transplantation with SRT compounds, NB-DNJ or N-butyldeoxygalactonojirimycin (NB-DGJ) provided a synergistic effect and extended lifespan to as much as 215 days. A delay of symptom onset was observed and Hex levels were approximately 5-28% of wild type levels in well-engrafted areas. Animals with higher Hex expression survived longer. Glycosphingolipid storage was 40% less in mNSC transplanted animals and also had reduced neuroinflammation.¹³⁵

The dual strategy of mNSC transplantation and NB-DNJ treatment was tested in a juvenile setting of SD mice where mNSC transplantation occurred at postnatal day 0 with NB-DNJ treatment daily from postnatal day 9-15. Brains were analyzed for Hex activity and GM2 ganglioside content. No synergistic effect was noted in this context.¹³⁴

Bone marrow transplantation (BMT)

SD mice have been treated with BMT between 10 and 16 days of age and it was shown to increase their lifespan from 4.5 months up to 8 months of age ($P < 0.0001$) and delay neurological dysfunction, as measured by behavioral testing. Hex activity was mostly detected in the spleen and liver and GM2 ganglioside storage was reduced mostly in peripheral organs. Little Hex activity was seen in the brain as well as no reduction of glycolipid storage or neuropathology.¹³⁶ It was further shown that BMT could reduce the microglial activation and inflammatory response associated with the neurodegeneration in SD mice without the reduction of glycolipid storage at 4 months of age.¹³⁷ Unfortunately, no benefit to BMT was seen in human SD and TSD patients. Five GM2 gangliosidosis patients (2 SD, 3 TSD) underwent hematopoietic stem cell transplant (HSCT). Their average age of symptom onset was 3.8 ± 2.6 months and HSCT occurred on average at 10.4 ± 5.8 months. No benefits were observed. At the conclusion of the study 4/5 patients had died. One died from complications of the transplant while the other three succumbed to disease related causes. The median lifespan of treated patients was 64 months, not significantly more than untreated patients.¹⁷ Therefore, it has been concluded that this is currently not a valid treatment option.

Novel isozymes that mimic HexA

Traditionally, both *HEXA* and *HEXB* genes are delivered to both SD and TSD animal models in order to produce ideal HexA isozyme overexpression.¹³⁸⁻
¹⁴⁰ This strategy also allows both TSD and SD to be treated by the same drug product and is mutation agnostic. Due to rAAV DNA packaging size limitations, successfully encoding both α - and β -subunits of HexA, along with promoter elements has been challenging. However, multiple groups have explored a strategy where novel hybrid subunits have been created by combining the critical stability domains as well as GM2 ganglioside and GM2AP interaction sites of the HexA α - and β -subunits into a new hybrid subunit. These novel subunits can dimerize and cleave GM2 ganglioside. One of these new isozymes, HexM, can be packaged into a self-complementary AAV vector. Self-complementary AAV vectors have been shown to be more efficient at gene expression by allowing transduction without being limited by second strand synthesis that needs to occur prior to single stranded rAAVs becoming transcriptionally active.¹⁴¹ Furthermore, HexM encoded by AAV9 vectors has been delivered intravenously and intracranially to TSD and SD mice and has been shown to ameliorate disease.¹⁴²⁻
¹⁴⁴ Another hybrid isozyme, mod2b, has been delivered through ICV enzyme replacement and was also able to reduce storage and extend lifespan of SD mice.^{145, 146} These hybrid isozymes may improve current therapeutic strategies, but also give hope to a vascular delivery approach to treat GM2 gangliosidoses since only one vector would have to infect a cell to create an enzyme that is

secreted, capable of cleaving GM2 ganglioside, and also uptaken by other cells through the M6P receptor system. This would theoretically also allow for lower rAAV doses to be delivered. This, in combination with AAV capsids capable of crossing the BBB and transducing the CNS, is likely to be the next generation for gene therapy for GM2 gangliosidoses. However, one has to consider that these new isozymes are not naturally occurring proteins and upon delivery to humans could elicit an immune response. Although, some patients, due to the nature of their mutation, make no enzyme at all so this problem is also relevant when delivering normal Hex subunits.

AAV mediated gene therapy for GM2 gangliosidoses

Although early gene therapies for GM2 gangliosidoses included retroviral and adenoviral vectors, the field has primarily shifted to using rAAV vectors.¹⁴⁷⁻¹⁴⁹ SD mice have been treated at one month of age by bilateral intracranial injections into the striatum and cerebellum or into the hippocampus and cerebellum with a combination of two AAV1 vectors, encoding human Hex α - and Hex β -subunits. Treated SD mice live as long as 2 years, or the normal lifespan of wild-type mice.^{15, 106} The timing of treatment is critical, with the best survival outcomes (615 days, $p < 0.0001$) occurring at the 4 week old time point, while 12 week old treated animals show a slight decrease (126 days, $p > 0.05$) in median survival compared to untreated SD mice (131 days).¹⁵⁰ Simultaneous delivery of two AAVrh8 vectors encoding feline Hex α - and Hex β -subunits has been

successful in treating feline SD CNS pathology and extending lifespan through bilateral injection into the thalamus alone or in combination with injection into the DCN.^{14, 151} This dissertation describes similar efficacy in treating SD mice using intracranial delivery of AAVrh8 vectors encoding mouse Hex subunits as shown previously for other AAV constructs.^{15, 106, 150, 152} Furthermore, a single injection of AAV vectors into the ICV is as effective as DCN injection in complementing the therapeutic effect of bilateral thalamic injections in mice and cats.¹⁵³ Because ICV injection is considered safer than DCN injection, we decided to conduct pre-clinical safety studies using bilateral thalamic injections in combination with ICV delivery of an equimolar formulation of two AAVrh8 vectors encoding Hex α - and Hex β -subunits.¹

Preclinical studies in non-human primates

Many pre-clinical safety studies have been conducted in non-human primates (NHPs) due to phylogenetic similarities to humans allowing testing of the feasibility to scale up from rodent models to humans. Numerous studies have been conducted in NHPs to assess safety of AAV gene therapy for metabolic and neurological diseases using systemic, cerebrospinal fluid, and intracranial delivery routes.^{66, 67, 93, 116, 154-158} However, such safety studies differ widely in delivery route, AAV vector design/dosing, therapeutic gene, and volume/rate of injection. Thus, extrapolation of safety to our paradigm is not advisable as we are using a novel capsid (AAVrh8) and target (thalamus), which have never been

tested in humans. Our previous studies using direct intracranial injections of AAVrh8 vectors encoding species-specific Hex α - or β -subunits at 1:1 ratio in mice, cats, and sheep have all indicated safety, widespread enzyme distribution, and therapeutic efficacy.^{14, 153} In this dissertation we optimize the gene therapy strategies used in SD cats for pre-clinical safety and feasibility using normal monkeys.

**CHAPTER II -
LONG-TERM CORRECTION OF SANDHOFF DISEASE BY AAVrh8-
MEDIATED GENE TRANSFER OF MOUSE β -N-ACETYLHEXOSAMINIDASE.**

Materials & Methods

AAVrh8-CBA-mHex α / β -WPRE and AAV8-TBG-mHex β vector production

A single stranded rAAV vector plasmid described previously¹⁵⁹ was used to generate the AAVrh8-CBA-mHex α -WPRE and AAVrh8-CBA-mHex β -WPRE plasmids. AAV8-TBG-mHex β carries a thyroxin-binding globulin (TBG) promoter to drive liver-specific gene expression¹⁶⁰ and was produced by transient transfection of 293 cells and purified by CsCl gradient ultracentrifugation (UMass Medical School, Horae Gene Therapy Center, Worcester, MA). AAVrh8 vectors were produced by triple transient transfection of 293T cells followed by purification with iodixanol gradient and fast protein liquid chromatography as previously described.¹⁶¹ Vectors were concentrated using Acrodisc® Units with Mustang® Q Membranes (Pall Corporation), buffer exchanged to phosphate-buffered saline using 10 kDa Slide-A-Lyzer™ Dialysis Cassettes (Thermo Fisher Scientific), and filtered using Millex-GV Syringe Filter Unit, 0.22 μ m, PVDF, 4 mm (EMD Millipore). The titers of the vectors were measured by real-time quantitative-PCR with primers and probe to the bovine growth hormone (BGH) polyadenylation signal common to all vectors as described.¹⁶¹

Animal procedures

Sandhoff disease (SV/129 Hexb^{-/-}) mice were originally obtained from Dr. Richard Proia (NIH).¹³ In this study, humane endpoint was defined by weight loss of 9-20% maximum body weight or the loss of the ability to right themselves within 15 seconds when turned on their back. Thirty-day-old mice were injected bilaterally into the thalamus with a 1:1 formulation of AAVrh8-CBA-mHex α -WPRE and AAVrh8-CBA-mHex β -WPRE (1 μ L each side at 0.1 μ L/min; stereotaxic coordinates from bregma in mm: \pm 1.5 ML, -2.0 AP, and -3.5 from skull surface) in addition to bilaterally into deep cerebellar nuclei (0.3 μ L each side at 0.1 μ L/min; stereotaxic coordinates from bregma in mm: \pm 1.5 ML, - 6.0 AP, - 3.0 from skull surface) injection or into the left lateral ventricle (2 μ L at 0.2 μ L/min; stereotaxic coordinates from bregma in mm: -1.0 ML, -0.2 AP, -2.0 from skull surface) as previously described.¹ The animals in the dose escalation groups (Figure 2.2) with 3×10^{11} vg AAV8-TBG-mHex β via the tail vein using a 27G insulin syringe (BD Biosciences). Upon sacrifice, one brain hemisphere and half of a spinal cord was embedded in Neg-50TM (Richard-Allan Scientific) freezing medium and frozen in a 2-methylbutane/dry ice bath (ThermoFisher Scientific) for histology. Cerebrum, cerebellum and brain stem were separated from the other brain hemisphere and along with the other half of the spinal cord were frozen on dry ice for biochemical analysis. All experiments were reviewed and approved by the Institutional Animal Care and Use Committee at Boston College (Chestnut

Hill, MA), and performed in compliance with the NIH Guide for Care and Use of Laboratory Animals, 8th edition.

Behavioral studies

Inverted screen testing was performed as described previously.^{122, 162} Animals were placed on a square wire mesh screen (30 cm² with 25 mm² openings). The screen was slowly inverted over two seconds until secured at a 60° angle. Latency to fall (2 minute maximum time) and number of hind leg movements that occurred while on screen were recorded. Rotarod performance was measured on a non-accelerating rotarod at 20 rpm. Mice were given a 1 minute training session at 4 rpm. The longest time spent on the rotarod of two trials was recorded (60 second maximum time, 20 minute break between trials). Wire hang performance was measured and scored as described previously.¹²²

GM2 ganglioside content

GM2 ganglioside content in the CNS was measured by liquid chromatography-tandem mass spectrometry (LC-MS/MS) using a modification on a method described previously at the University of Massachusetts Medical School Proteomics and Mass Spectrometry Facility.¹⁶² Briefly, 0.01 or 0.04 mg/ μ l of tissue homogenate was diluted in 0.01 M Phosphate Citrate Buffer with 0.1 %

Triton X-100 (VWR) pH 4.4 to 25 or 50 μ l respectively. Each sample was spiked with 200 ng of d3-labeled GM2 (resuspended in methanol, Matreya, LLC). Standard calibration curves were made with GM2-ganglioside (resuspended in methanol, Matreya, LLC) over the range of 10–5000 ng in Phosphate Citrate Buffer with 0.1 % Triton X-100 and also spiked with 200 ng of d3-GM2 and also put through the extraction process. Total lipids were extracted twice by vortexing and sonicating samples for 30 seconds with 1 mL isopronal:ethyl acetate:water (6:3:1), combining both supernatants after centrifugation. Samples were dried, and resuspended in 100 μ l of 1 part 0.1% (v/v) formic acid (mobile phase A) to 4 parts methanol:2-propanol:0.1% formic acid (47.5:47.5:4.9, mobile phase B). For each sample, 10 μ L was injected in duplicate onto a 2.1 x 50 mm Kinetex (Phenomenex) C18 (1.7 μ ,100Å) column using an Acquity HPLC (Waters Corporation) coupled to a Quattro Premier XE (Waters) mass spectrometer operating in the negative ion electrospray mode. Gangliosides were eluted at 270 μ L/min using the following gradient: 0-1 min (80% B); 1-5 min (80-100% B); 5-7 min (100% B); 7.1-12 min (80% B). Multiple reaction monitoring (MRM) transitions for GM2 (fatty acids: 18:0, d3-18:0, 20:0) were monitored by following corresponding (M-H)- precursor ions to the common sialic acid anion fragment at m/z 290 (cone voltage, 90V; collision energy, 70 eV; collision gas pressure, 2.2 μ bar). The area of all the individual GM2 lipid species (18:0, 20:0) were combined and normalized to the d3-18:0 GM2 lipid species internal standard. Briefly, 11.06% of the area of 18:0 GM2 lipid was subtracted from the area of d3-

18:0 GM2, to correct for d3-18:0 GM2/18:0 GM2 overlap. The ratio of the sum of the area of 18:0 GM2 and 20:0 GM2 to the corrected d3-18:0 GM2 was calculated and ng of GM2 lipid was determined from the standard curve. Total GM2 ganglioside concentrations were then normalized to total protein content in tissue homogenate, measured by QuickStart™ Bradford Protein Assay with serial dilutions of bovine serum albumin as standard (Bio-Rad).

Hexosaminidase activity

Freshly frozen tissue was lysed in 0.1 % Triton-X 100 in 0.01 M Phosphate Citrate Buffer pH 4.4 using a Qiagen TissueLyser II (Qiagen Inc., CA, USA) with 5 mm stainless steel beads (Qiagen Inc., CA, USA 69989) at 15 Hz for 20 seconds with three pulses. Lysates were flash frozen in a bath of dry ice and 95% ethanol and thawed three times and then spun at 13,000 rpm for 5 minutes. Hexosaminidase isozyme activities was measured from supernatant using 4-Methylumbelliferyl N-acetyl- β -D-glucosaminide (MUG, Sigma) and 4-Methylumbelliferyl 6-Sulfo-2-acetamido-2-deoxy- β -D-glucopyranoside Potassium Salt (MUGS, Toronto Research Chemicals) and normalized to total protein content measured by QuickStart™ Bradford Protein Assay with serial dilutions of bovine serum albumin as standard (Bio-Rad, CA, USA #5000201) as previously described.¹⁴ Enzyme activity is represented as nmol 4MU/hr/mg protein.

Results

Intracranial delivery of AAVrh8-mHexa/β vector extends lifespan and improves motor performance of Sandhoff disease mice.

A 1:1 formulation of AAVrh8 vectors encoding mouse Hexosaminidase (Hex) α- and β-subunits was injected intracranially in 4-week old Sandhoff disease (SD) mice via two approaches, either a combination of bilateral thalamic (TH) and deep cerebellar nuclei (DCN) injections (TH/DCN), or bilateral thalamic injections combined with a single lateral intracerebroventricular injection (TH/ICV). The behavioral performance of AAVrh8 treated SD mice (4.68×10^9 vg), and controls (untreated SD and wild type littermates) was assessed over time starting at 60 days of age (one month post-injection) (Figure 2.1). The inverted screen performance of TH/ICV AAVrh8 treated SD mice was significantly better than untreated SD mice at 120 days of age ($P \leq 0.05$), and both TH/ICV and TH/DCN AAVrh8 treated mice performed comparable to that of wild type controls at 180 days (Figure 2.1A). In the rotarod test, both cohorts of AAVrh8 treated SD mice performed better than untreated SD controls ($P \leq 0.01$) at 120 days of age, and their performance was comparable to wild type controls to at least 180 days of age (Figure 2.1B). No significant improvement was measured in the wire hang test (Figure 2.1C) compared to untreated SD mice.

Both intracranial delivery approaches resulted in similar extensions of lifespan compared to untreated SD mice ($P \leq 0.001$ TH/DCN, $P \leq 0.0001$ TH/ICV) and were not significantly different from each other ($P > 0.05$). Untreated SD mice had a median survival of 127 days while SD mice treated via TH/DCN

or TH/ICV, at a dose of 4.68×10^9 vg, had a median survival of 424 days and 423 days, respectively (Figure 2.1D)

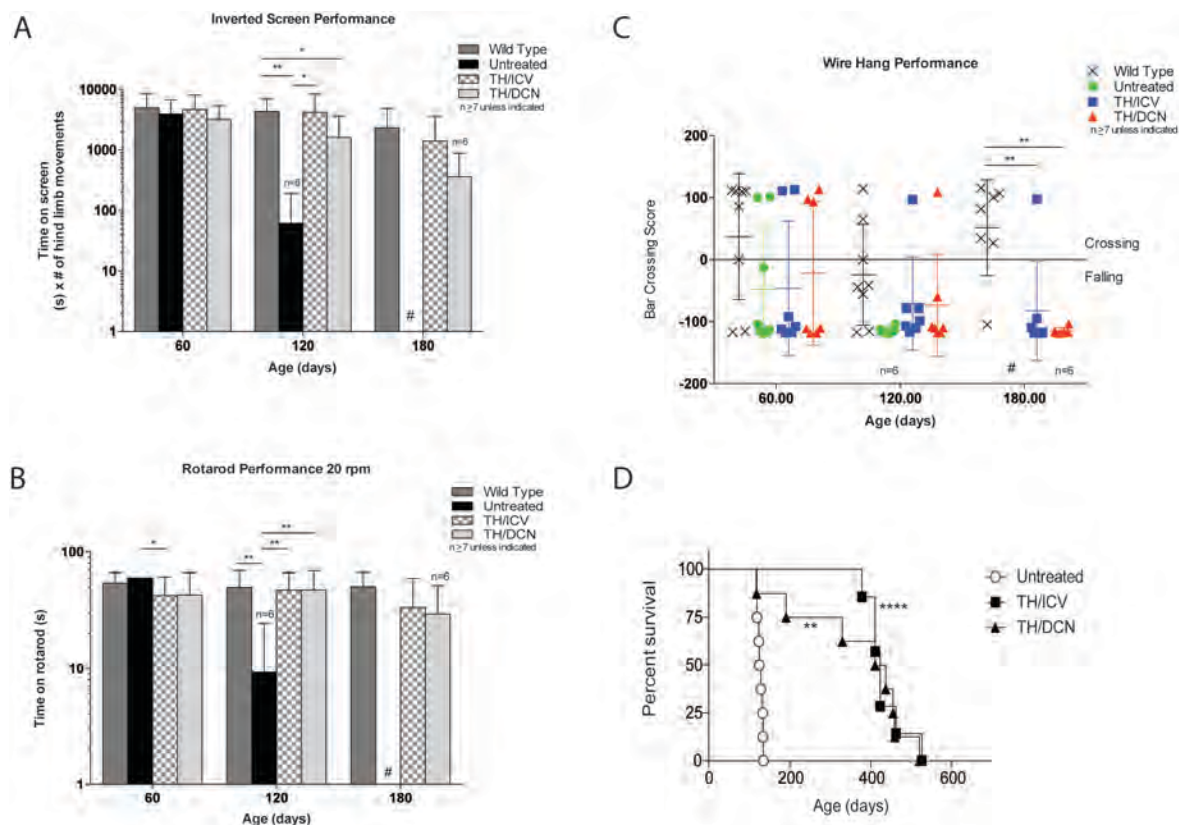


Figure 2.1 Intracranial AAVrh8-mHexa/β treatment increases lifespan of Sandhoff disease mice and results in retained motor performance. The performance of SD mice treated with 4.68×10^9 vg of AAVrh8-mHexa/β vector formulation via TH/ICV or TH/DCN delivery in (A) inverted screen, (B) rotarod, and (C) wire hang tests was evaluated at 60, 120 and 180 days of age. At 60 days wild type n=8, untreated SD mice n=8, TH/ICV treated n=7, TH/DCN treated n=7. At 120 days wild type n=8, untreated SD mice n=6, TH/ICV treated n=7, TH/DCN treated n=7. At 180 days wild type n=7, untreated SD mice n=0 (#: median survival of untreated SD mice was 127 days and therefore no mice remained at the 180 day timepoint), TH/ICV treated SD n=7, TH/DCN treated SD n=6. Results are shown as mean \pm SD, Tukey's multiple comparisons test. * ($P \leq 0.05$), ** ($P \leq 0.01$), *** ($P \leq 0.001$). (D) Kaplan-Meier survival plot of Sandhoff disease (SD) mice treated with 4.68×10^9 vg AAVrh8-mHexa/β intracranially showing that in combination with bilateral thalamic injections (TH), bilateral deep cerebellar nuclei (DCN) injections or a single intracerebral ventricular (ICV) injection results in comparable survival outcomes. Dose: 4.68×10^9 vg. Median survivals: untreated SD mice 127 days (n=8), TH/DCN 424 days (n=8), TH/ICV 423 days (n=7) Log-rank test between untreated SD mice and TH/DCN or TH/ICV. ** ($P \leq 0.01$), **** ($P \leq 0.0001$).

Dose-dependent extension in lifespan with prolonged motor performance in Sandhoff Disease mice with AAVrh8-mHexa/β treatment.

It has been shown that intravenous delivery of AAV8 encoding human acid sphingomyelinase (hASM), driven by a liver specific promoter, prior to intracranial delivery of AAV2-hASM in Niemann-Pick disease mice prevented hASM antibody generation and enhanced efficacy of brain injections.⁶⁴ We tested this systemic-mediated tolerization approach on SD (HexB^{-/-}) mice. Two days prior to intracranial TH/ICV infusion of AAVrh8-mHexa/β, SD mice were infused intravenously with AAV8-TBG-mHexβ (3 x 10¹¹ vg). Systemic injection of AAV8-TBG-mHexβ alone did not enhance survival of SD mice, as the median survival for untreated SD mice was 127 days while for SD mice treated with AAV8-TBG-mHexβ it was 128.5 days (Figures 2.1D and 2.2A). Furthermore, systemic-mediated tolerization combined with intracranial therapy did not significantly enhance median survival in SD mice compared to intracranial alone at 4.68 x 10⁸ vg (median survival of combination therapy 448.5 days, TH/ICV alone 423 days) (Figures 1.1D and 1.2A). A dose escalation experiment (4.68 x 10⁷, 4.68 x 10⁸ vg, 4.68 x 10⁹ vg, 1.17 x 10¹⁰ vg,) was performed on these mice as well. SD mice were pre-treated intravenously with AAV8-TBG-mHexβ before TH/ICV delivery of AAVrh8-mHexa/β vectors. Extension in survival was documented only for the two highest doses (4.68 x 10⁹ vg and 1.17 x 10¹⁰ vg, P ≤ 0.0001). Median survival of systemic-only treated SD mice was 128.5 days, 4.68 x 10⁷ vg: 110.5 days, 4.68 x 10⁸ vg: 135 days, 4.68 x 10⁹ vg: 448.5 days, 1.17 x 10¹⁰ vg: 591 days (Figure

2.2A). Despite living a maximum of 666 days (1.17×10^{10} vg dose), treated animals did eventually present with hind limb weakness and ataxia at time of euthanasia and some lost body weight and/or the ability to right themselves when placed on their back.

No significant differences in behavior performance was seen in these combination therapy mice treated with 4.68×10^9 vg or 1.17×10^{10} vg intracranial TH/ICV doses compared to intracranially untreated SD mice at 120 days when measured by inverted screen performance (Figure 2.2B), rotarod performance (Figure 2.2C), or wire hang test (Figure 2.2D). At 180 days of age TH/ICV mice dose performed comparable to wild type mice in inverted screen performance at both doses (Figure 2.2B). Also at 180 days of age, TH/ICV mice at both doses performed comparable to wild type mice in rotarod performance (Figure 2.2C). No significant improvement was measured in the wire hang test (Figure 2.2D) compared to intracranially untreated SD mice around the median survival age of untreated SD mice (120 days). However mice were still able to perform the test at 180 days when no untreated SD mice were surviving.

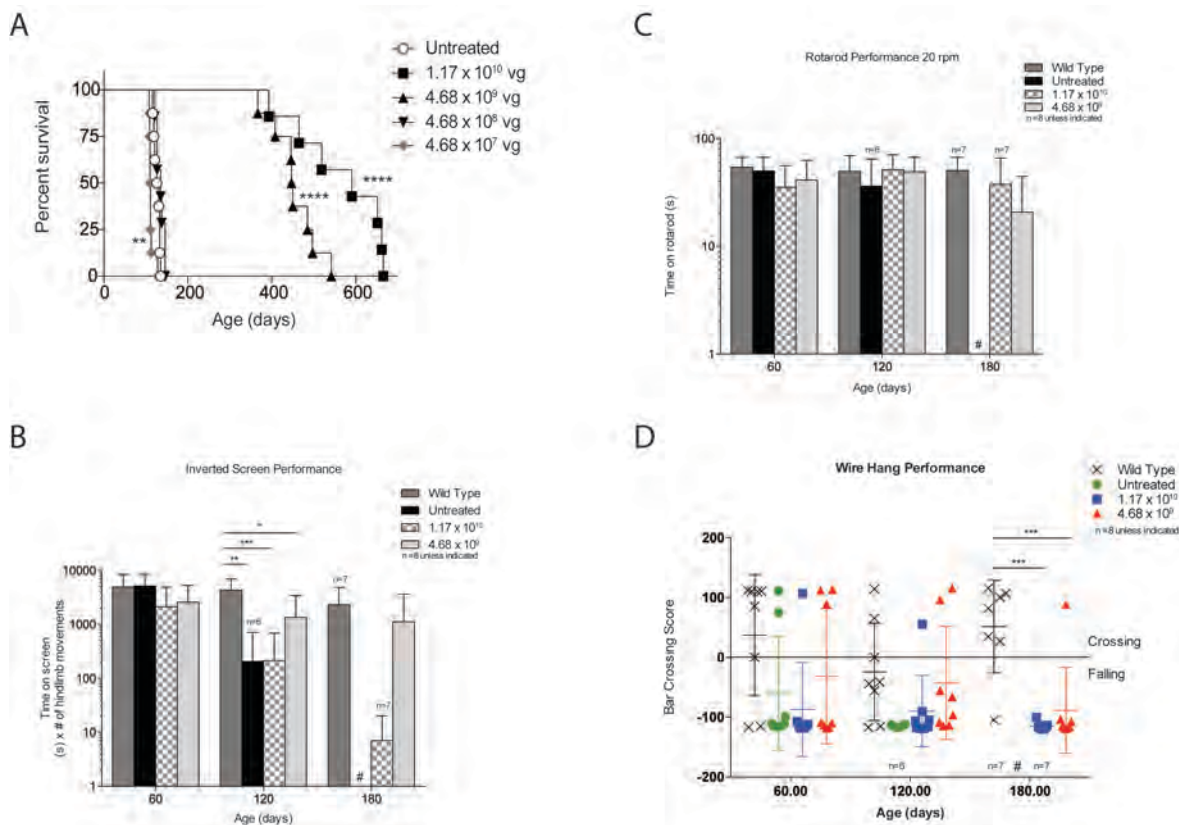


Figure 2.2 Intracranial AAVrh8-mHexa/β treatment in Sandhoff disease mice provides a dose-dependent extension in lifespan and prolongs motor performance. (A) Kaplan-Meier survival plot of a dose escalation experiment for AAVrh8-mHexa/β injected intracranially into the TH/ICV of 1 month SD mice showing a dose dependent increase in survival of Sandhoff mice treated with AAVrh8-mHexa/β bilaterally in the thalamus and intracerebral ventricle at 4.68×10^9 vg and 1.17×10^{10} vg. Median survivals: intracranially untreated SD mice - 128.5 days (n=8), 1.17×10^{10} vg - 591 days (n=7), 4.68×10^9 vg - 448.5 days (n=8), 4.68×10^8 vg - 135 days (n=7), 4.68×10^7 vg - 110.5 days (n=8). Log-rank test between untreated and injected groups. ** ($P \leq 0.01$), **** ($P \leq 0.001$). The performance of SD mice treated intracranially with 4.68×10^9 vg and 1.17×10^{10} vg of AAVrh8-mHexa/β vector formulation via TH/ICV delivery in (B) inverted screen, (C) rotarod, and (D) wire hang tests was evaluated at 60, 120 and 180 days of age. At 60 days wild type n=8, intracranially untreated SD mice n=8, TH/ICV treated 4.68×10^9 vg n=8, TH/ICV 1.17×10^{10} vg treated n=8. At 120 days wild type n=8, intracranially untreated SD mice n=6, TH/ICV 4.68×10^9 vg treated n=8, TH/ICV treated 1.17×10^{10} vg n=8. At 180 days wild type n=7, untreated SD mice n=0 (#: median survival of untreated SD mice was 128.5 days and therefore no mice remained at the 180 day time point), TH/ICV 1.17×10^{10} vg treated SD n=7, TH/ICV 4.68×10^9 vg treated SD n=8. Results are shown as mean \pm SD, Tukey's multiple comparisons test. * ($P \leq 0.05$), ** ($P \leq 0.01$), *** ($P \leq 0.001$), **** ($P \leq 0.0001$). Note: SD mice were also pretreated with intravenous AAV8-TBG-mHexβ (3×10^{11} vg) two days prior to intracranial AAVrh8-mHexa/β treatment.

Behavioral evaluation of AAVrh8 treated normal mice.

To assess the potential impact of intracranial AAVrh8 vector infusion in the absence of an underlying neurodegenerative process, age matched heterozygote (HZ) littermates (HexB^{+/-}) mice received intracranial injection of 4.68×10^9 vg AAVrh8 vector formulation via the same routes of administration. AAVrh8 treated HZ mice and untreated controls (wild type and HZ) were assessed in different behavioral tests over time (Figure 2.3). We did not observed gross alterations in the behavior of AAVrh8 injected HZ mice compared to controls, or any impact on survival. No differences among cohorts were apparent in the inverted screen test (Figure 2.3A). TH/DCN injected HZ mice performed slightly worse than untreated HZ and WT controls at 180 days in the rotarod test (Figure 2.3B). There were no significant differences in wire hang performance (Figure 2.3C) among cohorts at both 60 and 120 days of age. However, at 180 days TH/DCN injected HZ mice performed worse than untreated HZ animals ($P \leq 0.05$) and untreated WT animals ($P \leq 0.01$). There was no significant difference in performance of TH/ICV injected animals compared to untreated HZ or WT animals at 180 days of age.

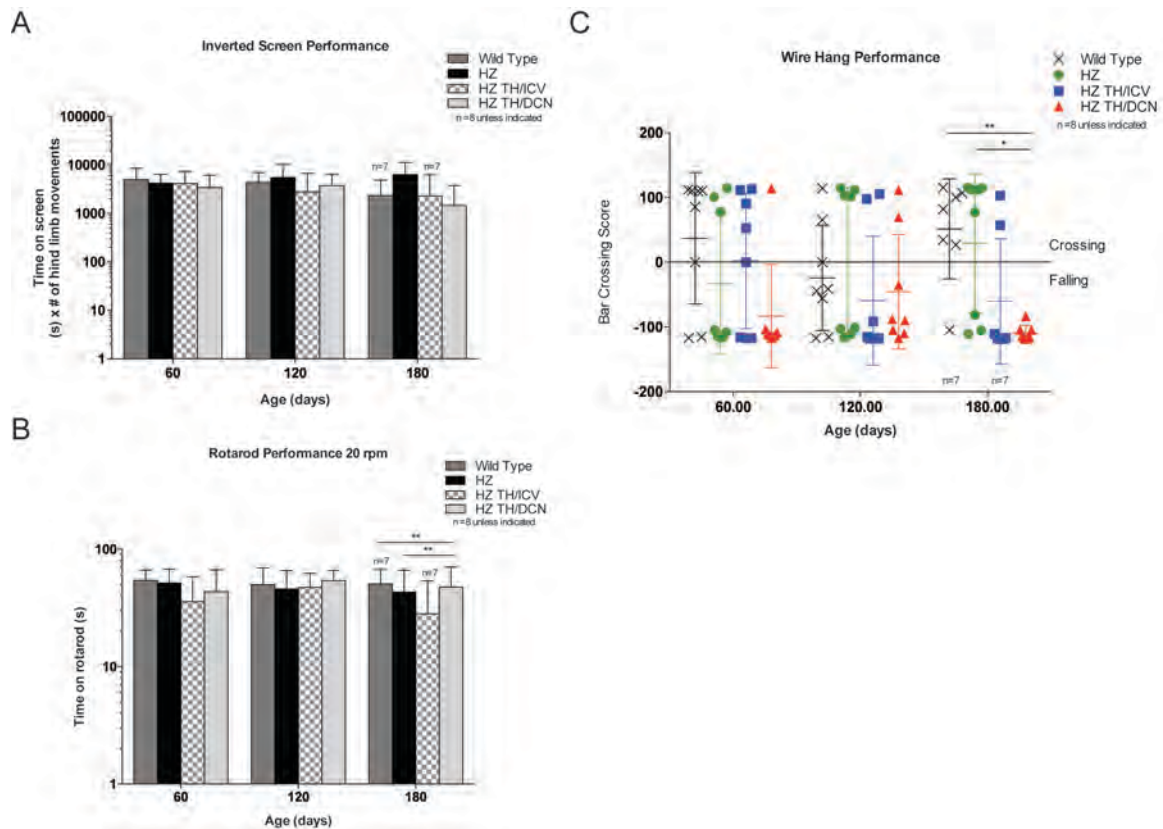


Figure 2.3 Intracranial delivery of AAVrh8-mHexa/β has minimal impact on motor performance of normal mice. The performance of heterozygous ($\text{HexB}^{+/-}$; HZ) mice treated by intracranial injection of 4.68×10^9 vg AAVrh8-mHexa/β through TH/ICV or TH/DCN delivery was assessed at 60, 120 and 180 days of age on the (A) inverted screen, (B) rotarod (B) and (C) wire hang tests. At 60 days wild type $n=8$, untreated HZ mice $n=8$, HZ TH/ICV treated $n=8$, HZ TH/DCN treated $n=8$. At 120 days wild type $n=8$, untreated HZ mice $n=8$, HZ TH/ICV treated $n=8$, HZ TH/DCN treated $n=8$. At 180 days wild type $n=7$, untreated HZ mice $n=8$, HZ TH/ICV treated $n=7$, HZ TH/DCN treated $n=8$. Results are shown as mean \pm SD, Tukey's multiple comparisons test. * ($P \leq 0.05$), ** ($P \leq 0.01$), *** ($P \leq 0.001$), **** ($P \leq 0.0001$).

Widespread CNS expression of Hexosaminidase and reduction of GM2 ganglioside storage in AAVrh8 treated SD mice.

GM2 ganglioside content and Hexosaminidase expression in the CNS were measured in TH/ICV AAVrh8 treated (1.17×10^{10} vg) SD mice, in untreated SD mice, and in untreated WT controls (Figure 2.4). We could not detect GM2 ganglioside, measured by LC-MS/MS, in the cerebrum of AAVrh8 treated

animals and significant reduction of GM2 ganglioside was seen in the cerebellum (91.1%), brainstem (99.6%), and spinal cord (99.8%) ($P \leq 0.0001$, Figure 2.4A).

Total Hexosaminidase activity was restored to the central nervous system of AAVrh8 treated SD mice. Levels of activity were above that of wild type in the cerebrum and comparable in the cerebellum, brainstem, and spinal cord.

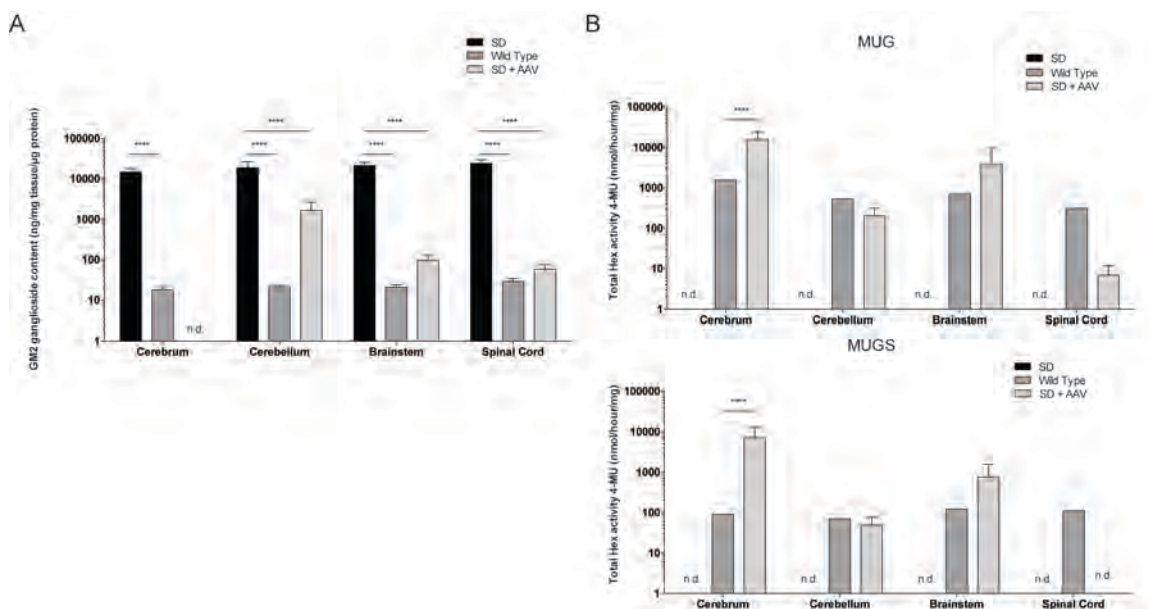


Figure 2.4 Intracranial AAVrh8-mHexa/β treatment reduces GM2 ganglioside storage and results in widespread Hexosaminidase expression in the central nervous system of Sandhoff disease mice. Sandhoff mice were treated by TH/ICV injection of 1.17×10^{10} vg AAVrh8-mHexa/β and at their humane endpoint the cerebrum, cerebellum, and spinal cord were analyzed for (A) GM2 ganglioside content and (B) Hexosaminidase activity using two artificial substrates, MUG (cleaved by HexA, HexB, and HexS isozymes) and MUGS substrate (cleaved by HexA and HexS isozymes). Results are shown as mean \pm SD, Tukey's multiple comparisons test. **** ($P \leq 0.0001$), n.d. (not detected). N=6 for all cohorts (3 males and 3 females).

**CHAPTER III -
DIRECT INTRACRANIAL INJECTION OF AAVrh8 ENCODING MONKEY β -N-
ACETYLHEXOSAMINIDASE CAUSES NEUROTOXICITY IN PRIMATE BRAIN.**

Materials & Methods

Electron Microscopy of AAVrh8 vector preparations

AAVrh8 vector preparations were analyzed by The Core Electron Microscopy Facility at the University of Massachusetts Medical School (Worcester, MA) using negative staining.

Silver stain of AAVrh8 vector & Densitometry

AAVrh8 vector purity was assessed by gel electrophoresis using 4-20% Mini-PROTEAN® TGX™ (Bio-Rad) precast gels followed by silver staining (Invitrogen) and densitometry.

Endotoxin detection

Endotoxin levels were measured on AAV vector preparations using the Endpoint Chromogenic LAL Assays (The QCL-1000™) from Lonza according to manufacturer's instructions.

AAVrh8-CBA-Hex α / β -WPRE^{mut6 Δ ATG} vector production

A single stranded rAAV vector plasmid described previously¹⁵⁹ was used to generate the AAVrh8-CBA-cmHex α -WPRE^{mut6 Δ ATG} and AAVrh8-CBA-cmHex β -WPRE^{mut6 Δ ATG} plasmids. The woodchuck hepatitis virus post-transcriptional

regulatory element was modified to include the previously described mut6 mutations in the putative promoter region of protein X¹⁶³ as well as replace all putative ATG codons with TTG. This modified WPRE^{mut6 Δ ATG} was synthesized by overlapping polymerase chain reaction (PCR).

Modified WPRE sequence:

GATAATCAACCTCTGGATTACAAAATTTGTGAAAGATTGACTGGTATTCTTAA
 CTTTGTGCTCCTTTTACGCTTTGTGGATACGCTGCTTTATTGCCTTTGTATC
 TTGCTATTGCTTCCCGTTTGGCTTTCATTTTCTCCTCCTTGTATAAATCCTGG
 TTGCTGTCTCTTTTTGAGGAGTTGTGGCCCGTTGTCAGGCAACGTGGCGTG
 GTGTGCACTGTGTTTGTGACGCAACCCCCACTGGTTGGGGCATTGCCACC
 ACCTGTCAGCTCCTTTCCGGGACTTTCGCTTTCCCCCTCCCTATTGCCACGG
 CGGAACTCATCGCCGCCTGCCTTGCCCGCTGCTGGACAGGGGCTCGGCTG
 TTGGGCACTGACAATTCCGTGGTGTGTCGGGGAAATCATCGTCCTTTTCCT
 GGCTGCTCGCCTGTGTTGCCACCTGGATTCTGCGCGGGACGTCCTTCTGCT
 ACGTCCCTTCGGCCCTCAATCCAGCGGACCTTCCTTCCCGCGGCCTGCTGC
 CGGCTCTGCGGCCTCTTCCGCGTCTTCGCCTTCGCCCTCAGACGAGTCGG
 ATCTCCCTTTGGGCCGCCTCCCCGCATCGGACTAG.

AAVrh8 vectors were produced by triple transient transfection of 293T cells followed by purification using iodixanol gradient and fast protein liquid chromatography as previously described.¹⁶¹ Vectors were then concentrated using Acrodisc® Units with Mustang® Q Membranes (Pall Corporation), buffer exchanged to phosphate-buffered saline using 10 kDa Slide-A-Lyzer™ Dialysis

Cassettes (Thermo Fisher Scientific), and filtered using Millex-GV Syringe Filter Unit, 0.22 μm , PVDF, 4 mm (EMD Millipore). The titers of the vectors were measured by real-time quantitative-PCR with primers and probe to the bovine growth hormone (BGH) polyadenylation signal as described.¹⁶¹

Non-human primates

Male and female cynomolgus macaques (1.5-2.5 year-old) were purchased from Worldwide Primates Inc. (Miami, FL) and selected for this study based on the absence of AAVrh8 neutralizing antibodies in serum (<1:10), measured as previously described.¹⁶⁴ All experiments were reviewed and approved by the Institutional Animal Care and Use Committee at the University of Massachusetts Medical School (Worcester, MA), and performed in compliance with the NIH Guide for Care and Use of Laboratory Animals, 8th edition.

Intracerebral injection of AAVrh8 vectors or PBS and imaging in animals

Three doses (3.2×10^{12} vg (1x cohort: n=3), 3.2×10^{11} vg (1/10th cohort: n=2), or 1.1×10^{11} vg (1/30th cohort, n=2)) containing a 1:1 ratio of AAVrh8 vectors encoding cmHex α - and cmHex β -subunits along with control groups injected with vehicle (phosphate buffered saline (PBS), n=1) or 3.2×10^{12} vg of an AAVrh8 vector without a transgene (TGE, n=2) were tested. Neurosurgical procedure, injection, and imaging were performed as previously described.^{1, 165,}

¹⁶⁶ Targeting and trajectory planning occurred through fusion of live operative

fluoroscopy and cone-beam computed tomography scans with pre-surgical magnetic resonance imaging (MRI). Bilateral injections into the thalamus occurred simultaneously (150 μ l per side) with an infusion rate of 2 μ l/min using a 16G SmartFlow™ neuroventricular cannula (MRI Interventions, Inc). Approximately 10 minutes after infusion the cannulas were withdrawn from the brain and followed by injection into the left cerebral lateral ventricle (300 μ l) at a rate of 50 μ l/min using a 16G SmartFlow™ neuroventricular cannula (MRI Interventions, Inc). In all cohorts each thalamus received 1/4th of the total AAV vector dose and the left cerebral lateral ventricle received half. Injection volumes were kept constant across cohorts.

Clinical Monitoring and Neurological Assessment

Monkeys were assessed in their home cage before surgery and weekly as described.¹⁶⁷ Behavior of monkeys in their home cage was also evaluated using a camcorder to document behavior before surgery and at 7, 15, 30, 60, and 90 days post-surgery. Spontaneous behavior (recording the monkey for 3.5 minutes while absent from the room), food presentation and response (to handing animal treats or placing treats in the food hopper for 1 minute), as well as response to threat (approaching animal's cage while looking directly at the monkey for 1 minute) were all documented.

Measurement of antibody titers in serum

Serum antibody titers towards AAVrh8 vector or purified human Hex α -subunit (Sigma) were measured using an ELISA assay as previously described.¹⁴

Titers $\leq 1:8$ were considered not detectable.

Tissue collection, processing, histopathology, histochemistry, and immunohistochemistry

Fresh, unperfused tissue was collected from animals in the highest dose cohort (3.2×10^{12} vg) as well as from the PBS control group. Animals from 3.2×10^{11} vg dose cohort, 1.1×10^{11} vg dose cohort, and control animals receiving AAVrh8 vector without a transgene were perfused with cold phosphate buffered saline prior to tissue collection. Following death, a complete necropsy was performed. All tissues collected were fixed in 10% neutral buffered formalin (NBF) and paraffin embedded according to standard procedures. Five μ m histologic sections were routinely processed and stained with hematoxylin and eosin (HE). Luxol fast blue histochemical staining was performed based on standard procedures. To characterize the immune cell infiltrate of the lesions, immunohistochemistry for CD3, CD20, and CD68 were performed. Briefly, all staining protocols used an antigen retrieval protocol of microwaving slide-mounted sections in 0.1M sodium citrate buffer for 20 minutes followed by 20 minutes of cooling at room temperature (RT). CD3 (Dako, Carpinteria, CA; catalog #A0452) was applied for 30 minutes at room temperature at a dilution of 1:600. CD20 (Dako, Carpinteria, CA; catalog #M0755) and CD68 (Dako,

Carpinteria, CA; catalog #M0814) were applied overnight at 4°C at a dilution of 1:179 and 1:410 respectively. Secondary antibodies were biotinylated horse anti-mouse (Vector Laboratories, Burlingame, CA) or biotinylated goat anti-rabbit (Vector Laboratories) as appropriate, diluted 1:200, and incubated for 30 minutes at room temperature. Tertiary reagent in each case was Vectastain ABC Elite reagent (CD3) or Vectastain ABC Standard reagent (CD20, CD68) incubated for 30 minutes at RT (Vector Laboratories). All slides were developed with DAB chromogen (Dako) and counterstained with Mayer's hematoxylin. Negative controls consisted of adjacent brain sections stained with irrelevant species-, isotype-, and concentration-matched antibodies. Lymph node served as a positive control tissue for all antibodies.

Western blotting

Tissues were lysed from 3 mm biopsy punches of the thalamus in T-PER™ Tissue Protein Extraction Reagent (Thermo Scientific) containing cOmplete Protease Inhibitor Cocktail (Roche). Total protein was measured using QuickStart™ Bradford Protein Assay with serial dilutions of bovine serum albumin as protein standard (Bio-Rad). Total protein lysates (20 µg) were resolved using SDS-polyacrylamide gel electrophoresis with 4-20% Mini-PROTEAN® TGX™ (Bio-Rad) precast gel in 25 mM Tris 190 mM Glycine 0.1% sodium dodecyl sulfate followed by wet transfer to a 0.22 µm nitrocellulose membrane (Maine Manufacturing, LLC) in 25 mM Tris 190 mM Glycine.

Membranes were blocked for 1 hour in 5% non-fat dry milk in Tris-Buffered Saline with 0.05% Tween™ 20 (TBST) and probed with rabbit anti-Hex α -subunit antibody (LifeSpan BioSciences, Inc.) or mouse anti- Hex β -subunit antibody¹⁴ diluted 1:1,000 in 5% non-fat dry milk in TBST and incubated overnight at 4°C. HRP-conjugated secondary antibodies (anti-mouse or anti-rabbit, GE Healthcare) were diluted 1:5,000 in 5% non-fat dry milk TBST and incubated for 1 hour at room temperature. Signal was detected using Pierce ECL Western Blotting Substrate (ThermoFisher Scientific) followed by exposure to Amersham Hyperfilm ECL (GE Healthcare). Membranes were stripped using 100 mM glycine (pH 4.0) for 25 minutes, washed in TBST and then blocked and probed again using HRP-conjugated mouse anti- β -actin antibody (GenScript) diluted 1:1,000 in 5% non-fat dry milk in TBST for 1 hour and detected as before.

Hexosaminidase activity

Hexosaminidase isozyme activities were measured from fresh frozen tissue either from 3 mm biopsy punches from the thalamus of 4 mm coronal blocks or from 2 mm slices from thoracic spinal cord coronal blocks. Enzyme activity was measured using 4-Methylumbelliferyl N-acetyl- β -D-glucosaminide (MUG, Sigma) and 4-Methylumbelliferyl 6-Sulfo-2-acetamido-2-deoxy- β -D-glucopyranoside Potassium Salt (MUGS, Toronto Research Chemicals) and normalized to total protein measured by QuickStart™ Bradford Protein Assay with serial dilutions of bovine serum albumin as protein standard (Bio-Rad) as

previously described.¹⁴ Enzyme activity is represented as nmol 4MU/hr/mg protein.

Fluorescent immunostaining

Formalin-fixed paraffin sections (5 μ m thick) were used for neuropathological evaluation. Paraffin was removed from tissue mounted slides with two 8 minute incubations in xylenes and then section were rehydrated with serial 4 minute incubations in 100%, 95%, and 80% ethanol followed by 1x phosphate buffered saline (PBS). For antigen retrieval, slides were boiled in 10mM Tris 1mM EDTA (pH 9.0) for five minutes and then cooled for 20 minutes. Blocking with permeabilization was done for 1 hour in 5% normal goat serum (SouthernBiotech) in PBS with 0.05% Tween-20 (Acros). Sections were incubated with primary antibodies diluted in 5% normal goat serum in PBS with 0.05% Tween-20 for 1 hour at room temperature at the following concentrations: rabbit anti-HEXA, 1:1000 (LifeSpan BioSciences, Inc.), mouse anti-HEXB, 1:1000,¹⁴ or NeuN, 1:1,000 (EMD Millipore). Sections were washed 3 times in TBST and secondary antibodies against the appropriate species and conjugated to the different fluorophores (Alexa-488 or Alexa-555, ThermoFisher) were diluted 1:1000 in 5% normal goat serum in PBS with 0.05% Tween-20 and incubated for 30 minutes followed by 3 washes in PBS. Sections were stained for 1 minutes in Thermo Scientific™ Pierce™ DAPI (4',6-diamidino-2-phenylindole)

Nuclear Counterstain diluted in PBS. Coverslips were mounted on slides using PermaFluor aqueous mounting medium (ThermoFisher).

In situ hybridization

RNAscope fluorescent multiplex kit (Advanced Cell Diagnostics) was used for *in situ* analysis of vector derived mRNA in tissue sections using a WPRE^{mut6 Δ ATG} specific probe set (Advanced Cell Diagnostics). Formalin-fixed 4 μ m paraffin brain sections were used according to the manufacturer's instructions.

Results

Experimental Design

The goal of this study was to assess the safety of a formulation of two AAVrh8 vectors (1:1 ratio) encoding Hex α - and β -subunits injected bilaterally into the thalamus and one cerebral lateral ventricle in cynomolgus macaques (cm). Vector purity, endotoxin levels, and empty capsid ratios were measured (Figure 3.1). These vectors encoded cm Hex proteins to reduce the likelihood of a confounding immune response triggered by delivery of Hex proteins from other species. All subjects were selected for the absence of AAVrh8 neutralizing antibody titers ($<1:10$). The study included three dosing cohorts: 3.2×10^{12} vg (1x cohort: n=3), 3.2×10^{11} vg (1/10th cohort: n=2), and 1.1×10^{11} vg (1/30th cohort, n=2) of AAVrh8-cmHex vectors, and control groups injected with vehicle PBS, n=1) or 3.2×10^{12} vg of an AAVrh8 vector without a transgene (TGE, n=2). The 1x dose was based on the efficacious dose in SD cats by vg/kg brain weight.¹⁵³ Safety was determined by neurological behavioral assessments, MRI data obtained at endpoint (90 days), and pathological examination of tissues.

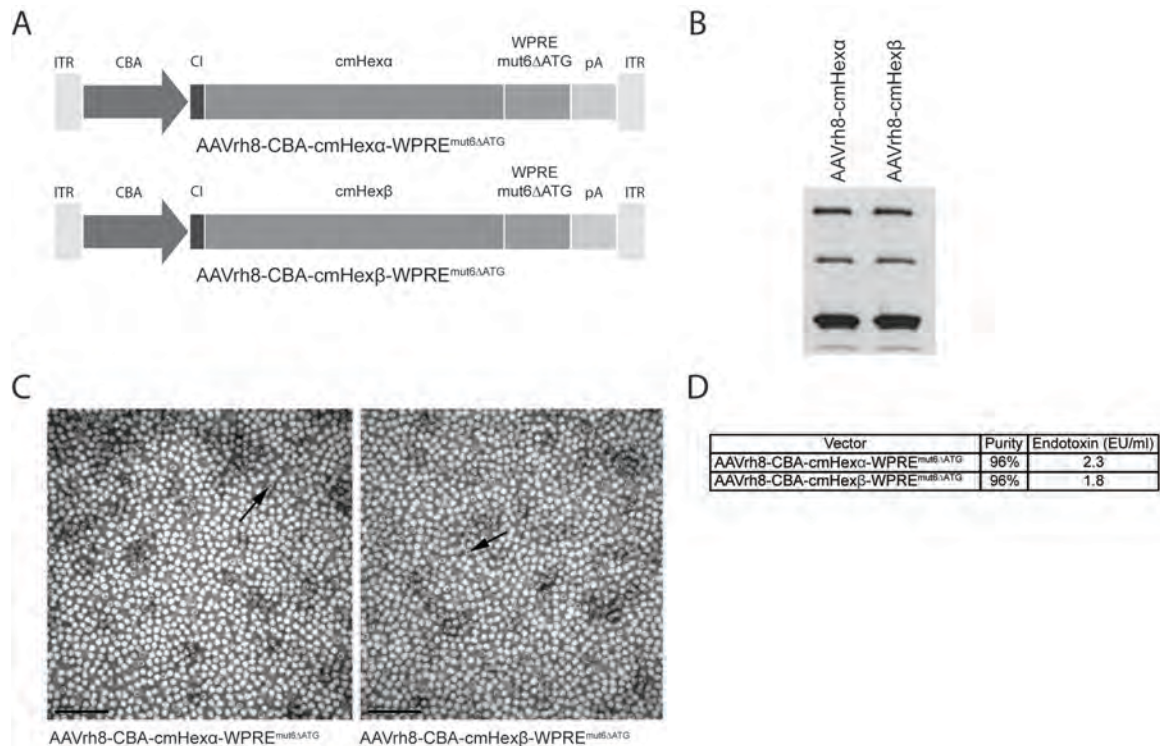


Figure 3.1 Characterization of AAVrh8 vectors. (A) Schematic of the two AAVrh8 vectors used in this study. ITR: inverted terminal repeat, CBA: CMV enhancer fused to chicken β -actin promoter, CI: chimeric intron, cm: cynomolgus macaque, Hex: Hexosaminidase, WPRE^{mut6 Δ ATG}: modified Woodchuck Hepatitis Virus Posttranscriptional Regulatory Element, pA: bovine growth hormone poly-adenylation site. (B) Silver stain on AAVrh8 viral preparations. (C) Electron microscopy of AAVrh8 preparations detected by negative stain. Darkly stained structures indicate empty viral capsids (arrows). (D) AAVrh8 preparation purity determined by densitometry of silver stain in (B) as well as endotoxin levels measured in AAVrh8 preparations.

Clinical Observations

All monkeys tolerated and recovered well from the surgical procedure. However, monkeys in the highest dose cohort (1x) started to show neurological symptoms at 2-3 weeks after injection. Symptoms included general weakness of limbs, ataxia, inability to perch, and reduced food intake. The neurological function of these animals declined rapidly and they became apathetic, which led to premature euthanasia between 20-28 days after surgery. In the 1/10th dosing

cohort, animals appeared normal until 33 and 48 days after injection when they began to develop chorea and dyskinesia during voluntary movement, such as when reaching out for food. From this cohort the animal that developed symptoms at 33 days required euthanasia at 57 days due to lethargy and non-responsiveness. However, the other animal in this cohort survived to the 90-day study endpoint. In the 1/30th dosing cohort, one animal lost voluntary use of its right arm at 59 days and required euthanasia due to lethargy at 66 days. The other animal in this cohort did not develop any major clinical signs and survived to the 90-day study endpoint (Table 3.1). Despite no outward clinical symptoms in this animal, a brain MRI before necropsy indicated alterations in the thalamus (Figure 3.2). No clinical signs were observed in the control cohorts, which consisted of a PBS injected animal as well as two animals injected with a transgene empty (TGE) AAVrh8 vector at the 1x dose (Table 3.1, Figure 3.2).

Animal ID	Vector dose	Symptom onset (days)	Survival (days)	Clinical signs
0908068	1x	14	20	lethargy, non-responsive
0908087	1x	17	23	ataxia, unable to perch
0909589	1x	27	28	generalized weakness especially of right leg, reduced food intake
8722431552	1/10 th	33	57	dyskinesias, chorea
09087133	1/10 th	48	> endpoint	dyskinesias, chorea
0909587	1/30 th	59	66	loss of voluntary use of right arm, eventual lethargy
0908997	1/30 th	n/a	> endpoint	none
8963934563	PBS	n/a	> endpoint	none
5347096796	TGE (1x)	n/a	> endpoint	none
7667353701	TGE (1x)	n/a	> endpoint	none

Table 3.1 Summary of neurological symptoms observed in study animals. For each animal, vector dose, day of symptom onset, length of survival, and observed clinical signs are indicated. The pre-determined endpoint of the study was 90 days. (TGE: transgene empty, PBS: phosphate buffered saline)

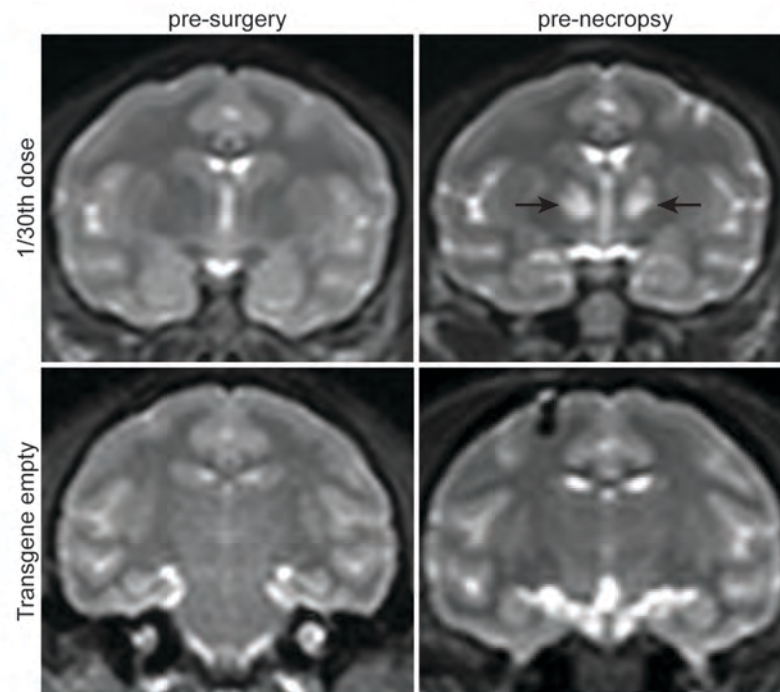


Figure 3.2 Corresponding coronal sections of brain T2-weighted MRI at pre-surgery and pre-necropsy indicating signal alterations at endpoint in treated animal. Hyperintensities (arrows) detected in the thalami of an animal injected with 1.1×10^{11} vg (1/30th dose) of AAVrh8 vector formulation encoding cmHex α or cmHex β subunits. No hyperintensities were noted at any time point in the thalami of an animal treated with a transgene empty vector.

Pathology

Serum antibody titers to human recombinant HexA and AAVrh8 capsid were measured at both pre-injection and necropsy. There were no detectable titers (<1:8) to the HexA protein before injection or at necropsy in all animals. At necropsy animals receiving vector (including TGE control) had AAVrh8 capsid serum antibody titers ranging from 1:128 – 1:49,152. The PBS injected animal did not have any AAVrh8 capsid antibody titers (Table 3.2).

Animal ID	Titer to hHex α -subunit		Titer to rh8 capsid	
	Pre-surgery	Necropsy	Pre-surgery*	Necropsy
1x				
0908068	ND 1:8	ND 1:8	ND	1:3,072
0908087	ND 1:8	ND 1:8	ND	1:2,048
0909589	ND 1:8	ND 1:8	ND	1:1,024
1/10th				
8722431552	ND 1:8	ND 1:8	ND	1:49,152
09087133	ND 1:8	ND 1:8	ND	1:49,152
1/30th				
0909587	ND 1:8	ND 1:8	ND	1:128
0908997	ND 1:8	ND 1:8	ND	1:384
PBS				
8963934563	ND 1:8	ND 1:8	ND	ND 1:8
Transgene Empty				
5347096796	ND 1:8	ND 1:8	ND	1:49,152
7667353701	ND 1:8	ND 1:8	ND	1:1,024

Table 3.2 Serum titers against recombinant human Hex α -subunit and AAVrh8 capsid. The pre-surgery and necropsy titers measured by ELISA against Hex α and AAVrh8 capsid for each animal and their dosing cohorts are indicated. ND: not detected. *Pre-surgery AAVrh8 titers were measured by neutralizing antibody screen to select animals.

Histological examination of the brain revealed widespread neuropathology in the thalamus of animals injected with AAVrh8 encoding Hex. Alterations included the presence of granular eosinophilic inclusions in neurons (Figure 3.3A), necrotic areas with vacuolation (Figure 3.3B), perivascular cuffing (Figure 3.3C), and white matter loss indicated by lack of luxol fast blue stain (Figure 3.3D). Neurons with eosinophilic inclusions were also observed in the thalamus of the other NHPs injected with lower doses of AAVrh8-cmHex vectors (Figure 3.3E). There was no evidence of neuropathology in other regions of the brain with the exception of that associated with needle tracks. All control cohorts had mostly normal histological appearance in the thalamus (Figure 3.3F) with only small lesions present near the injection site or needle tracks.

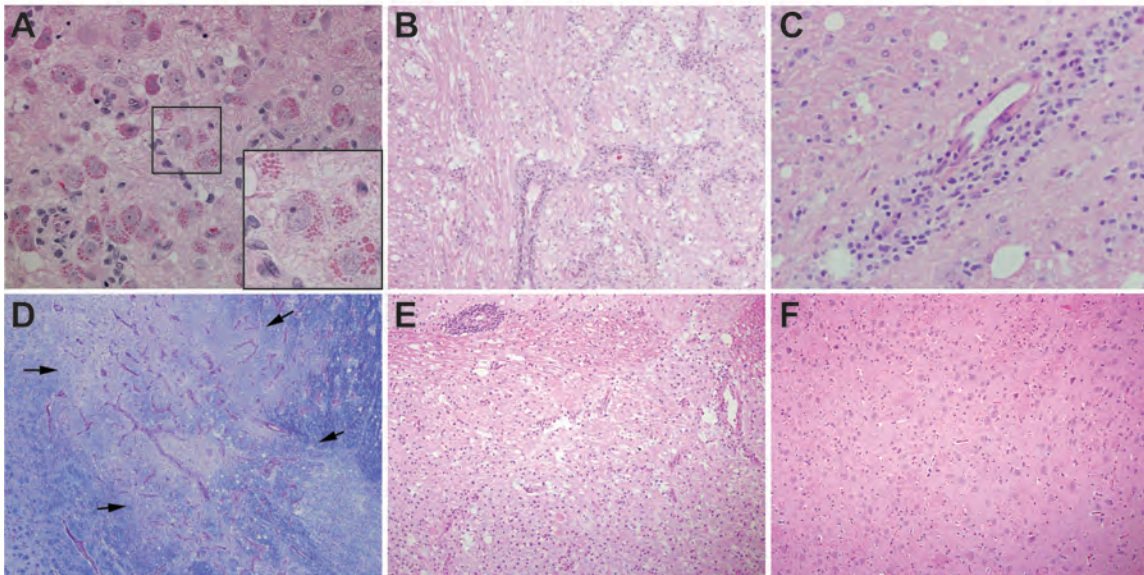


Figure 3.3 Neuropathology. (A) H&E staining indicating the presence of granular eosinophilic inclusions in neurons of the thalamus of injected animals. Box indicates location of magnified region. Magnification 40x. (B) Necrotic area in thalamus with vacuolation. Magnification 10x. (C) Example of peri-vascular cuff in thalamus. Magnification 20x. (D) In this Luxol fast blue-stained section, arrows delineate one large area of necrosis, vascular proliferation, and white matter loss (note pallor compared to adjacent dark blue color). Magnification 10x. (E) Similar neuropathology was seen even in the lowest dosing cohort. 10x (F) Normal thalamus in PBS injected animal Magnification 10x; (1x cohort, A-D; 1/30th cohort, E; PBS injected, F). Tissue sections for histological assessment shown in A, B, C, E, and F were stained with hematoxylin and eosin.

Analysis of the types of immune cells by immunohistochemistry revealed the presence of T-cells (CD3⁺) and B-cells (CD20⁺) in perivascular cuffs but little to none elsewhere in the thalamus (Figure 3.4A-B). However, there was a large macrophage/microglial presence as shown in CD68 immunostaining in the thalamus (Figure 3.4C). These findings were common to all subjects treated with AAV-cmHex vectors, but not in NHPs treated with either PBS or transgene-empty AAV vector.

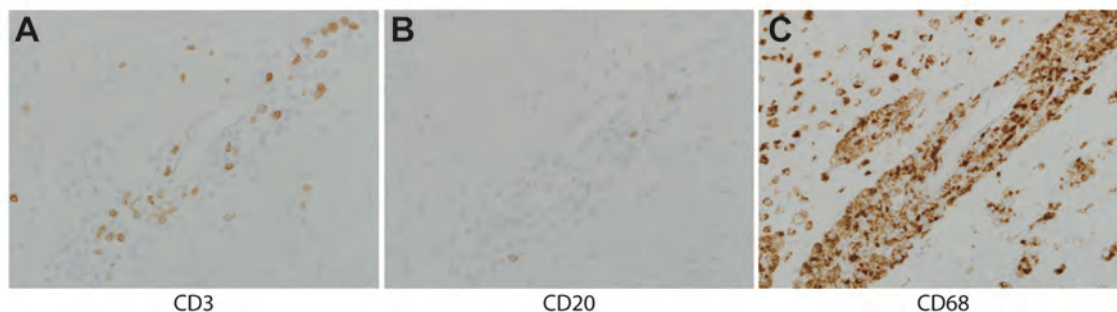


Figure 3.4 Immunological profile of perivascular cuffs in AAVrh8-cmHex α / β injected monkey thalamus. (A) CD3 immunostaining for T-cells. (B) CD20 immunostaining for B-cells. (C) CD68 immunostaining for macrophages/microglia. (A-C; 1/10th cohort animal) Magnification 20x.

Hexosaminidase expression and localization

Western blot analysis of Hex α - and Hex β -subunit protein levels revealed increased levels in the thalamus of animals injected with AAVrh8 vectors encoding cmHex α / β (Figure 3.5A). Accordingly, hexosaminidase activity in the thalamus and spinal cord of animals injected with AAVrh8 vectors encoding cmHex α / β was considerably higher than in control animals, in some instances by >100-fold (Figure 3.5B). This large increase in hexosaminidase expression was still present despite the neuronal loss observed in the thalamus (Figure 3.3).

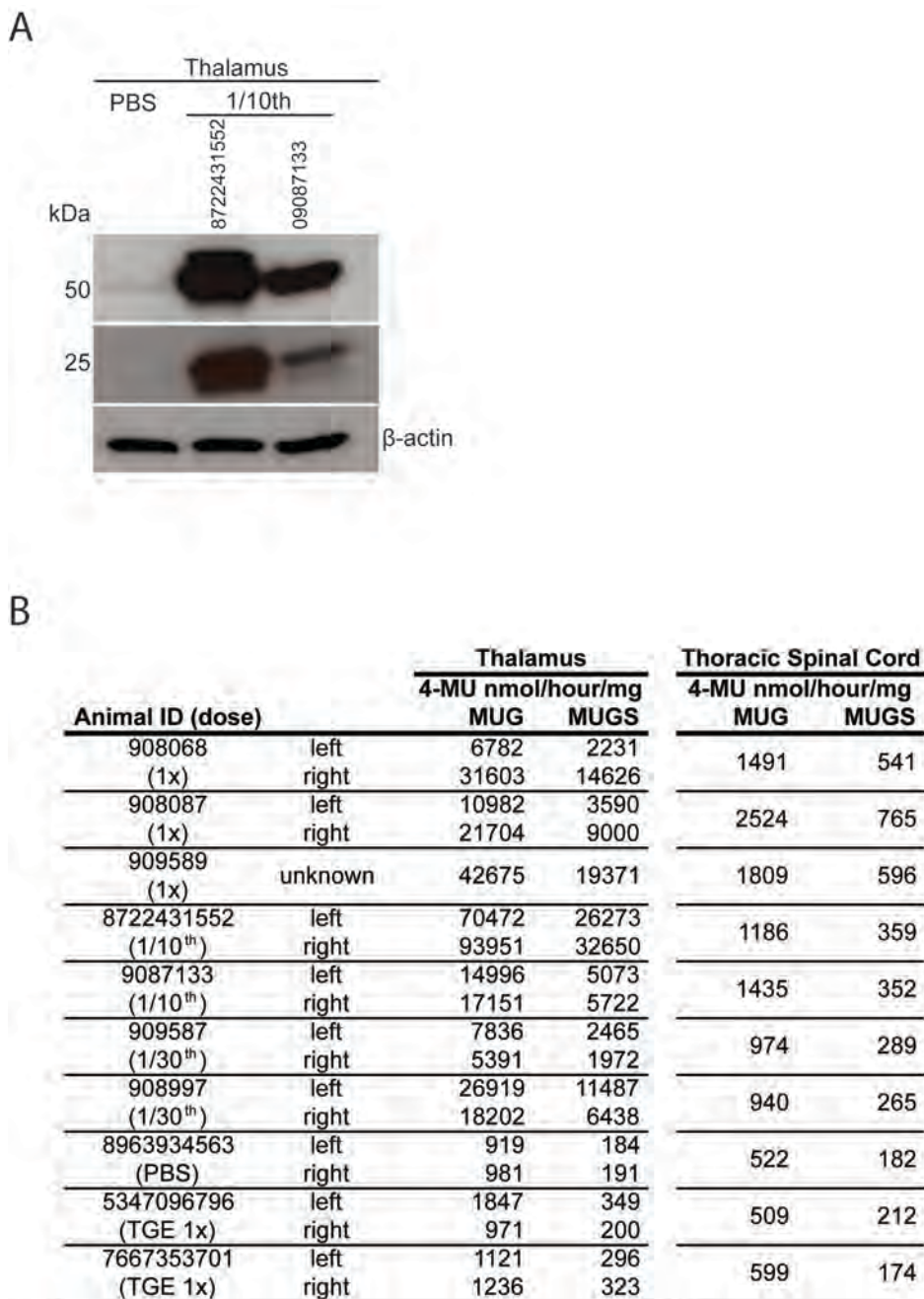


Figure 3.5 Increased Hex expression and activity in the CNS. (A) Western blot analysis of Hex α - or β -subunit protein levels in thalamus lysates from PBS injected control and two animals from 1/10th cohort. (B) Hex activity was measured in the thalamus and thoracic spinal cord on all cohorts. MUG substrate is cleaved by HexA, HexB, and HexS isozymes. MUGS substrate is preferentially cleaved by HexA and HexS isozymes. Note: Due to an emergency euthanasia and necropsy the identity of the thalamus (left or right) in animal is 909589 is unknown.

Despite massive neuronal loss (Figure 3.3) there were still numerous cells in the thalamus expressing both Hex subunits as shown by double immunofluorescence staining for Hex α - and Hex β -subunits (Figure 3.6A). Many transduced cells were neurons given the co-localization of Hex α -subunit with NeuN (Figure 3.6B). *In situ* hybridization in parallel sections using a WPRE probe indicated that cells overexpressing Hex subunits were likely to be AAV vector transduced cells (Figure 3.6C).

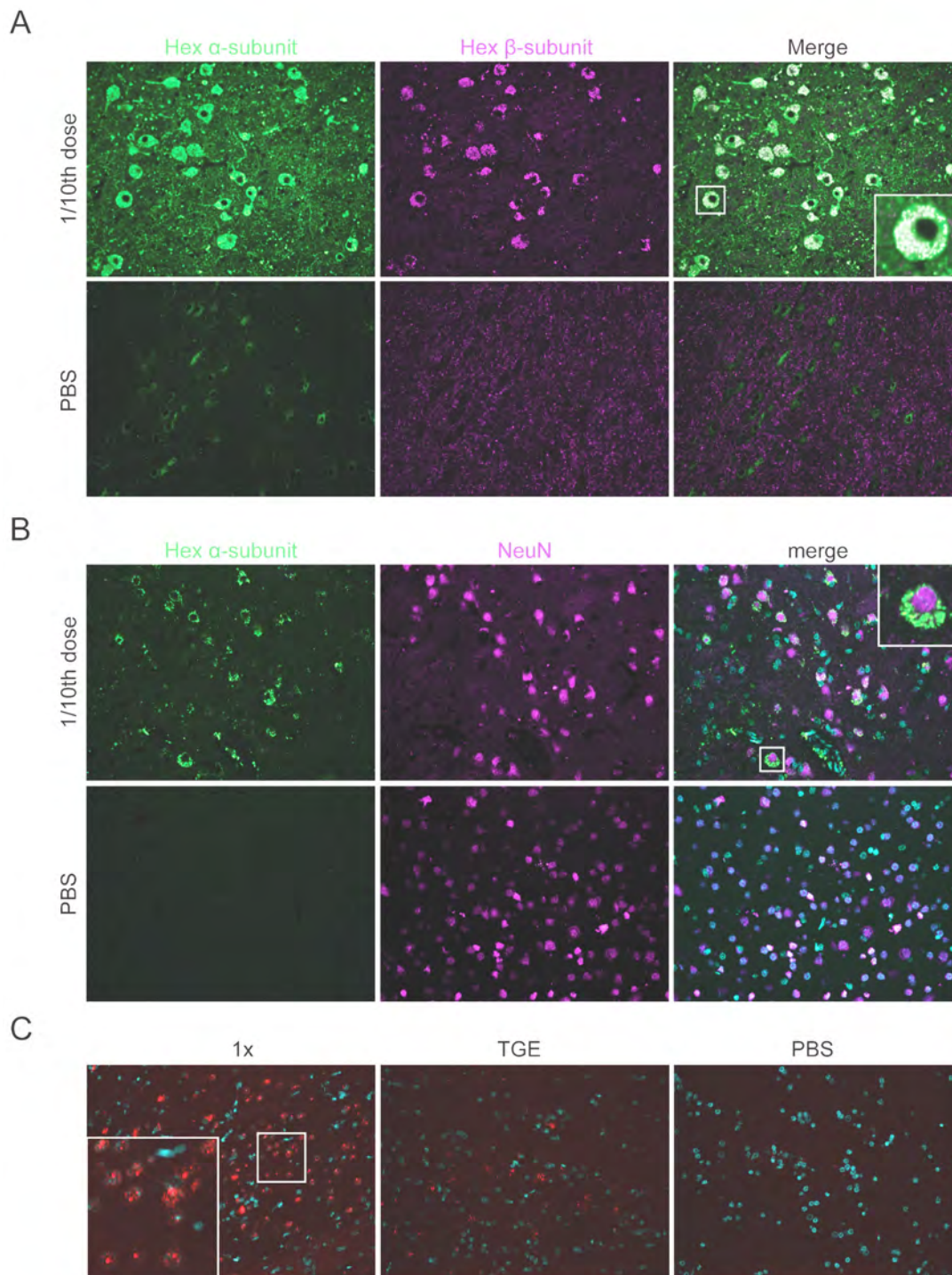


Figure 3.6 Hex α - or Hex β -subunit localization in monkey thalamus. (A) Immunofluorescence staining for Hex α (green) and Hex β (magenta) subunits and their co-localization (white). Box indicates location of magnified region. Magnification 40x. (B) Immunostaining for Hex α -subunit (green) and NeuN (magenta). Magnification 40x. (C) RNA *in situ* hybridization with probe for WPRE (red) expressed by AAV transduced cells. DAPI stain (cyan) Magnification 20x.

CHAPTER IV - OPTIMIZATION OF AAV VECTOR DESIGN FOR SAFE EXPRESSION OF β -N- ACETYLHEXOSAMINIDASE IN THE BRAIN FOR GM2 GANGLIOSIDOSES GENE THERAPY.

Materials & Methods

AAVrh8 vector production

A single stranded rAAV vector plasmid described previously¹⁵⁹ was used to generate AAVrh8-CBA-cmHexa/ β -WPRE^{mut6 Δ ATG}, AAVrh8-CBA-cmHexa/ β , AAVrh8-CB-CI-cmHexa/ β , AAVrh8-CB-cmHexa/ β , AAVrh8-P2-CI-cmHexa/ β , AAVrh8-P2-cmHexa/ β , AAVrh8-cmHexa/ β , AAVrh8-CBA-WPRE^{mut6 Δ ATG}, AAVrh8-CBA-mHexa/ β -WPRE^{mut6 Δ ATG}, and AAVrh8-CB-CI-mHexa/ β plasmids. The P2 promoter sequence is from US Patent No. US 6,346,415 B1, (example 1-7). Sequences of the promoters and other transcriptional elements can be found in Appendix A. AAVrh8 vectors were produced by triple transient transfection of 293T cells followed by purification using iodixanol gradient and fast protein liquid chromatography as previously described.¹⁶¹ Vectors were then concentrated using an Amicon Ultra-15 Centrifugal Filter Unit (100 kDa), buffer exchanged to phosphate-buffered saline using 10 kDa Slide-A-LyzerTM Dialysis Cassettes (Thermo Fisher Scientific), and filtered using Millex-GV Syringe Filter Unit, 0.22 μ m, PVDF, 4 mm (EMD Millipore). The titers of the vectors were measured by real-time quantitative-PCR with primers and probe to the bovine growth hormone (BGH) polyadenylation signal as described.¹⁶¹

Animal procedures

All experiments were reviewed and approved by the Institutional Animal Care and Use Committee at University of Massachusetts Medical School (Worcester, MA), and performed in compliance with the NIH Guide for Care and Use of Laboratory Animals, 8th edition.

AAVrh8 vector screen in nude mice

Ten- to twelve week-old male athymic nude mice were obtained from Charles River Laboratories and injected with an equal mixture of AAVrh8-cmHex α/β vectors bilaterally into the thalamus (2 μ L each side, 0.1 μ L/min, 1.5 mm medial and lateral, 2.0 mm posterior, 3.5 mm ventral to bregma) and into the left lateral ventricle (4 μ L, 0.2 μ L/min, 1.0 mm lateral, 0.2 mm posterior, 2.0 mm ventral to bregma) at a dose of 1.32×10^{10} vg as previously described.¹ Control groups included mice injected with an AAV vector without transgene (Chapter III), phosphate buffered saline (PBS), and non-injected mice (N=8 for all experimental and control groups). Mice were killed at 1 month post-injection for biochemical (n=4) and histological analysis (n=4). For biochemical analysis of Hexosaminidase expression the cerebrum was blocked into four coronal sections: C1: olfactory bulbs and first 3 mm, C2: following 2 mm, C3: following 3 mm, C4: following 2 mm, and the cerebellum, brainstem, and spinal cord were separated. Tissue was immediately frozen on dry ice and stored at -80°C. For

histology brains were fixed in 10% neutral buffered formalin (NBF) and paraffin embedded according to standard procedures at the University of Massachusetts Medical School Morphology Core Facility (Worcester, MA).

AAVrh8 vector screen in primates

Non-human primates

Male and female cynomolgus macaques (1.5-2.5 year-old) were purchased from Worldwide Primates Inc. (Miami, FL) and selected for this study based on the absence of AAVrh8 antibodies in serum (<1:10), measured by ELISA as previously described.¹⁴

Intracerebral injection of AAVrh8 vectors or PBS and imaging in animals

A 1:1 ratio of AAVrh8 vectors containing encoding cmHex α - and cmHex β - subunits at a dose of 3.2×10^{11} vg with 2 mM gadolinium (Magnevist®, Bayer) were injected into the thalamus and lateral ventricle of cynomolgus macaque (n=2 per group) as described earlier (Chapter III).

Clinical Monitoring and Neurological Assessment

Monkeys were assessed in their home cage before surgery and weekly. Behavior of monkeys in their home cage was also evaluated using a camcorder to document behavior before surgery and at 7, 15, 30, 60, and 90 days post-surgery as previously described (Chapter III).

Tissue collection

Monkeys were perfused with cold phosphate buffered saline prior to tissue collection. Brain was blocked into 4 mm coronal slices and every other slice was frozen on dry ice and stored at -80°C and the remaining slices and other tissues were fixed in 10% neutral buffered formalin (NBF) and paraffin embedded according to standard procedures at the New England Primate Research Center (Southborough, MA).

AAVrh8-CB-CI-mHexa/β efficacy studies in Sandhoff Disease mice

A colony of Sandhoff Disease (SV/129 Hexb^{-/-}) mice¹³ was established at the University of Massachusetts Medical School (Worcester, MA) from founders kindly provided by Dr. Gerhard Bauer at the University of California, Davis (Davis, CA) and Dr. Thomas Seyfried at Boston College (Boston, MA). For short-term biochemical analysis of GM2 ganglioside content and Hexosaminidase activity (Figure 3.11), thirty day old SD mice were injected with 1:1 mix of AAVrh8-mHexa/β vectors bilaterally into the thalamus (1 μL each side, 0.1 μL/min, stereotaxic coordinates from bregma in mm: AP: -2.0; ML: ± 2.0; DV from brain surface: -3.5) and into the left lateral ventricle (2 μL, 0.2 μL/min, stereotaxic coordinates from bregma in mm: AP: +0.2; ML: 1.0; DV from brain surface: -2.0) at doses of 4.68×10^9 vg or 2.34×10^{10} vg as previously described.¹ Control groups included mice injected with PBS and non-injected mice. Tissue from the

CNS was collected 8 weeks post infusion and immediately frozen on dry ice and stored at -80°C.

For survival studies (5 month of age endpoint), Sandhoff disease (SD) mice were injected with 2.34×10^{10} vg of an equal mixture of AAVrh8-CB-CI-mHexa/β into the thalamus (1 μL each side, 0.1 μL/min, same stereotaxic coordinates as above) and into the left lateral ventricle (2 μL, 0.2 μL/min, same stereotaxic coordinates as above) at 30 days of age (n=8). Control animals included untreated Sandhoff Disease mice (n=6). Humane endpoint was defined by weight loss of 9-20% maximum body weight or the loss of the ability to right themselves within 15 seconds when turned on their back.

For short-term biochemical analysis of GM2 ganglioside content after dose escalation of ICV dose (Figure 3.12), a 1:1 mix of AAVrh8-CB-CI-mHexa/β vectors were injected bilaterally into the thalamus (1.17×10^{10} vg, 1 μL each side, 0.1 μL/min, same stereotaxic coordinates as above) and into the left lateral ventricle at four different doses: (1.17×10^{10} vg- 2 μL, 2.34×10^{10} vg- 4 μL, 5.85×10^{10} vg- 10 μL, 5.00×10^{11} vg- 10 μL at 0.2 μL/min, same stereotaxic coordinates as above). Brain, cerebellum and spinal cord were collected 4 weeks post infusion and immediately frozen on dry ice and stored at -80°C.

Histology

Paraffin sections (5 μm) were routinely processed and stained with hematoxylin and eosin (H&E), or immunostained with Iba-1 (1:1000, Wako 019-

19741), and GFAP (1:340, Dako Z0334) at the University of Massachusetts Medical School Morphology Core Facility (Worcester, MA). Fluorescent immunostaining of Hexosaminidase was performed using rabbit anti-HEXA, (1:1000, LifeSpan BioSciences, Inc.) as described previously (Chapter III).

Hexosaminidase activity

Hexosaminidase isozyme activities were measured from fresh frozen tissue. Enzyme activity was measured using the artificial substrates 4-Methylumbelliferyl N-acetyl- β -D-glucosaminide (MUG, Sigma) and 4-Methylumbelliferyl 6-Sulfo-2-acetamido-2-deoxy- β -D-glucofuranoside Potassium Salt (MUGS, Toronto Research Chemicals) and normalized to total protein measured by QuickStart™ Bradford Protein Assay with serial dilutions of bovine serum albumin as standard (Bio-Rad) as previously described (Chapter II).¹⁴ Enzyme activity is represented as nmol 4MU/hr/mg protein.

GM2 ganglioside content

GM2 ganglioside content in the CNS was measured from fresh frozen tissue by liquid chromatography-tandem mass spectrometry (LC-MS/MS) as described earlier (Chapter II).

Results

Experimental Design

The goal of this study was to design a new AAVrh8 vector to express β -N-acetylhexosaminidase (Hexosaminidase, Hex) in the brain at therapeutic levels in the absence of the unexpected toxicity documented in monkeys injected with the original AAVrh8-CBA-cmHex α/β -WPRE^{mut6 Δ ATG} vector (Chapter III). Six new AAVrh8 vector designs encoding cynomolgus macaque Hex α - and β -subunits were generated by systematic removal and/or replacement of different elements likely to have an effect on the strength of transgene expression to generate a series of vectors covering a broad range of enzyme overexpression (Figure 4.1).

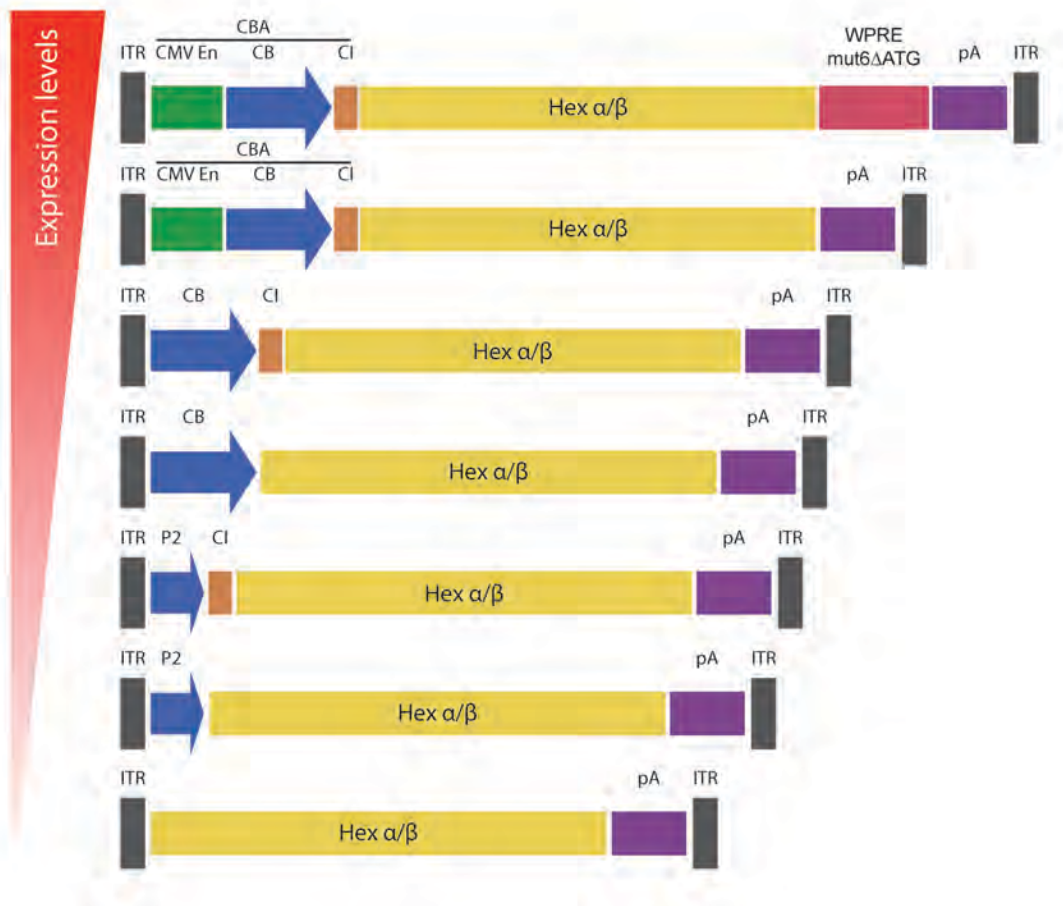


Figure 4.1 Panel of new AAV vectors with an expected gradient of HexA expression levels. Systematic removal of expression elements from the original AAV vector design (top) to its most basic form without a classical promoter element of ITR-flanked cDNA with a polyadenylation signal (bottom vector) in order to reduce expression levels of Hexosaminidase. ITR: Inverted terminal repeat, CMV En: cytomegalovirus enhancer, CB: chicken β -actin promoter, CI: chimeric intron, WPRE: woodchuck hepatitis virus posttranscriptional regulatory element, pA: polyadenylation signal.

Hexosaminidase activity and expression in nude mouse brain

Hex activity was measured in the CNS of athymic nude mice one month after intracranial delivery of 1.32×10^{10} vg AAVrh8-Hex α/β vectors (Figure 4.1) using the artificial substrates MUG (Figure 4.2), cleaved by all isozymes of Hex,

and MUGS (Figure 4.3), cleaved by HexA and HexS. Relative Hex activity in the coronal brain block containing the injection site is shown in Table 4.1 to summarize the findings and identify group numbers. The original AAV vector pair (Group 1) generated Hex activities ~400-1,700 fold above normal. Other AAV vector pairs generated Hex activities in the brain 123-563 fold (Group 2), 20-30 fold (Group 3), and 13-80 fold (Group 5) above normal providing the anticipated range of 1-2 log of activities in AAV-mediated Hex expression in brain. Other AAV vectors pairs (Groups 4, 6, and 7) did not generate Hex activity above normal levels in athymic nude mouse brain. In control groups (Groups 8, 9) the brain Hex activity was comparable to that in naïve mice (Group 10) (Figure 4.1, Table 4.1). Cynomolgus macaque Hexosaminidase expression was also detected in the nude mouse brain by immunostaining (Figure 4.4) with an antibody against human Hex α -subunit and correlated with measured activity levels. Staining revealed numerous cells expressing the enzyme in the thalamus and hippocampus of animals in Group 1 (Figure 4.4A, K), Group 2 (Figure 4.4B, L), Group 3 (Figure 4.4C, M), and Group 5 (Figure 4.4E, O).

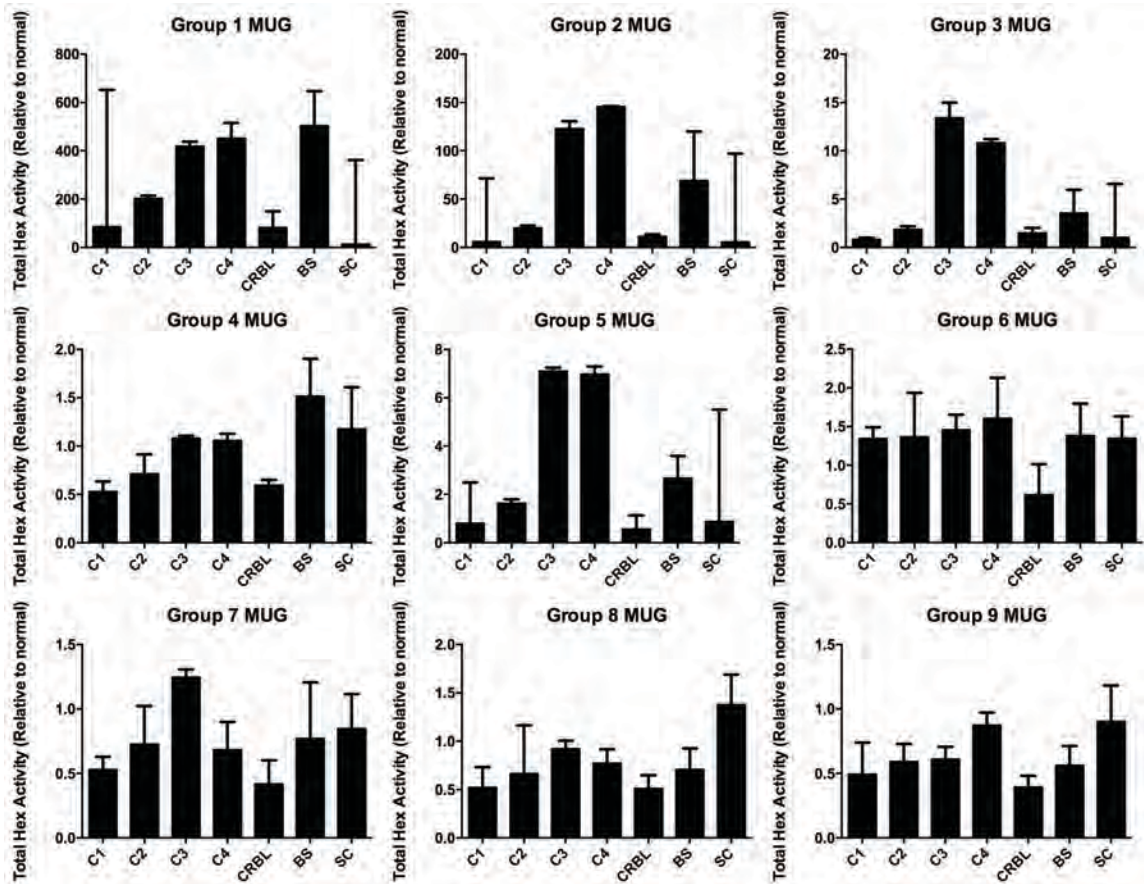


Figure 4.2 Total hexosaminidase isozyme activity in athymic nude mouse brain after intracranial delivery of AAVrh8 vectors encoding cynomolgus Hex α and Hex β . Athymic nude mice were injected intracranially with 1.32×10^{10} vg of AAVrh8 vectors and Hex activity was measured one month post injection. Hex activity was measured using MUG artificial substrate recognized by all Hex isoforms (HexA, B, and S) and normalized to baseline enzyme activity in naïve nude mouse brain. The brain was divided in coronal blocks for biochemical measurement of Hex activity - C1: olfactory bulbs and first 3 mm coronal slice of cerebrum, C2: following 2 mm coronal slice of cerebrum, C3: following 3 mm coronal slice of cerebrum which contain injection sites, C4: following 2 mm coronal slice of cerebrum, CRBL: cerebellum, BS: brain stem, SC: spinal cord).

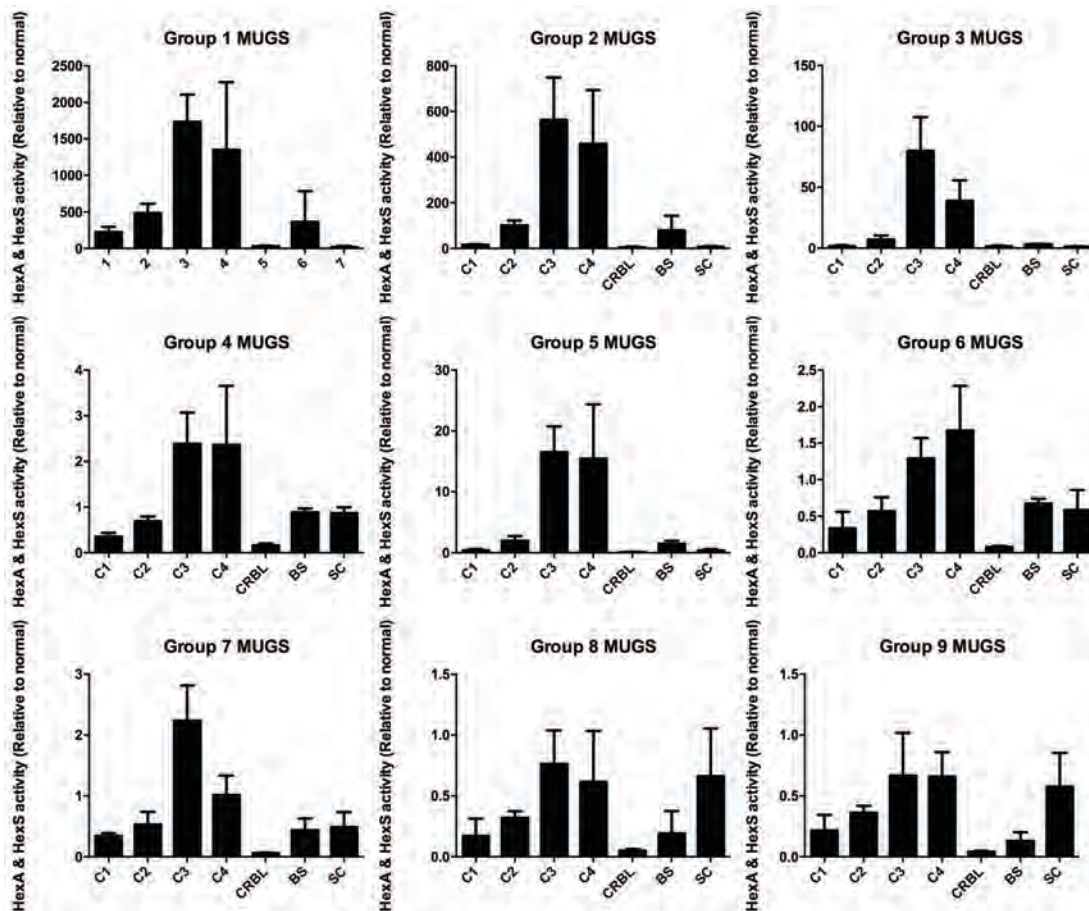


Figure 4.3. HexA and HexS isozyme activity in athymic nude mouse brain after intracranial delivery of AAVrh8 vectors encoding cynomolgus Hex α and Hex β . Combined HexA and HexS activity measured with MUGS substrate, normalized baseline enzyme activity in naïve nude mouse brain. The brain was divided in coronal blocks for biochemical measurement of Hex activity - C1: olfactory bulbs and first 3 mm coronal slice of cerebrum, C2: following 2 mm coronal slice of cerebrum, C3: following 3 mm coronal slice of cerebrum which contain injection sites, C4: following 2 mm coronal slice of cerebrum, CRBL: cerebellum, BS: brain stem, SC: spinal cord).

Group	Vector	Relative Enzyme Activity	
		MUG	MUGS
1	pAAV-CBA-cmHexa/ β -WPRE Δ 6ATGs	419.1	1732.3
2	pAAV-CBA-cmHexa/ β	123.0	563.1
3	pAAV-CB-CI-cmHexa/ β	13.4	80.0
4	pAAV-CB-cmHexa/ β	1.1	2.4
5	pAAV-P2-CI-cmHexa/ β	7.1	16.5
6	pAAV-P2-cmHexa/ β	1.5	1.3
7	pAAV-cmHexa/ β	1.3	2.2
8	pAAV-CBA-WPRE Δ 6ATGs	0.9	0.8
9	PBS	0.6	0.7
10	Naive	1.0	1.0

Table 4.1 Experimental groups and relative hexosaminidase activity in the injected coronal brain block. Treatment groups are shown with corresponding AAVrh8 vectors and average hexosaminidase activity determined with MUG and MUGS substrates (Figures 4.2 and 4.3).

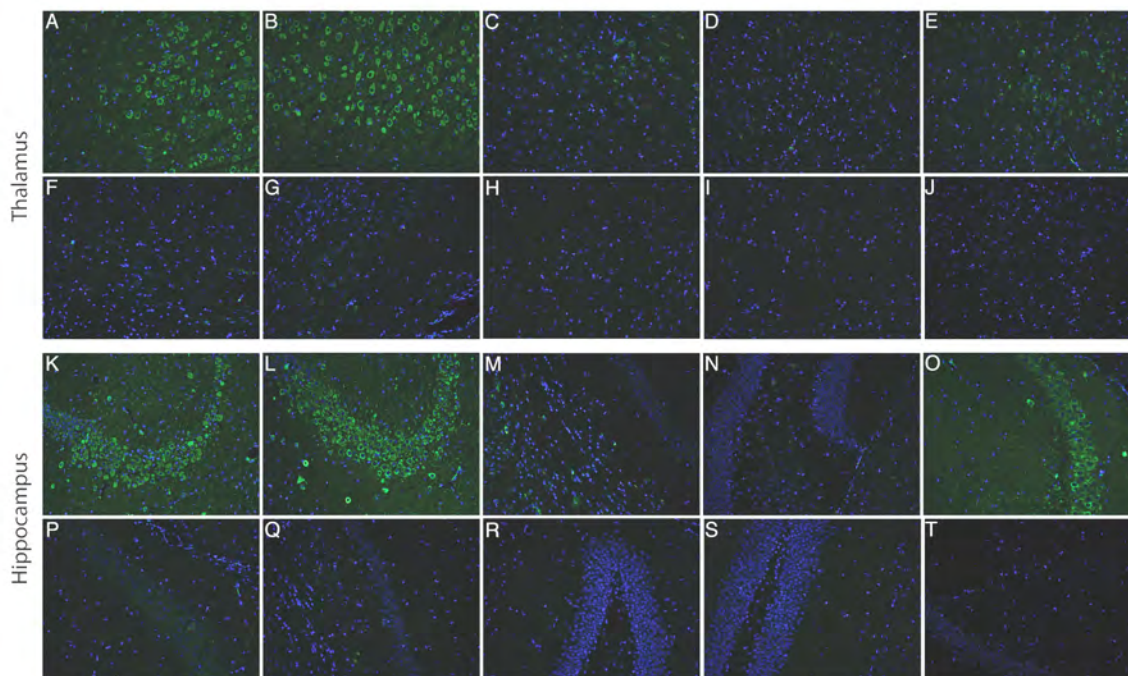


Figure 4.4 NHP hexosaminidase expression in athymic nude mouse brain varies among AAVrh8 vectors. Immunofluorescence detection of Hexa expression (green) in the thalamus and hippocampus of Group 1 (A, K), Group 2 (B, L), Group 3 (C,M), Group 4 (D,N), Group 5 (E,O), Group 6 (F,P), Group 7 (G,Q), Group 8(H,R), Group 9(I,S), and Group 10 (J,T) mice; Nuclei counterstained with DAPI (blue) Magnification 40x.

Neuropathology in nude mouse brain

Neuropathological examination of the brains revealed numerous thalamic neurons containing eosinophilic granules in Group 1 animals (Figure 4.5A). This finding is identical to our observations in monkeys injected with these AAV vectors used in Group 1 (Chapter III), but the number of these abnormal neurons appears considerably lower in mice than monkeys. This observation was also made in Group 2 animals, but the number of abnormal neurons was considerably lower than in Group 1 (Figure 4.5B). We also observed abnormal neurons in the hippocampus of Group 1 & 2 animals (Figure 4.5K, L). We found no evidence of neurons with eosinophilic granules in the brain of any other group.

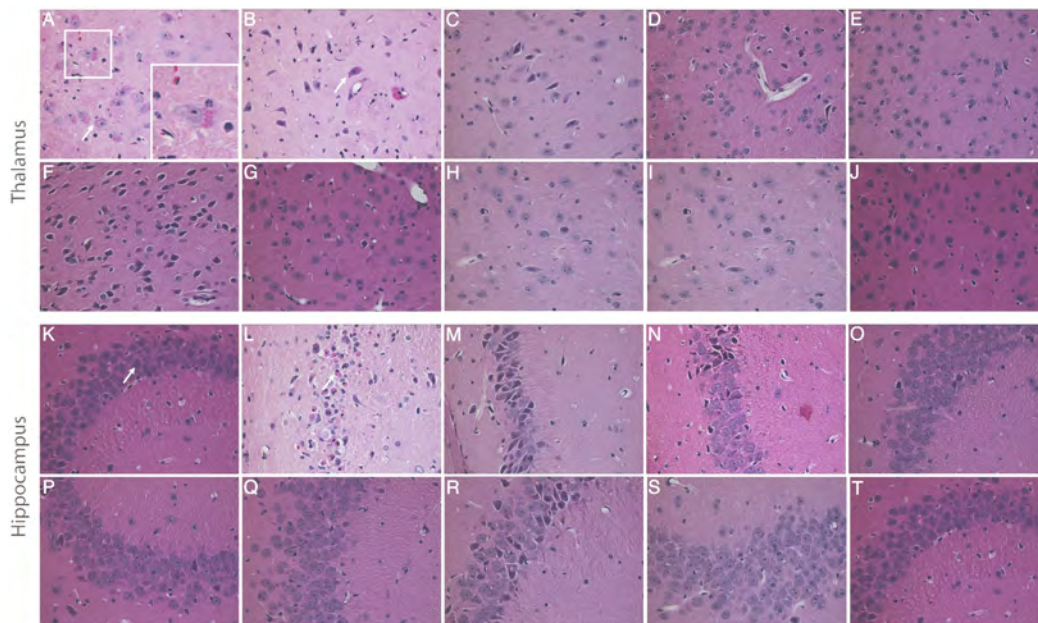


Figure 4.5 Mouse brains expressing highest levels of NHP hexosaminidase protein contain eosinophilic neurons. Hematoxylin and eosin stained tissue sections show the presence of neurons containing eosinophilic granules (example indicated by white arrows) that correlate with cynomolgus Hex expression levels in the hippocampus and thalamus. Group 1 (A, K), Group 2 (B, L), Group 3 (C,M), Group 4 (D,N), Group 5 (E,O), Group 6 (F,P), Group 7 (G,Q), Group 8(H,R), Group 9(I,S), and Group 10 (J,T) mice. Magnification 40x.

Lower Hexosaminidase overexpression results in less gliosis

Increased microglia activation, evaluated with Iba-1 staining, was observed in the thalamus and hippocampus in animals injected with the original AAVrh8 vector formulation (Figure 4.6A, K) compared to controls (Figure 4.6 H-J; R-T). This evidence of microglia activation was localized to the sites where Hex α -positive cells were detected by immunofluorescence staining (Figure 4.4) with no apparent changes in microglia elsewhere in the brain (data not shown). The increase in Iba-1 staining in thalamus and hippocampus was considerably milder in Groups 2 and 3 (Figure 4.6B-C; L-M), and essentially indistinguishable from controls in Groups 4-7 (Figure 4.6D-G; N-Q).

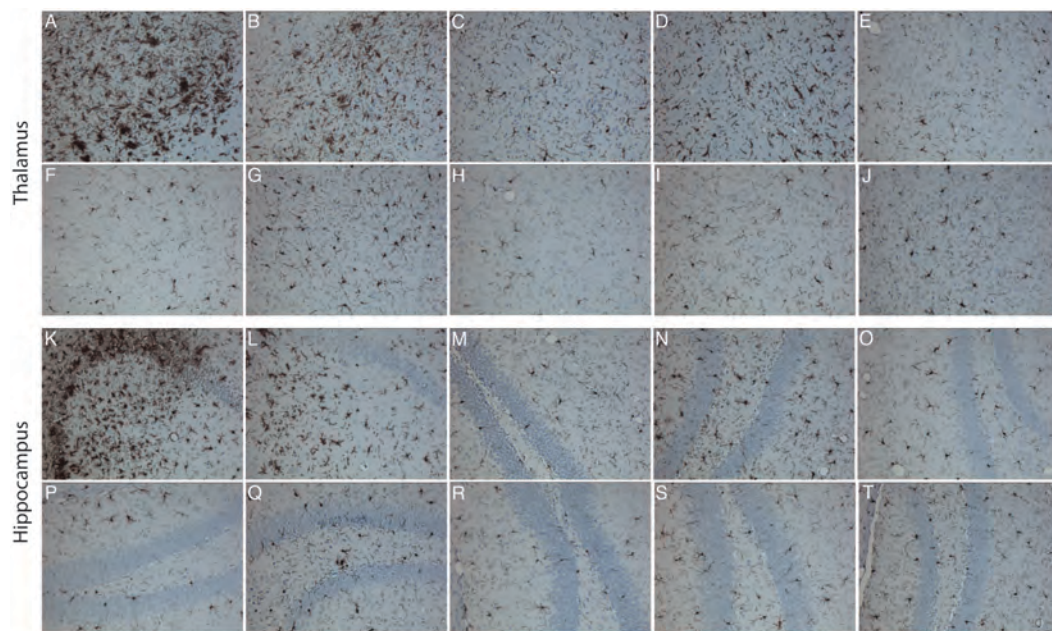


Figure 4.6 Absence of microglial activation in brains injected with AAVrh8 vectors expressing lower levels of NHP hexosaminidase. Iba-1 immunostaining showed reduced microglia activation in groups expressing lower NHP Hex levels in the hippocampus and thalamus. Group 1 (A, K), Group 2 (B, L), Group 3 (C,M), Group 4 (D,N), Group 5 (E,O), Group 6 (F,P), Group 7 (G,Q), Group 8(H,R), Group 9(I,S), and Group 10 (J,T). Magnification 40x.

We also analyzed the brain for evidence of reactive astrogliosis using GFAP immunostaining (Figure 4.7). In the thalamus there appeared to be some degree of astrogliosis in Groups 1, 2, and 4 (Figure 4.7A-B, D), and mild or indistinguishable from controls in Groups 3, and 5-7 (Figure 4.7C, E-G). In the hippocampus we only found evidence of reactive astrogliosis in animals injected with the original AAVrh8 vector formulation (Figure 4.7K). All others were indistinguishable from controls. We found no evidence of astrogliosis in other areas of the brain in any of the groups.

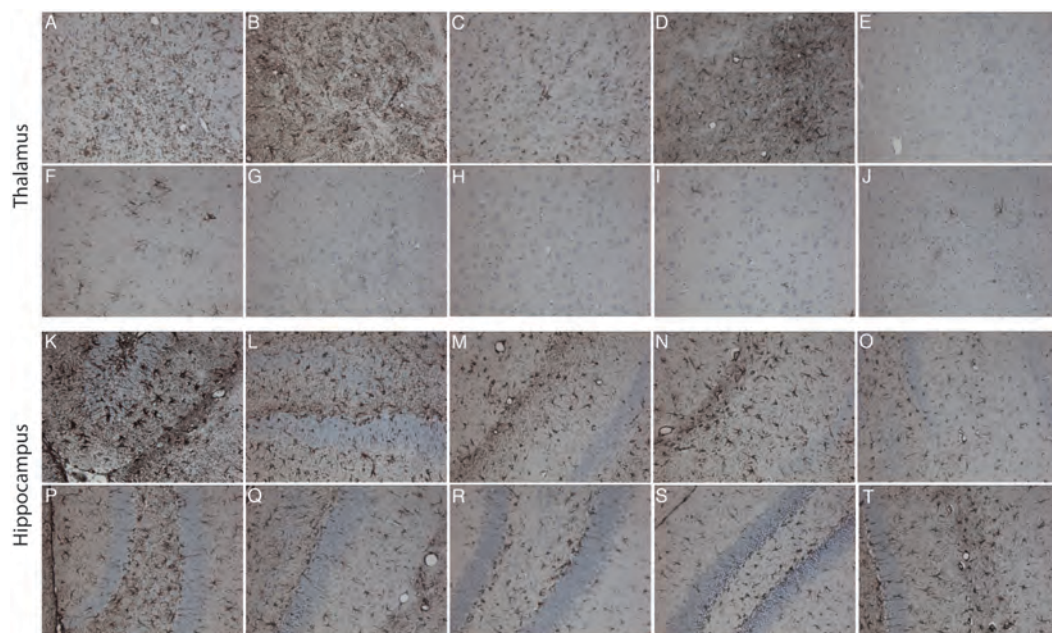


Figure 4.7 Absence of astrocyte activation in brains injected with AAVrh8 vectors expressing lower levels of NHP hexosaminidase. GFAP immunostaining showed reduced numbers of activated astrocytes in groups expressing lower NHP Hex levels in the hippocampus and thalamus. Group 1 (A, K), Group 2 (B, L), Group 3 (C,M), Group 4 (D,N), Group 5 (E,O), Group 6 (F,P), Group 7 (G,Q), Group 8(H,R), Group 9(I,S), and Group 10 (J,T). Magnification 40x.

Testing new vector designs in primates for Hexosaminidase expression and safety

Three of the six new AAVrh8 vector designs (Figure 4.8) were chosen from the screen in athymic nude mice that mediated overexpression of Hexosaminidase in brain with minimal inflammatory response compared to the original AAVrh8 vector. These three AAVrh8 vectors were injected (3.2×10^{11} vg) into the brain of NHPs (n=2 per cohort) screened for low neutralizing antibody titers to AAVrh8.

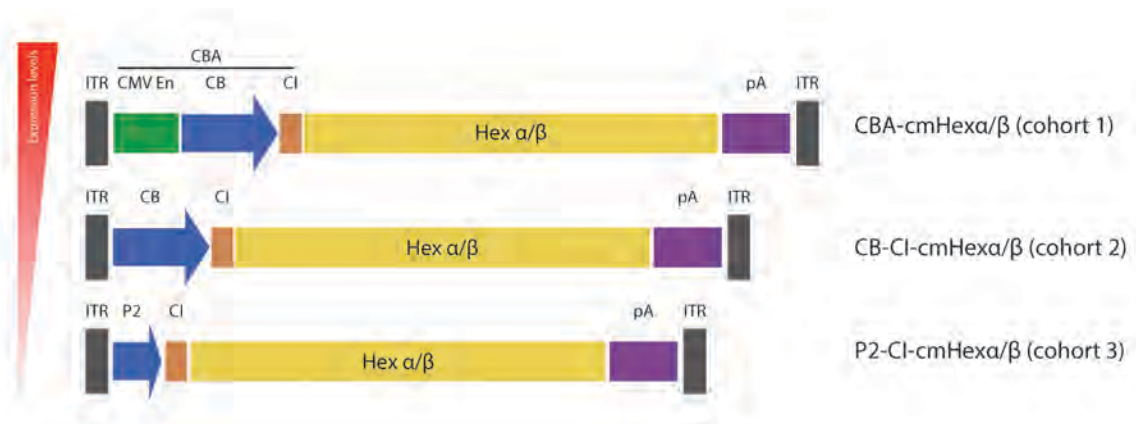


Figure 4.8 New AAVrh8 vectors selected for further testing in non-human primates. Three vectors were chosen from the nude mouse screen (Figure 4.1) to assess toxicity in NHP. AAVrh8-CBA-cmHexa/β (cohort 1) contains all elements of our original vector without the WPRE^{mut6ΔATG} element. AAVrh8-CB-CI-cmHexa/β (cohort 2) is further reduced from cohort 1 by the removal of the CMV enhancer. In AAVrh8-P2-CI-cmHexa/β (cohort 3) the CBA or CB promoter is replaced with a small weaker promoter sequence.

Clinical outcomes in primates

All NHPs tolerated the surgical procedure well with no complications. The behavior of all six AAVrh8-injected NHPs remained normal throughout the 90-day study. Brain MRI was carried out monthly. Small signal changes at the injection sites were documented in two monkeys (295748 and 295709) from cohorts 2

(AAVrh8-CB-CI-cmHexa/ β) and 3 (AAVrh8-P2-CI-cmHexa/ β) from 30 days onward. However, there were no significant changes over time (Figure 4.9). In one monkey (ID 295851) in cohort 1 there were no signal changes in brain MRIs at days 30 and 60 post-injection. However, a signal change was detected in the left thalamus at day 90 (Figure 4.9). Despite the appearance of this abnormal signal at day 90 the behavior of this monkey remained normal throughout the study.

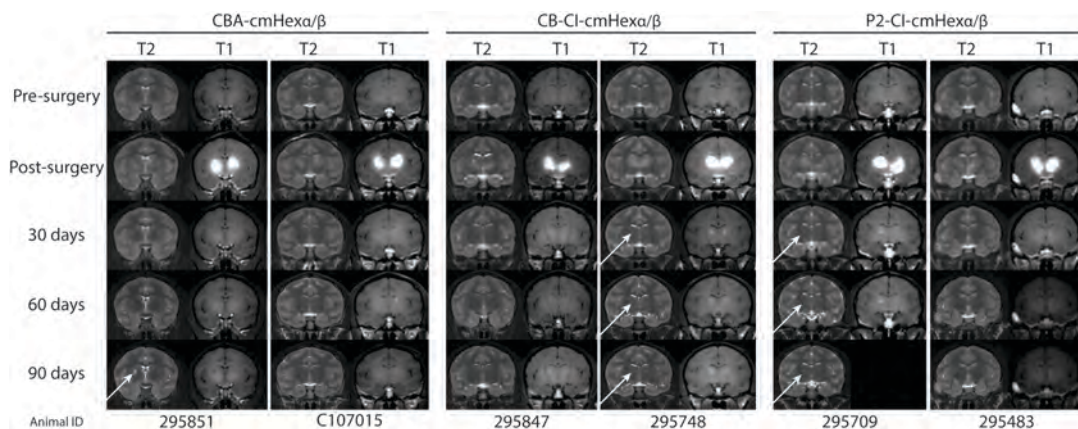


Figure 4.9 T2- and T1-weighted brain MRI sections of AAVrh8 injected non-human primates over time. AAVrh8 vectors were co-injected with gadolinium to assess distribution in the thalamus, through imaging, immediately after surgery (second row, bright signals). Arrows indicate regions of hyperintense signal in the thalamus in three NHPs.

Hexosaminidase activity in primate brain

As expected from our studies in athymic nude mice, total Hexosaminidase activity in thalamic punches was highest in cohort 1 (up to 87-fold above normal), and similar (up to 9-fold above normal) in cohorts 2 and 3 (Table 4.2).

Hex activity (fold over normal)	Location in thalamus	Animal	Group
87.6	Left top	295851	Cohort 1
14.7	Left bottom		
2	Right bottom		
86.6	Right top		
82.1	Left top	c107015	Cohort 1
12.9	Left bottom		
2.9	Right bottom		
53.5	Right top		
4.3	Left top	295748	Cohort 2
1.1	Left bottom		
0.9	Right bottom		
4.7	Right top		
4.7	Left top	295847	Cohort 2
0.7	Left bottom		
2.5	Right bottom		
1.1	Right top		
5.2	Left top	295483	Cohort 3
1	Left bottom		
1.6	Right bottom		
8.9	Right top		
4.5	Left top	295709	Cohort 3
0.8	Left bottom		
1.9	Right bottom		
2.1	Right top		

Table 4.2 Increase in hexosaminidase activity in the thalamus of AAVrh8 injected non-human primates. Hexosaminidase activity in 3 mm biopsy punches taken from dorsal and ventral thalamus of AAVrh8 injected monkeys measured using MUG substrate. Red indicates higher activity than normal.

Neuropathology in primate brain

Neuropathological evaluation of the brains revealed abundant accumulation of intraneuronal eosinophilic material in monkeys in cohort 1 (Figure 4.10A, black arrow). Moderate to severe neuronal degeneration (Figure 4.10A, red arrow) and neuronophagia (Figure 4.10A, purple arrow) was seen in

cohort 1 animals. In the left thalamus of one monkey (ID 295851) in cohort 1 there was severe necrosis with perivascular lymphoeosinophilic encephalitis 3 mm in diameter that extended 750 μm (Figure 4.10B, C). This lesion corresponded to the abnormal MRI signal that became evident in the left thalamus of this animal at day 90 (Figure 4.9).

In cohort 2 there was no accumulation of eosinophilic material and rare neuronal degeneration (Figure 4.10D). Focal inflammation of white matter with neuronal degeneration and mild multifocal gliosis, most likely associated with injection track trauma, was noted in one monkey (ID 295847) as was observed in cohort 3 (Figure 4.10F).

In cohort 3 there was no accumulation of intraneuronal eosinophilic material, rare neuronal degeneration (blue arrows) and satellitosis (Figure 4.10E). In one monkey (ID 295709) there was a focus of perivascular gitter cells likely associated with the cannula track (Figure 4.10F). Quantification of histopathology in the thalamus of low (cohort 3) and high (cohort 1) expressing animals can be found in Appendix B.

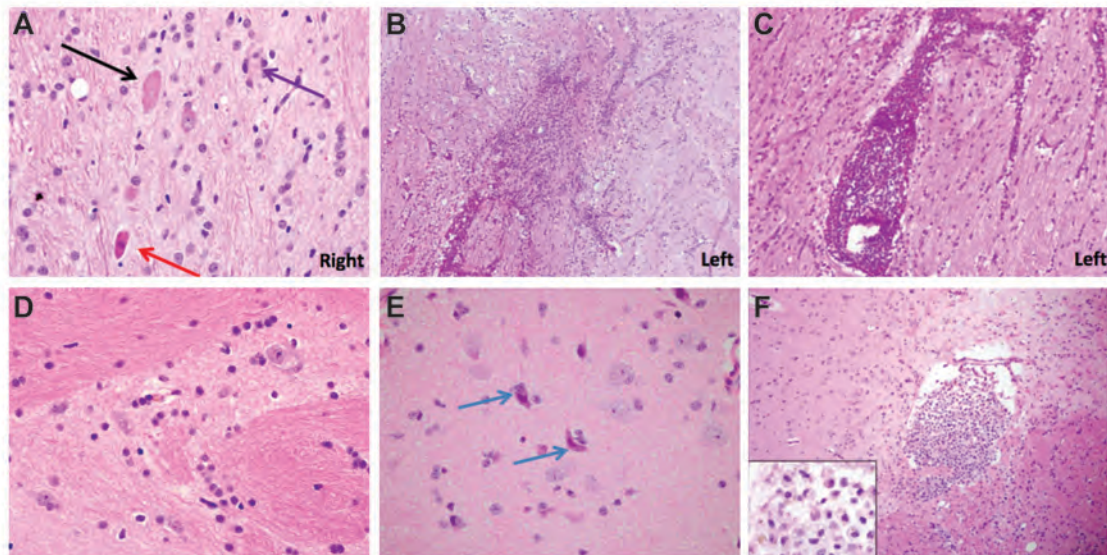


Figure 4.10 Neuropathological findings in the thalamus of AAVrh8 injected non-human primates. H&E staining indicating the presence of granular eosinophilic neurons in the thalamus of injected animals in cohort 1 (A, black arrows), neuronal degeneration (red arrow), and neuronophagia (purple arrow). In the left thalamus of animal 295851 of cohort 1 severe focal, necrotizing, perivascular, and lymphoeosinophilic encephalitis was observed (B, C). In cohort 2 animals there was no accumulation of eosinophilic material in neurons, rare neuronal degeneration, and mild multifocal gliosis likely due to injection trauma (D). In cohort 3 there was only minimal neuronal degeneration in the thalamus likely due to injection trauma (E). One animal in cohort 3 had the presence of perivascular gitter cells likely in the vicinity of the injection track (F). Magnification 10x.

Testing therapeutic efficacy and defining a new minimal effective dose of AAVrh8-CB-CI-mHexa/β in Sandhoff disease mouse model

For short-term biochemical analysis of the effect in CNS GM2 ganglioside content, SD mice were infused with AAVrh8-CB-CI-mHexa/β vector formulation encoding mouse Hexa/β (mHexa/β) subunits at two doses, 4.68×10^9 vg and 2.34×10^{10} vg and compared to the original AAVrh8 vector (AAVrh8-CBA-mHexa/β-WPRE^{mut6ΔATG}) injected at 4.68×10^9 vg, the dose previously shown to have a significant therapeutic effect (Chapter III). GM2 ganglioside content was significantly lower in the cerebrum of SD mice injected with either dose of AAVrh8-CB-CI-mHexa/β vector compared to PBS-injected SD mice, and the

92% reduction observed for the highest dose (2.34×10^{10} vg) of AAVrh8-CB-CI-mHexa/ β vector was comparable to that documented in SD mice injected with the original AAVrh8 vector (97%) (Figure 4.11A). We also observed significant reduction in GM2 ganglioside content in cerebellum and brainstem of SD mice injected with AAVrh8-CB-CI-mHexa/ β vector compared to PBS-injected SD mice, however, to a lesser extent than the original AAVrh8 vector. As expected the degree of GM2 reduction in the CNS of SD mice injected with AAVrh8-CB-CI-mHexa/ β vector was dose dependent (Figure 4.11A). Hexosaminidase activity in the brain of SD mice treated with AAVrh8-CB-CI-mHexa/ β vector was dose dependent and lower than the original AAVrh8 vector by 7-43 fold, but nonetheless 2-12 fold above normal (Figure 4.11B).

Another set of SD mice ($n=8$) was injected with 2.34×10^{10} vg AAVrh8-CB-CI-mHexa/ β to test therapeutic efficacy using survival to 5 months of age (one month past the median survival of untreated SD mice) as outcome measure. The majority of AAV-treated SD mice (6 of 8) survived to 5 months of age. However, only 2/6 animals appeared asymptomatic at 5 months (Figure 4.11C). The remaining four mice presented with varying degrees of hind limb impairment or weakness. The hind limb impairment may be explained by the more modest reduction in spinal cord GM2 ganglioside content with the new AAVrh8 vector formulation compared to the original CBA vector (Figure 4.11A, 35% vs. 70%).

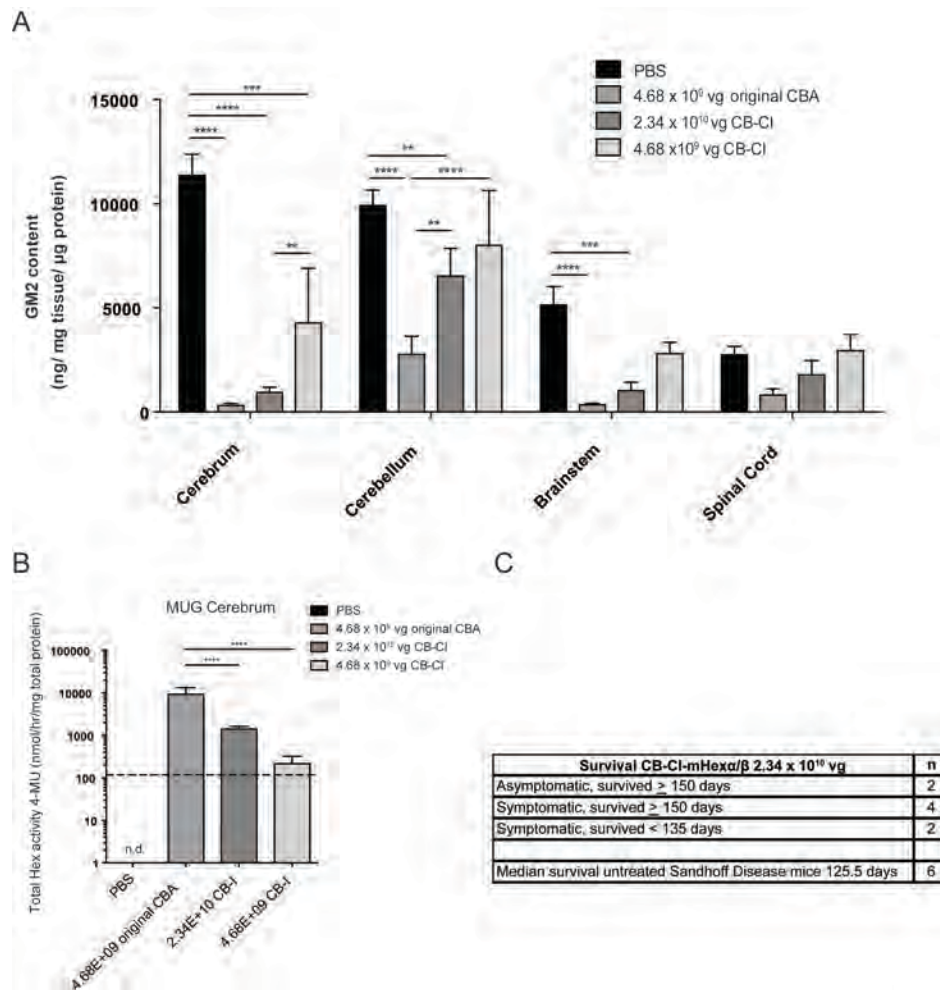


Figure 4.11 Intracranial injection of AAVrh8-CB-CI-mHexa/β vector reduces GM2 ganglioside storage in CNS with a concomitant increase in hexosaminidase activity leads to improved survival of Sandhoff disease mice. SD mice received intracranial injection of AAVrh8-CB-CI-mHexa/β vector at total doses of 4.68×10^9 vg or 2.34×10^{10} vg, or of original vector (4.68×10^9 vg), or PBS. A) GM2 ganglioside content measured by LC-MS/MS in CNS 8 weeks after injection. B) Cerebrum hexosaminidase activity measured using MUG substrate 8 weeks after injection. Dashed line indicates average activity of untreated wild type animals. Results are shown as mean \pm SD, Tukey's multiple comparisons test, * ($P \leq 0.05$), ** ($P \leq 0.01$), *** ($P \leq 0.001$), **** ($P \leq 0.0001$), $n=4$ PBS, $n=4$ original CBA-mHexa/β, $n=6$ 2.34×10^{10} vg CB-CI-mHexa/β and 4.68×10^9 vg CB-CI-mHexa/β. n.d. (not detected) C) Survival and symptom presentation of (5 month study endpoint) of Sandhoff disease mice injected with 2.34×10^{10} vg of AAVrh8-CB-CI-mHexa/β ($n=8$). Median survival of untreated Sandhoff disease mice was 125.5 days ($n=6$).

In order to improve the effect on GM2 ganglioside storage in the spinal cord and cerebellum we increased the dose delivered to CSF via the lateral

ventricles while maintaining the thalamic dose (1.17×10^{10} vg) constant. SD mice were injected with increasing CSF doses of AAVrh8-CB-CI-mHexa/β - 1.17×10^{10} vg, 2.34×10^{10} vg, 5.85×10^{10} vg, 5.00×10^{11} vg (n=3 per cohort). The reduction in GM2 ganglioside content in the spinal cord (Figure 4.12A) and cerebellum (Figure 4.12B) at one month after injection was dose dependent with the highest dose (5.2×10^{11} vg total) showing an effect similar to the original AAVrh8 vector injected at 4.68×10^9 vg.

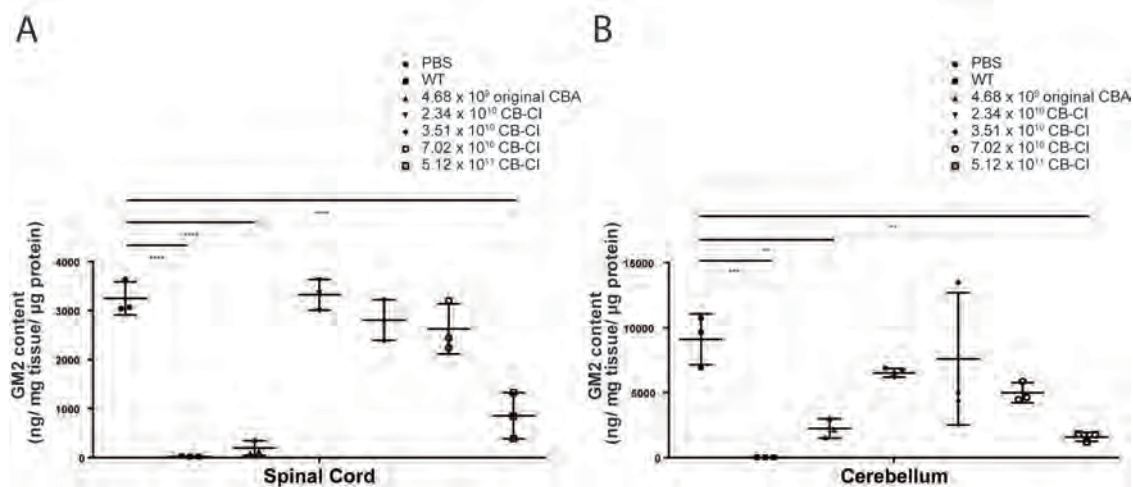


Figure 4.12 Increasing doses of CSF delivered AAVrh8-CB-CI-mHexa/β vector further reduce GM2 ganglioside storage in spinal cord and cerebellum. SD mice were injected with 1.17×10^{10} vg of AAVrh8-CB-CI-mHexa/β into the thalamus with increasing CSF doses (1.17×10^{10} vg, 2.34×10^{10} vg, 5.85×10^{10} vg, 5.00×10^{11} vg). Four weeks after injection GM2 ganglioside content measured by LC-MS/MS in spinal cord (A) and cerebellum (B). Results are shown as mean \pm SD, Dunnet's multiple comparisons tests* ($P \leq 0.05$), ** ($P \leq 0.01$), *** ($P \leq 0.001$), n=3.

Scaling up AArh8 doses from mouse to monkey to humans per kg of brain weight (Table 10.3) would require 1.02×10^{15} vg using our highest ventricular dose. Given the feasibility of manufacturing enough AAVrh8 to move forward clinically we believe 3.51×10^{10} vg in mice ($\sim 7.02 \times 10^{13}$ vg in humans) shows

sufficient evidence of therapeutic benefit and safety to begin further IND-enabling studies in SD mice and non-human primates.

Mouse : NHP : Human Dose comparison
1x : 130x : 2,000x

Thalamus dose (vg)	ICV dose (vg)	Total vg	
1.17×10^{10}	1.17×10^{10}	2.34×10^{10}	mouse
1.52×10^{12}	1.52×10^{12}	3.04×10^{12}	monkey
2.34×10^{13}	2.34×10^{13}	4.68×10^{13}	human
1.17×10^{10}	2.34×10^{10}	3.51×10^{10}	mouse
1.52×10^{12}	3.04×10^{12}	4.56×10^{12}	monkey
2.34×10^{13}	4.68×10^{13}	7.02×10^{13}	human
1.17×10^{10}	5.85×10^{10}	7.02×10^{10}	mouse
1.52×10^{12}	7.61×10^{12}	9.13×10^{12}	monkey
2.34×10^{13}	1.17×10^{14}	1.40×10^{14}	human
1.17×10^{10}	5.00×10^{11}	5.12×10^{11}	mouse
1.52×10^{12}	6.50×10^{13}	6.66×10^{13}	monkey
2.34×10^{13}	1.00×10^{15}	1.02×10^{15}	human

Table 4.3 Dosing scale from mouse to monkey to human. AAV doses corresponding to the brain weight of mouse, monkey, and humans,¹⁶⁸ distributed between thalami and lateral ventricle. Thalamus dose is divided between left and right sides.

CHAPTER V – DISCUSSION

Direct CNS administration of AAVrh8 vectors encoding for mouse β -N-acetylhexosaminidase subunits is well tolerated and leads to long-term survival as well as prolonged motor performance of treated Sandhoff disease mice. Furthermore, in addition to bilateral thalamic injections, a single injection into the lateral ventricle is just as efficacious as bilateral deep cerebellar nuclei injections. Targeting the lateral ventricle and avoiding cerebellar injections may ease clinical translation. Widespread enzyme expression and therapeutic benefit has also been shown in Sandhoff disease cats and Tay-Sachs disease sheep using this therapeutic strategy encoding for species-specific subunits.^{14, 151, 153} Despite treated Sandhoff disease mice living a maximum of 666 days, euthanasia was usually required due to hind limb ataxia and weakness. These findings could be the result of insufficient Hex enzyme expression in the spinal cord. Although there was great reduction of GM2 ganglioside storage in the spinal cord, enzyme expression was lower than in wild type levels as it was undetected using the MUGS substrate. This may be improved upon by increasing ICV dose and volumes, as was done in the Sandhoff disease mice treated with our new AAVrh8-CB-CI-mHex α/β vector in Chapter IV (Figure 4.12).

Production of Hex through direct thalamic and ventricular delivery of AAVrh8 vectors encoding species-specific subunits proved to be toxic in normal NHPs, probably due to overexpression. The severe neurological symptoms that manifested over time were surprising given the demonstrated efficacy and safety

of bilateral injections of AAV-Hex vectors (AAV1, AAV2, and AAVrh8) in normal and GM2 affected disease mice, cats, and sheep.^{14, 15, 106, 150, 151, 153} The absence of neuropathology elsewhere in the central nervous system (CNS) suggests that delivery of AAVrh8-Hex vectors into cerebral spinal fluid through the cerebral lateral ventricles is safe.

The most likely explanation for the neurologic deterioration is the extensive neuronal loss in the thalamus, revealed by MRI imaging and neuropathological examination of the NHP brains injected with AAVrh8-cmHex α/β . Unlike the severe histological findings documented here, a prior study in NHPs injected with an AAV2 vector expressing human acid sphingomyelinase in the thalamus and brainstem also developed severe neurological symptoms but with no apparent neuronal loss. Instead there was robust infiltration of injected brain structures with inflammatory cells.¹⁶⁹

Several lines of evidence in the present study suggest the neurodegenerative process triggered by thalamic injection of AAVrh8-cmHex α/β vectors in normal NHPs is unlikely to have been caused by an immunological response. The human and cynomolgus macaque hexosaminidase α - and β -subunits differ by 11 and 23 amino acids, respectively (Figures 5.1 and 5.2). Intracranial injection of AAV vectors encoding non-self-proteins in NHPs and other species has been shown to trigger strong immune responses resulting in extensive neuronal loss. In addition to the antigenic nature of the transgene, the AAV capsid tropism to antigen presenting cells in the brain may also be a

contributing factor.^{170, 171} Moreover, as patients afflicted with lysosomal storage diseases treated by enzyme replacement therapy often develop antibodies to recombinant human proteins,^{172, 173} we considered the differences in Hex subunits between species a significant factor that could confound interpretation of the results. As such, the AAVrh8-Hex vectors encoded cynomolgus macaque hexosaminidase α - and β -subunits, which would make it unlikely that neuronal loss was caused by an adaptive immune response to the transgenes. The presence of large numbers of transduced neurons in the thalamus near areas of heavy neuronal loss further supports the notion of a non-immune mechanism. In addition, inflammatory cells in thalamus were mostly of the macrophage lineage (CD68+) with very few CD3+ T-cells only found near some blood vessels. These findings suggest that the inflammatory cell infiltration was likely secondary to a primary neurodegenerative insult. Also, we found no evidence of antibodies to HexA at the endpoint, although this finding has a caveat that the ELISA assay was based on commercially available human Hex, and thus it is possible that it failed to detect antibodies to NHP specific epitopes.

Despite having low or absent neutralizing antibodies to AAVrh8 (titer <1:10) prior to injection, all NHPs injected with AAVrh8 vectors had high anti-capsid antibody titers at the endpoint. However, a humoral response to the capsid is unlikely to have a significant contribution to the neuronal loss as control NHPs injected with the transgene-empty AAVrh8 vector showed no evidence of neuropathology beyond that associated with the needle track. Moreover,

previous studies have reported the presence of high anti-AAV antibody titers after intracranial delivery in NHPs with no apparent adverse effects.^{156, 157} Therefore, this study highlights the safety of an AAV vector, but also uncovers the toxicity that can be associated with a biochemical mechanism, such as overexpression, that is not related to AAV vector or transgene immunogenicity.

Despite extensive neuronal loss, Hex activity in the thalamus of NHP injected with AAVrh8-cmHex α/β vector was >100 fold above normal. These high Hex expression levels appear to be driven by the remaining transduced neurons laden with eosinophilic granules filled with Hex as indicated by co-immunofluorescence staining with antibodies to Hex α - and β -subunits. Neurons with identical intracellular features were also found in the thalamus of long-lived cats treated with AAVrh8 vectors encoding feline Hex subunits, but with no evidence of neuronal loss or neurological deficits.¹⁴ Transgenic mice overexpressing lysosomal beta-glucuronidase (GUSB) also displayed eosinophilic granules in different cell types, and brain expression levels were ~100-700 fold above normal with no apparent neurological deficits. This indicates that massive overexpression of at least GUSB in neurons is well tolerated.¹⁷⁴ However, there are fundamental differences between transgenesis and AAV mediated *de novo* overexpression, namely developmental adaptation of cellular pathways to high-level expression of a lysosomal enzyme. Also, tissue level activity in transgenic mice is likely the result of relatively uniform enzyme activity in most cells in the tissue. On the other hand, the efficiency of AAV gene delivery

to the brain by intraparenchymal injection is far from achieving transduction of all cells in a particular structure and thus the measured activities are the result of enzyme expression in a subset of cells. The >100 fold above normal HexA levels in the thalamus of AAVrh8 injected NHPs at endpoint appeared to be produced by a relatively small number of neurons, and thus it is likely that activities in those cells are considerably higher than the average measured in tissue punches but are still compatible with survival. It seems reasonable to postulate that HexA expression crossed an unknown threshold in some cells that triggered a neurodegenerative process. A possible mechanism is that continuous high-level expression of HexA overtaxes the protein folding capacity in some AAV transduced neurons leading to a chronic unfolded protein response that ultimately results in cell death.¹⁷⁵ It has been demonstrated in other fields that vector mediated over expression of RNAi, with the use of strong promoters such as U6, leads to cellular toxicity due to saturation of the miRNA pathway.¹⁷⁶ The exact limit of overexpression tolerated by neurons is unknown, but the notion that lysosomal enzymes can be expressed at any level with no consequences to genetically modified cells should be reconsidered, although we are unable to exclude the possibility that these adverse events are HexA specific. An example of overexpression-associated toxicity of a lysosomal enzyme in a particular target cell type is that described for *ex vivo* lentivirus gene therapy in Krabbe disease where galactocerebrosidase proved to be toxic to hematopoietic stem cells but not to their progeny.¹⁷⁷ This has not been documented for other lysosomal

enzymes where this *ex vivo* strategy has been successful for storage diseases such as metachromatic leukodystrophy.^{53, 54} A recent study using systemic delivery of AAV9 encoding another lysosomal enzyme, α -N-acetylglucosaminidase, to treat mucopolysaccharidosis (MPS) IIIB resulted in liver toxicity associated with transgene overexpression in wild type but not MPS IIIB mice.¹⁷⁸ Presently, we are unable to exclude the possibility that toxicity is the result of unique properties of cynomolgus macaque hexosaminidase subunits. However, we have also seen similar histopathology and Hex overexpression that was demonstrated in Chapter IV, when we inject nude mice with AAVrh8 vectors that encode for the human transgene as well (data not shown). Further studies with hexosaminidases from different species will be necessary to address this possibility.

The reasons for the difference in outcomes between NHPs and normal cats injected with AAVrh8 vectors carrying the same expression elements at comparable doses are unknown. It is possible the CBA promoter and/or WPRE in the transgene expression cassette have different potencies across species, and also that AAVrh8 transduces NHP cells more efficiently given that it was cloned from rhesus macaque tissues.¹⁷⁹ Other AAV serotypes that efficiently transduce the CNS could also be explored. Alternatively, there could be species-specific thresholds of sensitivity for overexpression. The 3×10^{12} vg dose tested in NHP was based on a prior study¹⁵³ where GM2 cats were treated with 1.1×10^{12} vg of AAVrh8 vector delivered bilaterally to the thalamus and CSF via the lateral

ventricle. The dose/brain weight is comparable at 5.3×10^{13} vg/kg considering average brain weights of 60.4 ± 5.5 g and 20.9 ± 1.6 g in young cynomolgus macaques and cats, respectively. An important aspect to consider is that the thalamic dose in cats was delivered in a columnar fashion where the needle was raised 0.15 cm after each 10-20 μ L bolus, while in NHP we used convection enhanced delivery in a single site in the thalamus. The two infusion techniques likely generate different patterns of AAV vector distribution in the thalamus and possibly transduction efficiency that might be reflected in differences in AAV genome copy number per cell. Nonetheless a 30-fold reduction in AAV vector dose in NHP was insufficient to prevent toxicity in NHP. This suggests that differences in infusion technique and ultimately AAV distribution in thalamus are unlikely to explain the surprising difference in outcomes in monkeys and cats. The degree of neuronal loss documented in monkeys prevents a meaningful comparison of AAV vector genome content in the thalamus between the two species and others, as it is impossible to know how much of the initial dose has been lost in monkeys due to toxicity. Presently there is no information on the degree of enzyme overexpression in individual AAV transduced cells (neurons) in the brain that is compatible with long-term safety and efficacy. The difference in safety outcomes across and within species raises concerns about the predictive value of pre-clinical dose ranging and safety studies when translating AAV gene therapies from animals to humans.

Prior studies assessing the safety of multisite intracranial delivery of AAVrh10 vectors in NHPs reported no serious adverse events.^{157, 180} However, neuropathological examination revealed neuronal loss at the injection sites, but because the studies were carried out with AAVrh10 vectors encoding human enzymes, it is not possible to distinguish between an immunologically driven effect and toxicity due to overexpression as documented here. The absence of neurological side effects in those studies may simply be due to the small injection volumes per site (10 μ L) in non-motor cortical regions where the effect of neuronal loss in small numbers may not be easily detectable. It is also possible that thalamic neurons, or a subdivision of the thalamus, may be more sensitive. The mechanistic basis for the neuronal loss/spongiosis observed in those studies has different implications for the success in translation of these multisite approaches to patients. Clinical trials have been initiated with AAVrh10 vectors tested in NHPs and the outcomes in patients will ultimately reveal the safety and efficacy of the multisite delivery approach (NCT01801709). If successful, this multisite approach may be a better strategy to treat GM2 gangliosidosis as well. It could also be a strategy to overcome a decrease in vector load or lower expression levels in humans while still maintaining widespread distribution of enzyme. However, this superficial multisite approach may not treat deep brain structures, such as the thalamus, which in GM2 gangliosidosis patients are compromised as indicated by alterations in both CT and MRI (T1 and T2 weighted) imaging.^{181, 182} Aside from the safety differences among species as

demonstrated here, the differences in brain sizes and CSF flow from mice to cats, to primates, and to humans may all play a role in vector and enzyme distribution and subsequent expression levels.^{168, 183} We assume that the brain of a child less than 1 year of age will weigh approximately 500 g.¹⁶⁸ A comparable infusion volume will require the infusion of approximately 3 mL in each thalamus. However, we think such volumes would be an unacceptable risk to the patients and would require a delivery time of greater than 13 hours, assuming a delivery rate of 2 μ L/min and 3.2 mL in the thalamus distributed over 2 sites (1.6 mL/site). Therefore, we may initially have to limit infusion volumes in patients and develop strategies to safely increase infusion rates.

Since dose reduction was not enough to overcome this toxicity other strategies to reduce Hex expression while maintaining AAV vector dose, and therefore vector and enzyme distribution was employed. Six new AAVrh8 vector designs were created by the removal and/or replacement of promoters and other transcriptional elements, which achieved the predicted gradient of Hex expression. A vector screen in mice revealed three new formulations with reduced enzyme expression and low toxicity compared to our original vector. Testing of AAVrh8-CBA-cmHex α/β , AAVrh8-CB-CI-cmHex α/β , and AAVrh8-P2-CI-cmHex α/β in primates revealed AAVrh8-CBA-cmHex α/β to have the highest Hex expression, but showed toxicity in 1 out of 4 injection sites. It is possible that the exact placement of the cannula in the brain parenchyma could impact viral vector distribution and therefore transduction efficiency, affecting expression

levels which then leads to toxicity. AAVrh8-CB-CI-cmHexa/β and AAVrh8-P2-CI-cmHexa/β had similar expression levels of Hex to each other and showed minimal toxicity. Since vector elements of AAVrh8-CB-CI-cmHexa/β are most similar to original formulation and are widely used in the field, we believe it will be the best candidate to move forward to the clinic. In comparison to our original formulation, AAVrh8-CB-CI-cmHexa/β does not contain the CMV enhancer or the WPRE^{mut6ΔATG} element. Reduction of expression through alterations of vector design does have negative consequences on therapeutic efficacy when delivered at similar doses to our original vector in Sandhoff disease mice. We were able to successfully treat the cerebrum comparably to our original vector by increasing vector dose 2-5 fold. However, treating other areas of the CNS as well as with our original vector, particularly in the spinal cord, requires large increases in the vector dose and volumes delivered to the lateral ventricle. It may be possible to test alternative routes of vector delivery to treat the spinal cord such as cisterna magna or intrathecal delivery, which has proven successful in other lysosomal storage and CNS disorders.⁹³

Overexpression and secretion of lysosomal enzymes from genetically modified cells is the fundamental tenet of the current *ex vivo* and *in vivo* gene therapy approaches for lysosomal storage diseases. Though the exact tolerability limits for lysosomal enzyme overexpression in neurons is unknown and may vary across enzymes, the notion that these proteins can be safely expressed at any level with no consequences should be evaluated carefully.

Future Directions

Now that we have shown safety and efficacy with our newly optimized AAVrh8-Hex α/β vectors, formal IND-enabling studies for safety and efficacy will need to be performed in Sandhoff mice along with a formal IND-enabling toxicity study in primates in order to move this therapy forward to clinical trials. These studies will be done using doses flanking and including our newly defined minimum effective dose (3.51×10^{10} vg in mice, 4.56×10^{12} in monkeys, and 7.02×10^{13} vg in humans). A concern with translating this therapy to the clinic will be the possibility of a patient's immune response to the AAV capsid and transgene product. Ideally patients chosen for the trial will not have preexisting antibodies towards AAVrh8. In addition, the initial patients enrolled in the study will ideally be those with juvenile form of TSD or SD since these patients will have some endogenous Hex expression, albeit a mutated form. Clinical trials using AAV8 to treat Hemophilia B (NCT00979238) have shown a short course of glucocorticoids can limit immune response to the capsid allowing for long-term transgene expression.¹⁸⁴

Monkey	1	MASSRLWFSLLLAAAFAGRATALWPPQN	I	QTS	QRYVLYPNNFQFQYD	I	SSAAQPGCSV	60																																																		
Human		MTSSRLWFSLLLAAAFAGRATALWPPQN	F	QTS	QRYVLYPNNFQFQYD	V	SSAAQPGCSV																																																			
Monkey	61	LDEAFQRYRDLLFGSGSWPRPYR	I	TGKRHT	I	EKNVLVSVVTPGCNQLPTLESVENYTLTI	120																																																			
Human		LDEAFQRYRDLLFGSGSWPRPYL	T	TGKRHT	L	EKNVLVSVVTPGCNQLPTLESVENYTLTI																																																				
Monkey	121	NDDQCLLSETVWGALRGLETFSQLVWKS	AEGTFF	INKTE	IEDFPRFPHRGLLLDTSRHY	180																																																				
Human		NDDQCLLSETVWGALRGLETFSQLVWKS	AEGTFF	INKTE	IEDFPRFPHRGLLLDTSRHY																																																					
Monkey	181	LPLSSILDTLDMAYNKLNVFHWHLVDDP	SFPY	SFTFPELMRKG	SYNPVTHIYTAQDVK	240																																																				
Human		LPLSSILDTLDMAYNKLNVFHWHLVDDP	SFPY	SFTFPELMRKG	SYNPVTHIYTAQDVK																																																					
Monkey	241	EVIEYARLRGIRVLAEFDTPGH	TLSW	GGPIGLLTPCYSG	SEPSGTFGPVNPSLNNTYEF	300																																																				
Human		EVIEYARLRGIRVLAEFDTPGH	TLSW	GGPIGLLTPCYSG	SEPSGTFGPVNPSLNNTYEF																																																					
Monkey	301	MSTFFLE	I	SSVFPDFYLHLGG	DEVDFTCWKS	N	P	I	QDFMRKKGFGEDFKQLESFYIQTLL	360																																																
Human		MSTFFLE	V	SSVFPDFYLHLGG	DEVDFTCWKS	N	P	I	QDFMRKKGFGEDFKQLESFYIQTLL																																																	
Monkey	361	DIVSSYGKGYVVWQEVFDNKVKI	R	PD	T	I	QVWRE	I	P	V	N	M	K	E	L	E	L	V	T	K	A	G	F	R	A	L	L	S	A	P	W	420																										
Human		DIVSSYGKGYVVWQEVFDNKVKI	Q	PD	T	I	QVWRE	I	P	V	N	M	K	E	L	E	L	V	T	K	A	G	F	R	A	L	L	S	A	P	W																											
Monkey	421	YLNRI	S	Y	G	P	D	W	K	D	F	Y	I	V	E	P	L	A	F	E	G	T	P	E	Q	K	A	L	V	I	G	G	E	A	C	M	W	G	E	Y	V	D	N	T	N	L	V	P	R	L	W	P	R	A	G	A	V	480
Human		YLNRI	S	Y	G	P	D	W	K	D	F	Y	I	V	E	P	L	A	F	E	G	T	P	E	Q	K	A	L	V	I	G	G	E	A	C	M	W	G	E	Y	V	D	N	T	N	L	V	P	R	L	W	P	R	A	G	A	V	
Monkey	481	AERLWSNKL	T	S	D	L	T	F	A	Y	E	R	L	S	H	F	R	C	E	L	L	R	R	G	V	Q	A	Q	P	L	H	V	G	Y	C	E	Q	E	F	E	Q	T	529															
Human		AERLWSNKL	T	S	D	L	T	F	A	Y	E	R	L	S	H	F	R	C	E	L	L	R	R	G	V	Q	A	Q	P	L	N	V	G	F	C	E	Q	E	F	E	Q	T																

Figure 5.1 β -N-acetylhexosaminidase α -subunit amino acid sequences. Amino acid sequence alignment of monkey (cynomolgus macaque) and human. Differences highlighted in yellow.

Monkey	1	MELCGLGLPRPPMLLALLLATLLAAMLALLTQVALVVQVAEAT	R	A	P	G	V	S	A	A	R	G	P	A	L	W	P	L	P	60																																						
Human		MELCGLGLPRPPMLLALLLATLLAAMLALLTQVALVVQVAEAA	R	A	P	S	V	S	A	K	P	G	P	A	L	W	P	L	P																																							
Monkey	61	LSVKMTPNLLHLAPENFYISHSPNSTAGP	S	C	T	L	L	E	E	A	F	R	R	Y	H	S	I	F	G	F	Y	K	W	D	H	E	P	A	K	S	Q	A	120																									
Human		LSVKMTPNLLHLAPENFYISHSPNSTAGP	S	C	T	L	L	E	E	A	F	R	R	Y	H	G	Y	I	F	G	F	Y	K	W	H	E	P	A	E	F	Q	A																										
Monkey	121	TAQL	Q	Q	L	L	V	S	I	T	L	Q	S	E	C	D	A	F	P	N	I	S	S	D	E	S	Y	T	L	L	V	K	E	P	V	A	L	K	A	N	R	V	W	G	A	L	R	G	L	E	T	F	S	Q	L	V	180	
Human		KTQV	Q	Q	L	L	V	S	I	T	L	Q	S	E	C	D	A	F	P	N	I	S	S	D	E	S	Y	T	L	L	V	K	E	P	V	A	L	K	A	N	R	V	W	G	A	L	R	G	L	E	T	F	S	Q	L	V		
Monkey	181	QDSC	G	T	F	T	I	N	E	S	T	I	I	D	S	P	R	F	H	R	G	I	L	I	D	T	S	R	H	L	P	V	K	I	I	L	K	T	L	D	A	M	A	F	N	K	F	N	V	L	H	W	H	I	V	D	240	
Human		QDSY	G	T	F	T	I	N	E	S	T	I	I	D	S	P	R	F	S	H	R	G	I	L	I	D	T	S	R	H	L	P	V	K	I	I	L	K	T	L	D	A	M	A	F	N	K	F	N	V	L	H	W	H	I	V	D	
Monkey	241	DQSF	P	Y	Q	S	I	A	F	P	E	L	S	N	K	G	S	Y	S	L	S	H	V	T	P	N	D	V	R	M	V	I	E	Y	A	R	L	R	G	I	R	V	L	P	E	F	D	T	P	G	H	T	L	S	W	G	K	300
Human		DQSF	P	Y	Q	S	I	T	F	P	E	L	S	N	K	G	S	Y	S	L	S	H	V	T	P	N	D	V	R	M	V	I	E	Y	A	R	L	R	G	I	R	V	L	P	E	F	D	T	P	G	H	T	L	S	W	G	K	
Monkey	301	GQKDL	L	T	P	C	Y	S	R	Q	N	K	L	D	S	F	G	P	I	N	P	T	L	N	T	T	Y	S	F	L	T	T	F	F	K	E	I	S	E	V	F	P	D	Q	F	I	H	L	G	G	D	E	V	E	F	K	C	360
Human		GQKDL	L	T	P	C	Y	S	R	Q	N	K	L	D	S	F	G	P	I	N	P	T	L	N	T	T	Y	S	F	L	T	T	F	F	K	E	I	S	E	V	F	P	D	Q	F	I	H	L	G	G	D	E	V	E	F	K	C	
Monkey	361	WESNPKIQDFMKQKGF	K	D	F	K	K	L	E	S	F	Y	I	Q	K	V	L	D	I	I	A	T	I	N	K	G	S	I	V	W	Q	E	V	F	D	D	K	V	K	L	A	P	G	T	I	420												
Human		WESNPKIQDFMRQKGF	T	D	F	K	K	L	E	S	F	Y	I	Q	K	V	L	D	I	I	A	T	I	N	K	G	S	I	V	W	Q	E	V	F	D	D	K	A	K	L	A	P	G	T	I													
Monkey	421	VEVW	K	D	N	A	Y	P	E	E	L	S	K	V	T	A	S	G	F	P	V	I	L	S	A	P	W	Y	L	D	L	I	S	Y	Q	D	W	R	K	Y	K	V	E	P	L	D	F	G	G	T	R	E	Q	K	Q	L	480	
Human		VEVW	K	D	S	A	Y	P	E	E	L	S	R	V	T	A	S	G	F	P	V	I	L	S	A	P	W	Y	L	D	L	I	S	Y	Q	D	W	R	K	Y	K	V	E	P	L	D	F	G	G	T	Q	K	Q	L				
Monkey	481	FIGGE	A	C	L	W	G	E	Y	V	D	A	T	N	L	T	P	R	L	W	P	R	A	S	A	V	G	E	R	L	W	S	K	D	V	R	D	M	D	G	A	Y	D	R	L	T	R	H	R	C	R	M	V	E	R	G	540	
Human		FIGGE	A	C	L	W	G	E	Y	V	D	A	T	N	L	T	P	R	L	W	P	R	A	S	A	V	G	E	R	L	W	S	K	D	V	R	D	M	D	D	A	Y	D	R	L	T	R	H	R	C	R	M	V	E	R	G		
Monkey	541	IAAQ	P	L	Y	A	G	Y	C	N	H	E	N	V	556																																											
Human		IAAQ	P	L	Y	A	G	Y	C	N	H	E	N	M																																												

Figure 5.2 β -N-acetylhexosaminidase β -subunit amino acid sequences. Amino acid sequence alignment of monkey (cynomolgus macaque) and human. Differences highlighted in yellow.

APPENDIX A SEQUENCES OF PROMOTERS AND OTHER TRANSCRIPTIONAL ELEMENTS

Sequence of CMV enhancer (CMVEn):

```

1 CTGAATTCGG TACCCTAGTT ATTAATAGTA ATCAATTACG GGGTCATTAG TTCATAGCCC
61 ATATATGGAG TTCCGCGTTA CATAACTTAC GGTAATGGC CCGCCTGGCT GACCGCCCAA
121 CGACCCCGC CCATGACGT CAATAATGAC GTATGTTCC ATAGTAACGC CAATAGGGAC
181 TTTCCATTGA CGTCAATGGG TGGACTATTT ACGGTAAACT GCCCACTTGG CAGTACATCA
241 AGTGTATCAT ATGCCAAGTA CGCCCCCTAT TGACGTCAAT GACGGTAAAT GGCCCGCTG
301 GCATTATGCC CAGTACATGA CCTTATGGGA CTTTCCTACT TGGCAGTACA TCTACGTATT
361 AGTCATCGCT ATTAC

```

Sequence of CB promoter:

```

1 CATGGTCGAG GTGAGCCCA CGTTCTGCTT CACTCTCCC ATCTCCCCC CCTCCCCACC
61 CCAATTTTG TATTTATTTA TTTTTAATT ATTTTGTGCA GCGATGGGG CGGGGGGGG
121 GGGGGGGCG GCGCAGGCG GGGCGGGCG GGGCGAGGG CGGGCGGGG CGAGGCGGAG
181 AGGTGCGCG GCAGCCAATC AGAGCGGCG GCTCCGAAAG TTTCTTTTA TGGCGAGCG
241 GCGGCGGCG CGGCCCTATA AAAAGCGAAG CGCGCGGCG GCG

```

Sequence of chimeric intron (CI):

```

1 GTGAGCGGC GGGACGCC TTTCTCTCCG GGCTGTAAT AGCGCTTGGT TTAATGACGG
61 CTTGTTTTCTT TTCTGTGGCT GCGTGAAAGC CTTGAGGGGC TCCGGGAGCT AGAGCCTCTG
121 CTAACCATGT TCATGCCTT TTTCTTTTCC TACAGCTCCT GGGCAACGTG CTGGTTATTG
181 TGCTGTCTCA TCATTTTGGC AAAGAATTCC TCGAAGATCC GAAGGGGTTT AGGAGTCGT
241 GCGACGCTGC CTTGCCCCG TGCCCCGCTC CGCCGCGCC TCGCGCCGCC CGCCCCGGT
301 CTGACTGACC GCGTTACTCC CACAG

```

Sequence of modified WPRE:

```

1 GATAATCAAC CTCTGGATTA CAAAATTGT GAAAGATTGA CTGGTATTCT TAACTTTGTT
61 GCTCCTTTTA CGCTTTGTGG ATACGCTGCT TTATTGCCTT TGTATCTTGC TATTGCTTCC
121 CGTTTGGCTT TCATTTTCTC CTCCTTGAT AAATCCTGGT TGCTGTCTCT TTTTGAGGAG
181 TTGTGGCCCG TTGTCAGGCA ACGTGGCGTG GTGTGCACTG TGTTTGCTGA CGCAACCC
241 ACTGGTTGGG GCATGCCCAC CACCTGTCAG CTCCTTTCCG GGACTTTCG TTTCCCTC
301 CCTATTGCCA CGGCGGAACT CATCGCCGCC TGCCTTGCCC GCTGCTGGAC AGGGGCTCGG
361 CTGTTGGGCA CTGACAATTC CGTGGTGTG TCGGGGAAAT CATGCTCCTT TCCTTGGCTG
421 CTCGCCTGTG TTGCCACCTG GATTCTGCGC GGGACGTCCT TCTGCTACGT CCCTTCGGCC
481 CTCAATCCAG CGGACCTTCC TTCCCGCGG CTGCTGCCGG CTCTGCCGCC TCTTCCGCGT
541 CTTCCCTTC GCCCTCAGAC GAGTCGGATC TCCCTTTGGG CCGCCTCCCC GCATCGGACT
601 AG

```

Sequence of P2 promoter:

```

1 CTGGAGCCGG TGTCAGGTTG CTCCGTAAC GGTGACGTGC ACGCGTGGG GGAGCCATCA
61 GCGAGGTTGC TATATAAGCA GAGCTCGTTT AGTGAACCGT CAGA

```

APPENDIX B HISTOPATHOLOGIC CHANGES SEEN IN SHORT TERM PRE-CLINICAL SAFETY FOR GENE THERAPY FOR TAY-SACHS AND SANDHOFF DISEASE

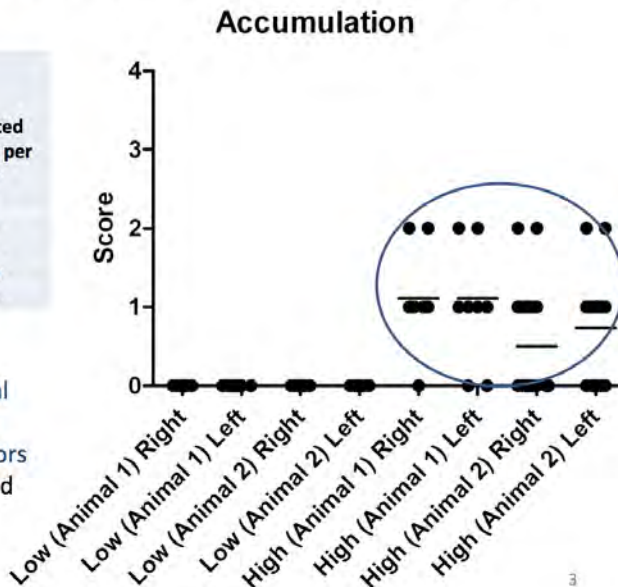
Keiko Petrosky
 October 30, 2014
 Division of Comparative Pathology New England Primate Research Center
 Harvard Medical School Southborough, MA

Serial sections (150 microns apart) were taken of the right and left thalamus of animals in high expressors (Cohort 1, n = 2) and low expressors (Cohort 3, n = 2) for analysis. Unfortunately, embedding and cutting of cohort 2 resulted in poor quality sections and could not be used for quantitative analysis. However, qualitative analysis of cohort 2 and cohort 3 indicate similar levels of histopathological changes.

Neuronal changes in high-expressors (Cohort 1) v. low-expressors (Cohort 3)

Accumulation Score		
Score	Description	# affected neurons per HPF
0	None	0
1	Minimal	1-2
2	Mild	3-5
3	Moderate	6-10
4	Severe	10+

- Accumulation of intraneuronal intracytoplasmic eosinophilic material seen in high-expressors
- Distribution similar in right and left thalamus



BIBLIOGRAPHY

1. Golebiowski D, Bradbury A, Kwon C-S et al. Aav Gene Therapy Strategies for Lysosomal Storage Disorders with Central Nervous System Involvement [Http://Dx.Doi.Org/10.1007/978-1-4939-2306-9_11](http://dx.doi.org/10.1007/978-1-4939-2306-9_11). In: Gene Delivery and Therapy for Neurological Disorders. X Bo and J Verhaagen, eds. (Springer New York). 2015; pp. 265-295.
2. Arfi A, Richard M, Scherman D. Innovative Therapeutic Approaches for Improving Patient Life Condition with a Neurological Lysosomal Disease. In: Latest Findings in Intellectual and Developmental Disabilities Research, Üner Tan (Ed). (InTech). 2012.
3. Suzuki K. Globoid Cell Leukodystrophy (Krabbe's Disease): Update. *J Child Neurol* 2003;18:595-603.
4. Sano R, Annunziata I, Patterson A et al. Gm1-Ganglioside Accumulation at the Mitochondria-Associated Er Membranes Links Er Stress to Ca(2+)-Dependent Mitochondrial Apoptosis. *Mol Cell* 2009;36:500-511.
5. Voccoli V, Tonazzini I, Signore G et al. Role of Extracellular Calcium and Mitochondrial Oxygen Species in Psychosine-Induced Oligodendrocyte Cell Death. *Cell Death Dis* 2014;5:e1529.
6. Fuller M, Meikle PJ, Hopwood JJ. Epidemiology of Lysosomal Storage Diseases: An Overview. In: Fabry Disease: Perspectives from 5 Years of Fos. A Mehta, M Beck and G Sunder-Plassmann, eds. (Oxford). 2006.
7. Mahuran DJ. Biochemical Consequences of Mutations Causing the Gm2 Gangliosidosis. *Biochim Biophys Acta* 1999;1455:105-138.
8. Carstea ED, Morris JA, Coleman KG et al. Niemann-Pick C1 Disease Gene: Homology to Mediators of Cholesterol Homeostasis. *Science* 1997;277:228-231.
9. Meikle PJ, Hopwood JJ, Clague AE et al. Prevalence of Lysosomal Storage Disorders. *JAMA* 1999;281:249-254.
10. Byrne BJ, Falk DJ, Pacak CA et al. Pompe Disease Gene Therapy. *Hum Mol Genet* 2011;20:R61-68.
11. Rozenberg R, Pereira Lda V. The Frequency of Tay-Sachs Disease Causing Mutations in the Brazilian Jewish Population Justifies a Carrier Screening Program. *Sao Paulo Med J* 2001;119:146-149.
12. Roy A Gravel MMK, Richard L Proia, Konrad Sandhoff, Kinuko Suzuki, and Kunihiko Suzuki. The Gm2 Gangliosidosis. In: *The Metabolic and Molecular Bases of Inherited Disease*. (McGraw-Hill Companies, Inc.). 2001.
13. Sango K, Yamanaka S, Hoffmann A et al. Mouse Models of Tay-Sachs and Sandhoff Diseases Differ in Neurologic Phenotype and Ganglioside Metabolism. *Nat Genet* 1995;11:170-176.
14. Bradbury AM, Cochran JN, McCurdy VJ et al. Therapeutic Response in Feline Sandhoff Disease Despite Immunity to Intracranial Gene Therapy. *Mol Ther* 2013;21:1306-1315.

15. Cachon-Gonzalez MB, Wang SZ, McNair R et al. Gene Transfer Corrects Acute Gm2 Gangliosidosis--Potential Therapeutic Contribution of Perivascular Enzyme Flow. *Mol Ther* 2012;20:1489-1500.
16. Pellegrini M, Zicari E, Dotti MT et al. Dysautonomic Achalasia in Two Siblings with Sandhoff Disease. *J Neurol Sci* 2006;241:107-109.
17. Bley AE, Giannikopoulos OA, Hayden D et al. Natural History of Infantile G(M2) Gangliosidosis. *Pediatrics* 2011;128:e1233-1241.
18. Phaneuf D, Wakamatsu N, Huang JQ et al. Dramatically Different Phenotypes in Mouse Models of Human Tay-Sachs and Sandhoff Diseases. *Hum Mol Genet* 1996;5:1-14.
19. Cork LC, Munnell JF, Lorenz MD et al. Gm2 Ganglioside Lysosomal Storage Disease in Cats with Beta-Hexosaminidase Deficiency. *Science* 1977;196:1014-1017.
20. Porter BF, Lewis BC, Edwards JF et al. Pathology of Gm2 Gangliosidosis in Jacob Sheep. *Vet Pathol* 2011;48:807-813.
21. Torres PA, Zeng BJ, Porter BF et al. Tay-Sachs Disease in Jacob Sheep. *Mol Genet Metab* 2010;101:357-363.
22. Baker HJ, Reynolds GD, Walkley SU et al. The Gangliosidoses: Comparative Features and Research Applications. *Vet Pathol* 1979;16:635-649.
23. Martin DR, Krum BK, Varadarajan GS et al. An Inversion of 25 Base Pairs Causes Feline Gm2 Gangliosidosis Variant. *Exp Neurol* 2004;187:30-37.
24. Rattazzi MC, Appel AM, Baker HJ. Enzyme Replacement in Feline Gm2 Gangliosidosis: Catabolic Effects of Human Beta-Hexosaminidase A. *Prog Clin Biol Res* 1982;94:213-220.
25. Walkley SU, Baker HJ, Rattazzi MC. Initiation and Growth of Ectopic Neurites and Meganeurites During Postnatal Cortical Development in Ganglioside Storage Disease. *Brain Res Dev Brain Res* 1990;51:167-178.
26. Walkley SU, Baker HJ, Rattazzi MC et al. Neuroaxonal Dystrophy in Neuronal Storage Disorders: Evidence for Major Gabaergic Neuron Involvement. *J Neurol Sci* 1991;104:1-8.
27. Walkley SU, Wurzelmann S, Rattazzi MC et al. Distribution of Ectopic Neurite Growth and Other Geometrical Distortions of Cns Neurons in Feline Gm2 Gangliosidosis. *Brain Res* 1990;510:63-73.
28. Wood PA, McBride MR, Baker HJ et al. Fluorescence Polarization Analysis, Lipid Composition, and Na⁺, K⁺-Atpase Kinetics of Synaptosomal Membranes in Feline Gm1 and Gm2 Gangliosidosis. *J Neurochem* 1985;44:947-956.
29. Ioannou YA, Bishop DF, Desnick RJ. Overexpression of Human Alpha-Galactosidase a Results in Its Intracellular Aggregation, Crystallization in Lysosomes, and Selective Secretion. *J Cell Biol* 1992;119:1137-1150.
30. Neufeld EF. Enzyme Replacement Therapy - a Brief History. In: Fabry Disease: Perspectives from 5 Years of Fos. A Mehta, M Beck and G Sunder-Plassmann, eds. (Oxford). 2006.

31. Sands MS, Davidson BL. Gene Therapy for Lysosomal Storage Diseases. *Mol Ther* 2006;13:839-849.
32. Desnick RJ, Schuchman EH. Enzyme Replacement Therapy for Lysosomal Diseases: Lessons from 20 Years of Experience and Remaining Challenges. *Annu Rev Genomics Hum Genet* 2012;13:307-335.
33. Enns GM, Huhn SL. Central Nervous System Therapy for Lysosomal Storage Disorders. *Neurosurg Focus* 2008;24:E12.
34. Johnson WG, Desnick RJ, Long DM et al. Intravenous Injection of Purified Hexosaminidase a into a Patient with Tay-Sachs Disease. *Birth Defects Orig Artic Ser* 1973;9:120-124.
35. Auclair D, Finnie J, Walkley SU et al. Intrathecal Recombinant Human 4-Sulfatase Reduces Accumulation of Glycosaminoglycans in Dura of Mucopolysaccharidosis Vi Cats. *Pediatr Res* 2012;71:39-45.
36. Cabrera-Salazar MA, Bercury SD, Ziegler RJ et al. Intracerebroventricular Delivery of Glucocerebrosidase Reduces Substrates and Increases Lifespan in a Mouse Model of Neuronopathic Gaucher Disease. *Exp Neurol* 2010;225:436-444.
37. Chang M, Cooper JD, Sleat DE et al. Intraventricular Enzyme Replacement Improves Disease Phenotypes in a Mouse Model of Late Infantile Neuronal Ceroid Lipofuscinosis. *Mol Ther* 2008;16:649-656.
38. Dickson P, McEntee M, Vogler C et al. Intrathecal Enzyme Replacement Therapy: Successful Treatment of Brain Disease Via the Cerebrospinal Fluid. *Mol Genet Metab* 2007;91:61-68.
39. Dodge JC, Clarke J, Treleaven CM et al. Intracerebroventricular Infusion of Acid Sphingomyelinase Corrects Cns Manifestations in a Mouse Model of Niemann-Pick a Disease. *Exp Neurol* 2009;215:349-357.
40. Hemsley KM, Norman EJ, Crawley AC et al. Effect of Cisternal Sulfamidase Delivery in Mps liia Huntaway Dogs--a Proof of Principle Study. *Mol Genet Metab* 2009;98:383-392.
41. Lee WC, Tsoi YK, Troendle FJ et al. Single-Dose Intracerebroventricular Administration of Galactocerebrosidase Improves Survival in a Mouse Model of Globoid Cell Leukodystrophy. *FASEB J* 2007;21:2520-2527.
42. Ziegler RJ, Salegio EA, Dodge JC et al. Distribution of Acid Sphingomyelinase in Rodent and Non-Human Primate Brain after Intracerebroventricular Infusion. *Exp Neurol* 2011;231:261-271.
43. Mader KM, Beard H, King BM et al. Effect of High Dose, Repeated Intra-Cerebrospinal Fluid Injection of Sulphamidase on Neuropathology in Mucopolysaccharidosis Type liia Mice. *Genes Brain Behav* 2008;7:740-753.
44. Boado RJ, Zhang Y, Zhang Y et al. Genetic Engineering of a Lysosomal Enzyme Fusion Protein for Targeted Delivery across the Human Blood-Brain Barrier. *Biotechnol Bioeng* 2008;99:475-484.
45. Bockenhoff A, Cramer S, Wolte P et al. Comparison of Five Peptide Vectors for Improved Brain Delivery of the Lysosomal Enzyme Arylsulfatase A. *J Neurosci* 2014;34:3122-3129.

46. Grubb JH, Vogler C, Tan Y et al. Infused Fc-Tagged Beta-Glucuronidase Crosses the Placenta and Produces Clearance of Storage in Utero in Mucopolysaccharidosis Vii Mice. *Proc Natl Acad Sci U S A* 2008;105:8375-8380.
47. Meng Y, Sohar I, Sleat DE et al. Effective Intravenous Therapy for Neurodegenerative Disease with a Therapeutic Enzyme and a Peptide That Mediates Delivery to the Brain. *Mol Ther* 2014;22:547-553.
48. Osborn MJ, McElmurry RT, Peacock B et al. Targeting of the Cns in Mps-1h Using a Nonviral Transferrin-Alpha-L-Iduronidase Fusion Gene Product. *Mol Ther* 2008;16:1459-1466.
49. Papademetriou J, Garnacho C, Serrano D et al. Comparative Binding, Endocytosis, and Biodistribution of Antibodies and Antibody-Coated Carriers for Targeted Delivery of Lysosomal Enzymes to Icam-1 Versus Transferrin Receptor. *J Inherit Metab Dis* 2013;36:467-477.
50. Spencer BJ, Verma IM. Targeted Delivery of Proteins across the Blood-Brain Barrier. *Proc Natl Acad Sci U S A* 2007;104:7594-7599.
51. Biffi A. Gene Therapy for Lysosomal Storage Disorders: A Good Start. *Hum Mol Genet* 2016;25:R65-75.
52. Doerr J, Bockenhoff A, Ewald B et al. Arylsulfatase a Overexpressing Human Ipsc-Derived Neural Cells Reduce Cns Sulfatide Storage in a Mouse Model of Metachromatic Leukodystrophy. *Mol Ther* 2015;23:1519-1531.
53. Biffi A, Montini E, Lorioli L et al. Lentiviral Hematopoietic Stem Cell Gene Therapy Benefits Metachromatic Leukodystrophy. *Science* 2013;341:1233158.
54. Sessa M, Lorioli L, Fumagalli F et al. Lentiviral Haemopoietic Stem-Cell Gene Therapy in Early-Onset Metachromatic Leukodystrophy: An Ad-Hoc Analysis of a Non-Randomised, Open-Label, Phase 1/2 Trial. *Lancet* 2016;388:476-487.
55. Bosch A, Perret E, Desmaris N et al. Reversal of Pathology in the Entire Brain of Mucopolysaccharidosis Type Vii Mice after Lentivirus-Mediated Gene Transfer. *Hum Gene Ther* 2000;11:1139-1150.
56. Consiglio A, Quattrini A, Martino S et al. In Vivo Gene Therapy of Metachromatic Leukodystrophy by Lentiviral Vectors: Correction of Neuropathology and Protection against Learning Impairments in Affected Mice. *Nat Med* 2001;7:310-316.
57. Brooks AI, Stein CS, Hughes SM et al. Functional Correction of Established Central Nervous System Deficits in an Animal Model of Lysosomal Storage Disease with Feline Immunodeficiency Virus-Based Vectors. *Proc Natl Acad Sci U S A* 2002;99:6216-6221.
58. Afione SA, Conrad CK, Flotte TR. Gene Therapy Vectors as Drug Delivery Systems. *Clin Pharmacokinet* 1995;28:181-189.
59. Nault JC, Datta S, Imbeaud S et al. Recurrent Aav2-Related Insertional Mutagenesis in Human Hepatocellular Carcinomas. *Nat Genet* 2015;47:1187-1193.
60. Berns KI, Byrne BJ, Flotte TR et al. Adeno-Associated Virus Type 2 and Hepatocellular Carcinoma? *Hum Gene Ther* 2015;26:779-781.

61. Hastie E, Samulski RJ. Adeno-Associated Virus at 50: A Golden Anniversary of Discovery, Research, and Gene Therapy Success--a Personal Perspective. *Hum Gene Ther* 2015;26:257-265.
62. Ciesielska A, Hadaczek P, Mittermeyer G et al. Cerebral Infusion of Aav9 Vector-Encoding Non-Self Proteins Can Elicit Cell-Mediated Immune Responses. *Mol Ther* 2013;21:158-166.
63. Franco LM, Sun B, Yang X et al. Evasion of Immune Responses to Introduced Human Acid Alpha-Glucosidase by Liver-Restricted Expression in Glycogen Storage Disease Type II. *Mol Ther* 2005;12:876-884.
64. Passini MA, Bu J, Fidler JA et al. Combination Brain and Systemic Injections of Aav Provide Maximal Functional and Survival Benefits in the Niemann-Pick Mouse. *Proc Natl Acad Sci U S A* 2007;104:9505-9510.
65. Ciron C, Desmaris N, Colle MA et al. Gene Therapy of the Brain in the Dog Model of Hurler's Syndrome. *Ann Neurol* 2006;60:204-213.
66. Colle MA, Piguet F, Bertrand L et al. Efficient Intracerebral Delivery of Aav5 Vector Encoding Human Arsa in Non-Human Primate. *Hum Mol Genet* 2010;19:147-158.
67. Murrey DA, Naughton BJ, Duncan FJ et al. Feasibility and Safety of Systemic Raav9-Hnaglu Delivery for Treating Mucopolysaccharidosis IIb: Toxicology, Biodistribution, and Immunological Assessments in Primates. *Hum Gene Ther Clin Dev* 2014;25:72-84.
68. Maguire CA, Ramirez SH, Merkel SF et al. Gene Therapy for the Nervous System: Challenges and New Strategies. *Neurotherapeutics* 2014;11:817-839.
69. Kugler S, Lingor P, Scholl U et al. Differential Transgene Expression in Brain Cells in Vivo and in Vitro from Aav-2 Vectors with Small Transcriptional Control Units. *Virology* 2003;311:89-95.
70. Lee Y, Messing A, Su M et al. Gfap Promoter Elements Required for Region-Specific and Astrocyte-Specific Expression. *Glia* 2008;56:481-493.
71. de Leeuw CN, Dyka FM, Boye SL et al. Targeted Cns Delivery Using Human Minipromoters and Demonstrated Compatibility with Adeno-Associated Viral Vectors. *Mol Ther Methods Clin Dev* 2014;1:5.
72. Flotte TR, Afione SA, Solow R et al. Expression of the Cystic Fibrosis Transmembrane Conductance Regulator from a Novel Adeno-Associated Virus Promoter. *J Biol Chem* 1993;268:3781-3790.
73. Haberman RP, McCown TJ, Samulski RJ. Novel Transcriptional Regulatory Signals in the Adeno-Associated Virus Terminal Repeat a/D Junction Element. *J Virol* 2000;74:8732-8739.
74. Loeb JE, Cordier WS, Harris ME et al. Enhanced Expression of Transgenes from Adeno-Associated Virus Vectors with the Woodchuck Hepatitis Virus Posttranscriptional Regulatory Element: Implications for Gene Therapy. *Hum Gene Ther* 1999;10:2295-2305.
75. Powell SK, Rivera-Soto R, Gray SJ. Viral Expression Cassette Elements to Enhance Transgene Target Specificity and Expression in Gene Therapy. *Discov Med* 2015;19:49-57.

76. Cearley CN, Wolfe JH. Transduction Characteristics of Adeno-Associated Virus Vectors Expressing Cap Serotypes 7, 8, 9, and Rh10 in the Mouse Brain. *Mol Ther* 2006;13:528-537.
77. Lawlor PA, Bland RJ, Mouravlev A et al. Efficient Gene Delivery and Selective Transduction of Glial Cells in the Mammalian Brain by Aav Serotypes Isolated from Nonhuman Primates. *Mol Ther* 2009;17:1692-1702.
78. Markakis EA, Vives KP, Bober J et al. Comparative Transduction Efficiency of Aav Vector Serotypes 1-6 in the Substantia Nigra and Striatum of the Primate Brain. *Mol Ther* 2010;18:588-593.
79. Daya S, Berns KI. Gene Therapy Using Adeno-Associated Virus Vectors. *Clin Microbiol Rev* 2008;21:583-593.
80. Burger C, Gorbatyuk OS, Velardo MJ et al. Recombinant Aav Viral Vectors Pseudotyped with Viral Capsids from Serotypes 1, 2, and 5 Display Differential Efficiency and Cell Tropism after Delivery to Different Regions of the Central Nervous System. *Mol Ther* 2004;10:302-317.
81. Cearley CN, Vandenberghe LH, Parente MK et al. Expanded Repertoire of Aav Vector Serotypes Mediate Unique Patterns of Transduction in Mouse Brain. *Mol Ther* 2008;16:1710-1718.
82. Foust KD, Nurre E, Montgomery CL et al. Intravascular Aav9 Preferentially Targets Neonatal Neurons and Adult Astrocytes. *Nat Biotechnol* 2009;27:59-65.
83. Gray SJ, Matagne V, Bachaboina L et al. Preclinical Differences of Intravascular Aav9 Delivery to Neurons and Glia: A Comparative Study of Adult Mice and Nonhuman Primates. *Mol Ther* 2011;19:1058-1069.
84. Klein RL, Dayton RD, Leidenheimer NJ et al. Efficient Neuronal Gene Transfer with Aav8 Leads to Neurotoxic Levels of Tau or Green Fluorescent Proteins. *Mol Ther* 2006;13:517-527.
85. Klein RL, Dayton RD, Tatom JB et al. Aav8, 9, Rh10, Rh43 Vector Gene Transfer in the Rat Brain: Effects of Serotype, Promoter and Purification Method. *Mol Ther* 2008;16:89-96.
86. Sondhi D, Hackett NR, Peterson DA et al. Enhanced Survival of the Linc1 Mouse Following Cln2 Gene Transfer Using the Rh.10 Rhesus Macaque-Derived Adeno-Associated Virus Vector. *Mol Ther* 2007;15:481-491.
87. Yang B, Li S, Wang H et al. Global Cns Transduction of Adult Mice by Intravenously Delivered Raavrh.8 and Raavrh.10 and Nonhuman Primates by Raavrh.10. *Mol Ther* 2014;22:1299-1309.
88. Zhang H, Yang B, Mu X et al. Several Raav Vectors Efficiently Cross the Blood-Brain Barrier and Transduce Neurons and Astrocytes in the Neonatal Mouse Central Nervous System. *Mol Ther* 2011;19:1440-1448.
89. Choudhury SR, Hudry E, Maguire CA et al. Viral Vectors for Therapy of Neurologic Diseases. *Neuropharmacology* 2016. Feb 21. pii: S0028-3908(16)30048-X. doi: 10.1016/j.neuropharm.2016.02.013. [Epub ahead of print]
90. Choudhury SR, Fitzpatrick Z, Harris AF et al. In Vivo Selection Yields Aav-B1 Capsid for Central Nervous System and Muscle Gene Therapy. *Mol Ther* 2016;24:1247-1257.

91. Choudhury SR, Harris AF, Cabral DJ et al. Widespread Central Nervous System Gene Transfer and Silencing after Systemic Delivery of Novel Aav-as Vector. *Mol Ther* 2016;24:726-735.
92. Deverman BE, Pravdo PL, Simpson BP et al. Cre-Dependent Selection Yields Aav Variants for Widespread Gene Transfer to the Adult Brain. *Nat Biotechnol* 2016;34:204-209.
93. Hocquemiller M, Giersch L, Audrain M et al. Adeno-Associated Virus-Based Gene Therapy for Cns Diseases. *Hum Gene Ther* 2016;27:478-496.
94. Masat E, Pavani G, Mingozzi F. Humoral Immunity to Aav Vectors in Gene Therapy: Challenges and Potential Solutions. *Discov Med* 2013;15:379-389.
95. Leinekugel P, Michel S, Conzelmann E et al. Quantitative Correlation between the Residual Activity of Beta-Hexosaminidase a and Arylsulfatase a and the Severity of the Resulting Lysosomal Storage Disease. *Hum Genet* 1992;88:513-523.
96. Broekman ML, Tierney LA, Benn C et al. Mechanisms of Distribution of Mouse Beta-Galactosidase in the Adult Gm1-Gangliosidosis Brain. *Gene Ther* 2009;16:303-308.
97. Griffey M, Macauley SL, Ogilvie JM et al. Aav2-Mediated Ocular Gene Therapy for Infantile Neuronal Ceroid Lipofuscinosis. *Mol Ther* 2005;12:413-421.
98. Hennig AK, Levy B, Ogilvie JM et al. Intravitreal Gene Therapy Reduces Lysosomal Storage in Specific Areas of the Cns in Mucopolysaccharidosis Vii Mice. *J Neurosci* 2003;23:3302-3307.
99. Hennig AK, Ogilvie JM, Ohlemiller KK et al. Aav-Mediated Intravitreal Gene Therapy Reduces Lysosomal Storage in the Retinal Pigmented Epithelium and Improves Retinal Function in Adult Mps Vii Mice. *Mol Ther* 2004;10:106-116.
100. Luca T, Givogri MI, Perani L et al. Axons Mediate the Distribution of Arylsulfatase a within the Mouse Hippocampus Upon Gene Delivery. *Mol Ther* 2005;12:669-679.
101. Passini MA, Lee EB, Heuer GG et al. Distribution of a Lysosomal Enzyme in the Adult Brain by Axonal Transport and by Cells of the Rostral Migratory Stream. *J Neurosci* 2002;22:6437-6446.
102. Liu G, Martins I, Wemmie JA et al. Functional Correction of Cns Phenotypes in a Lysosomal Storage Disease Model Using Adeno-Associated Virus Type 4 Vectors. *J Neurosci* 2005;25:9321-9327.
103. Cearley CN, Wolfe JH. A Single Injection of an Adeno-Associated Virus Vector into Nuclei with Divergent Connections Results in Widespread Vector Distribution in the Brain and Global Correction of a Neurogenetic Disease. *J Neurosci* 2007;27:9928-9940.
104. Salegio EA, Samaranch L, Kells AP et al. Axonal Transport of Adeno-Associated Viral Vectors Is Serotype-Dependent. *Gene Ther* 2013;20:348-352.
105. Bosch A, Perret E, Desmaris N et al. Long-Term and Significant Correction of Brain Lesions in Adult Mucopolysaccharidosis Type Vii Mice Using Recombinant Aav Vectors. *Mol Ther* 2000;1:63-70.

106. Cachon-Gonzalez MB, Wang SZ, Lynch A et al. Effective Gene Therapy in an Authentic Model of Tay-Sachs-Related Diseases. *Proc Natl Acad Sci U S A* 2006;103:10373-10378.
107. Skorupa AF, Fisher KJ, Wilson JM et al. Sustained Production of Beta-Glucuronidase from Localized Sites after Aav Vector Gene Transfer Results in Widespread Distribution of Enzyme and Reversal of Lysosomal Storage Lesions in a Large Volume of Brain in Mucopolysaccharidosis VII Mice. *Exp Neurol* 1999;160:17-27.
108. Dodge JC, Clarke J, Song A et al. Gene Transfer of Human Acid Sphingomyelinase Corrects Neuropathology and Motor Deficits in a Mouse Model of Niemann-Pick Type a Disease. *Proc Natl Acad Sci U S A* 2005;102:17822-17827.
109. Baek RC, Broekman ML, Leroy SG et al. Aav-Mediated Gene Delivery in Adult Gm1-Gangliosidosis Mice Corrects Lysosomal Storage in Cns and Improves Survival. *PLoS One* 2010;5:e13468.
110. Kells AP, Hadaczek P, Yin D et al. Efficient Gene Therapy-Based Method for the Delivery of Therapeutics to Primate Cortex. *Proc Natl Acad Sci U S A* 2009;106:2407-2411.
111. Worgall S, Sondhi D, Hackett NR et al. Treatment of Late Infantile Neuronal Ceroid Lipofuscinosis by Cns Administration of a Serotype 2 Adeno-Associated Virus Expressing Cln2 Cdna. *Hum Gene Ther* 2008;19:463-474.
112. Tardieu M, Zerah M, Husson B et al. Intracerebral Administration of Adeno-Associated Viral Vector Serotype Rh.10 Carrying Human Sgsh and Sumf1 Cdnas in Children with Mucopolysaccharidosis Type IIa Disease: Results of a Phase I/II Trial. *Hum Gene Ther* 2014;25:506-516.
113. Salegio EA, Kells AP, Richardson RM et al. Magnetic Resonance Imaging-Guided Delivery of Adeno-Associated Virus Type 2 to the Primate Brain for the Treatment of Lysosomal Storage Disorders. *Hum Gene Ther* 2010;21:1093-1103.
114. Liu G, Martins IH, Chiorini JA et al. Adeno-Associated Virus Type 4 (Aav4) Targets Ependyma and Astrocytes in the Subventricular Zone and Rms. *Gene Ther* 2005;12:1503-1508.
115. Haurigot V, Marco S, Ribera A et al. Whole Body Correction of Mucopolysaccharidosis IIa by Intracerebrospinal Fluid Gene Therapy. *J Clin Invest* 2013;123:3254-3271.
116. Meyer K, Ferraiuolo L, Schmelzer L et al. Improving Single Injection Csf Delivery of Aav9-Mediated Gene Therapy for Sma: A Dose-Response Study in Mice and Nonhuman Primates. *Mol Ther* 2015;23:477-487.
117. Chen YH, Claflin K, Geoghegan JC et al. Sialic Acid Deposition Impairs the Utility of Aav9, but Not Peptide-Modified Aavs for Brain Gene Therapy in a Mouse Model of Lysosomal Storage Disease. *Mol Ther* 2012;20:1393-1399.
118. Fischer PB, Karlsson GB, Butters TD et al. N-Butyldeoxynojirimycin-Mediated Inhibition of Human Immunodeficiency Virus Entry Correlates with

- Changes in Antibody Recognition of the V1/V2 Region of Gp120. *J Virol* 1996;70:7143-7152.
119. Fischl MA, Resnick L, Coombs R et al. The Safety and Efficacy of Combination N-Butyl-Deoxynojirimycin (Sc-48334) and Zidovudine in Patients with Hiv-1 Infection and 200-500 Cd4 Cells/Mm3. *J Acquir Immune Defic Syndr* 1994;7:139-147.
120. Baek RC, Kasperzyk JL, Platt FM et al. N-Butyldeoxygalactonojirimycin Reduces Brain Ganglioside and Gm2 Content in Neonatal Sandhoff Disease Mice. *Neurochem Int* 2008;52:1125-1133.
121. Elliot-Smith E, Speak AO, Lloyd-Evans E et al. Beneficial Effects of Substrate Reduction Therapy in a Mouse Model of Gm1 Gangliosidosis. *Mol Genet Metab* 2008;94:204-211.
122. Jeyakumar M, Butters TD, Cortina-Borja M et al. Delayed Symptom Onset and Increased Life Expectancy in Sandhoff Disease Mice Treated with N-Butyldeoxynojirimycin. *Proc Natl Acad Sci U S A* 1999;96:6388-6393.
123. Jeyakumar M, Smith DA, Williams IM et al. Nsaids Increase Survival in the Sandhoff Disease Mouse: Synergy with N-Butyldeoxynojirimycin. *Ann Neurol* 2004;56:642-649.
124. Platt FM, Neises GR, Reinkensmeier G et al. Prevention of Lysosomal Storage in Tay-Sachs Mice Treated with N-Butyldeoxynojirimycin. *Science* 1997;276:428-431.
125. Brady RO. Enzyme Replacement for Lysosomal Diseases. *Annu Rev Med* 2006;57:283-296.
126. Cox T, Lachmann R, Hollak C et al. Novel Oral Treatment of Gaucher's Disease with N-Butyldeoxynojirimycin (Ogt 918) to Decrease Substrate Biosynthesis. *Lancet* 2000;355:1481-1485.
127. Elstein D, Hollak C, Aerts JM et al. Sustained Therapeutic Effects of Oral Miglustat (Zavesca, N-Butyldeoxynojirimycin, Ogt 918) in Type I Gaucher Disease. *J Inherit Metab Dis* 2004;27:757-766.
128. Maegawa GH, Banwell BL, Blaser S et al. Substrate Reduction Therapy in Juvenile Gm2 Gangliosidosis. *Mol Genet Metab* 2009;98:215-224.
129. Shapiro BE, Pastores GM, Gianutsos J et al. Miglustat in Late-Onset Tay-Sachs Disease: A 12-Month, Randomized, Controlled Clinical Study with 24 Months of Extended Treatment. *Genet Med* 2009;11:425-433.
130. Bembi B, Marchetti F, Guerci VI et al. Substrate Reduction Therapy in the Infantile Form of Tay-Sachs Disease. *Neurology* 2006;66:278-280.
131. Masciullo M, Santoro M, Modoni A et al. Substrate Reduction Therapy with Miglustat in Chronic Gm2 Gangliosidosis Type Sandhoff: Results of a 3-Year Follow-Up. *J Inherit Metab Dis* 2010;33 Suppl 3:S355-361.
132. Tallaksen CM, Berg JE. Miglustat Therapy in Juvenile Sandhoff Disease. *J Inherit Metab Dis* 2009;32 Suppl 1:S289-293.
133. Ashe KM, Bangari D, Li L et al. Iminosugar-Based Inhibitors of Glucosylceramide Synthase Increase Brain Glycosphingolipids and Survival in a Mouse Model of Sandhoff Disease. *PLoS One* 2011;6:e21758.

134. Arthur JR, Wilson MW, Larsen SD et al. Ethylenedioxy-Pip2 Oxalate Reduces Ganglioside Storage in Juvenile Sandhoff Disease Mice. *Neurochem Res* 2013;38:866-875.
135. Lee JP, Jeyakumar M, Gonzalez R et al. Stem Cells Act through Multiple Mechanisms to Benefit Mice with Neurodegenerative Metabolic Disease. *Nat Med* 2007;13:439-447.
136. Norflus F, Tifft CJ, McDonald MP et al. Bone Marrow Transplantation Prolongs Life Span and Ameliorates Neurologic Manifestations in Sandhoff Disease Mice. *J Clin Invest* 1998;101:1881-1888.
137. Wada R, Tifft CJ, Proia RL. Microglial Activation Precedes Acute Neurodegeneration in Sandhoff Disease and Is Suppressed by Bone Marrow Transplantation. *Proc Natl Acad Sci U S A* 2000;97:10954-10959.
138. Arfi A, Bourgoin C, Basso L et al. Bicistronic Lentiviral Vector Corrects Beta-Hexosaminidase Deficiency in Transduced and Cross-Corrected Human Sandhoff Fibroblasts. *Neurobiol Dis* 2005;20:583-593.
139. Guidotti JE, Mignon A, Haase G et al. Adenoviral Gene Therapy of the Tay-Sachs Disease in Hexosaminidase a-Deficient Knock-out Mice. *Hum Mol Genet* 1999;8:831-838.
140. Itakura T, Kuroki A, Ishibashi Y et al. Inefficiency in Gm2 Ganglioside Elimination by Human Lysosomal Beta-Hexosaminidase Beta-Subunit Gene Transfer to Fibroblastic Cell Line Derived from Sandhoff Disease Model Mice. *Biol Pharm Bull* 2006;29:1564-1569.
141. McCarty DM, Monahan PE, Samulski RJ. Self-Complementary Recombinant Adeno-Associated Virus (Scaav) Vectors Promote Efficient Transduction Independently of DNA Synthesis. *Gene Ther* 2001;8:1248-1254.
142. Karumuthil-Melethil S, Nagabhushan Kalburgi S, Thompson P et al. Novel Vector Design and Hexosaminidase Variant Enabling Self-Complementary Adeno-Associated Virus for the Treatment of Tay-Sachs Disease. *Hum Gene Ther* 2016;27:509-521.
143. Osmon KJ, Woodley E, Thompson P et al. Systemic Gene Transfer of a Hexosaminidase Variant Using an Scaav9.47 Vector Corrects Gm2 Gangliosidosis in Sandhoff Mice. *Hum Gene Ther* 2016;27:497-508.
144. Tropak MB, Yonekawa S, Karumuthil-Melethil S et al. Construction of a Hybrid Beta-Hexosaminidase Subunit Capable of Forming Stable Homodimers That Hydrolyze Gm2 Ganglioside in Vivo. *Mol Ther Methods Clin Dev* 2016;3:15057.
145. Kitakaze K, Mizutani Y, Sugiyama E et al. Protease-Resistant Modified Human Beta-Hexosaminidase B Ameliorates Symptoms in Gm2 Gangliosidosis Model. *J Clin Invest* 2016;126:1691-1703.
146. Matsuoka K, Tamura T, Tsuji D et al. Therapeutic Potential of Intracerebroventricular Replacement of Modified Human Beta-Hexosaminidase B for Gm2 Gangliosidosis. *Mol Ther* 2011;19:1017-1024.

147. Bourgoin C, Emiliani C, Kremer EJ et al. Widespread Distribution of Beta-Hexosaminidase Activity in the Brain of a Sandhoff Mouse Model after Coinjection of Adenoviral Vector and Mannitol. *Gene Ther* 2003;10:1841-1849.
148. Kyrkanides S, Miller JH, Brouxhon SM et al. Beta-Hexosaminidase Lentiviral Vectors: Transfer into the Cns Via Systemic Administration. *Brain Res Mol Brain Res* 2005;133:286-298.
149. Kyrkanides S, Miller JN, Tallents RH et al. Intraperitoneal Inoculation of Sandhoff Mouse Neonates with an Hiv-1 Based Lentiviral Vector Exacerbates the Attendant Neuroinflammation and Disease Phenotype. *J Neuroimmunol* 2007;188:39-47.
150. Cachon-Gonzalez MB, Wang SZ, Ziegler R et al. Reversibility of Neuropathology in Tay-Sachs-Related Diseases. *Hum Mol Genet* 2014;23:730-748.
151. McCurdy VJ, Rockwell HE, Arthur JR et al. Widespread Correction of Central Nervous System Disease after Intracranial Gene Therapy in a Feline Model of Sandhoff Disease. *Gene Ther* 2015;22:181-189.
152. Sargeant TJ, Wang S, Bradley J et al. Adeno-Associated Virus-Mediated Expression of Beta-Hexosaminidase Prevents Neuronal Loss in the Sandhoff Mouse Brain. *Hum Mol Genet* 2011;20:4371-4380.
153. Rockwell HE, McCurdy VJ, Eaton SC et al. Aav-Mediated Gene Delivery in a Feline Model of Sandhoff Disease Corrects Lysosomal Storage in the Central Nervous System. *ASN Neuro* 2015;7.
154. Bevan AK, Duque S, Foust KD et al. Systemic Gene Delivery in Large Species for Targeting Spinal Cord, Brain, and Peripheral Tissues for Pediatric Disorders. *Mol Ther* 2011;19:1971-1980.
155. Cederfjall E, Nilsson N, Sahin G et al. Continuous Dopa Synthesis from a Single Aav: Dosing and Efficacy in Models of Parkinson's Disease. *Sci Rep* 2013;3:2157.
156. Sondhi D, Peterson DA, Giannaris EL et al. Aav2-Mediated Cln2 Gene Transfer to Rodent and Non-Human Primate Brain Results in Long-Term Tpp-I Expression Compatible with Therapy for Incl. *Gene Ther* 2005;12:1618-1632.
157. Zerah M, Piguet F, Colle MA et al. Intracerebral Gene Therapy Using Aavrh.10-Harsa Recombinant Vector to Treat Patients with Early-Onset Forms of Metachromatic Leukodystrophy: Preclinical Feasibility and Safety Assessments in Nonhuman Primates. *Hum Gene Ther Clin Dev* 2015;26:113-124.
158. San Sebastian W, Kells AP, Bringas J et al. Safety and Tolerability of Mri-Guided Infusion of Aav2-Haacdc into the Mid-Brain of Non-Human Primate. *Mol Ther Methods Clin Dev* 2014;3.
159. Broekman ML, Baek RC, Comer LA et al. Complete Correction of Enzymatic Deficiency and Neurochemistry in the Gm1-Gangliosidosis Mouse Brain by Neonatal Adeno-Associated Virus-Mediated Gene Delivery. *Mol Ther* 2007;15:30-37.

160. Yan Z, Yan H, Ou H. Human Thyroxine Binding Globulin (Tbg) Promoter Directs Efficient and Sustaining Transgene Expression in Liver-Specific Pattern. *Gene* 2012;506:289-294.
161. Broekman ML, Comer LA, Hyman BT et al. Adeno-Associated Virus Vectors Serotyped with Aav8 Capsid Are More Efficient Than Aav-1 or -2 Serotypes for Widespread Gene Delivery to the Neonatal Mouse Brain. *Neuroscience* 2006;138:501-510.
162. Weismann CM, Ferreira J, Keeler AM et al. Systemic Aav9 Gene Transfer in Adult Gm1 Gangliosidosis Mice Reduces Lysosomal Storage in Cns and Extends Lifespan. *Hum Mol Genet* 2015;24:4353-4364.
163. Zanta-Boussif MA, Charrier S, Brice-Ouzet A et al. Validation of a Mutated Pre Sequence Allowing High and Sustained Transgene Expression While Abrogating Whv-X Protein Synthesis: Application to the Gene Therapy of Was. *Gene Ther* 2009;16:605-619.
164. Calcedo R, Vandenberghe LH, Gao G et al. Worldwide Epidemiology of Neutralizing Antibodies to Adeno-Associated Viruses. *J Infect Dis* 2009;199:381-390.
165. van der Bom IM, Moser RP, Gao G et al. Finding the Striatum in Sheep: Use of a Multi-Modal Guided Approach for Convection Enhanced Delivery. *J Huntingtons Dis* 2013;2:41-45.
166. van der Bom IM, Moser RP, Gao G et al. Frameless Multimodal Image Guidance of Localized Convection-Enhanced Delivery of Therapeutics in the Brain. *J Neurointerv Surg* 2013;5:69-72.
167. Spetzler RF, Selman WR, Weinstein P et al. Chronic Reversible Cerebral Ischemia: Evaluation of a New Baboon Model. *Neurosurgery* 1980;7:257-261.
168. Nieuwenhuys R, Donkelaar HJt, Nicholson C. *The Central Nervous System of Vertebrates.* (Springer, Berlin ; New York). 1998.
169. Salegio EA, Samaranch L, Jenkins RW et al. Safety Study of Adeno-Associated Virus Serotype 2-Mediated Human Acid Sphingomyelinase Expression in the Nonhuman Primate Brain. *Hum Gene Ther* 2012;23:891-902.
170. Hadaczek P, Forsayeth J, Mirek H et al. Transduction of Nonhuman Primate Brain with Adeno-Associated Virus Serotype 1: Vector Trafficking and Immune Response. *Hum Gene Ther* 2009;20:225-237.
171. Samaranch L, San Sebastian W, Kells AP et al. Aav9-Mediated Expression of a Non-Self Protein in Nonhuman Primate Central Nervous System Triggers Widespread Neuroinflammation Driven by Antigen-Presenting Cell Transduction. *Mol Ther* 2014;22:329-337.
172. Bigger BW, Saif M, Linthorst GE. The Role of Antibodies in Enzyme Treatments and Therapeutic Strategies. *Best Pract Res Clin Endocrinol Metab* 2015;29:183-194.
173. van Gelder CM, Hoogeveen-Westerveld M, Kroos MA et al. Enzyme Therapy and Immune Response in Relation to Crim Status: The Dutch Experience in Classic Infantile Pompe Disease. *J Inherit Metab Dis* 2015;38:305-314.

174. Vogler C, Galvin N, Levy B et al. Transgene Produces Massive Overexpression of Human Beta -Glucuronidase in Mice, Lysosomal Storage of Enzyme, and Strain-Dependent Tumors. *Proc Natl Acad Sci U S A* 2003;100:2669-2673.
175. Hiramatsu N, Chiang WC, Kurt TD et al. Multiple Mechanisms of Unfolded Protein Response-Induced Cell Death. *Am J Pathol* 2015;185:1800-1808.
176. Grimm D. The Dose Can Make the Poison: Lessons Learned from Adverse in Vivo Toxicities Caused by Rnai Overexpression. *Silence* 2011;2:8.
177. Gentner B, Visigalli I, Hiramatsu H et al. Identification of Hematopoietic Stem Cell-Specific Mirnas Enables Gene Therapy of Globoid Cell Leukodystrophy. *Sci Transl Med* 2010;2:58ra84.
178. Meadows AS, Duncan FJ, Camboni M et al. A Glp-Compliant Toxicology and Biodistribution Study: Systemic Delivery of an Raav9 Vector for the Treatment of Mucopolysaccharidosis liib. *Hum Gene Ther Clin Dev* 2015;26:228-242.
179. Gao G, Vandenberghe LH, Alvira MR et al. Clades of Adeno-Associated Viruses Are Widely Disseminated in Human Tissues. *J Virol* 2004;78:6381-6388.
180. Sondhi D, Johnson L, Purpura K et al. Long-Term Expression and Safety of Administration of Aavrh.10hcln2 to the Brain of Rats and Nonhuman Primates for the Treatment of Late Infantile Neuronal Ceroid Lipofuscinosis. *Hum Gene Ther Methods* 2012;23:324-335.
181. Sharma S, Sankhyan N, Kalra V et al. Thalamic Changes in Tay-Sachs' Disease. *Arch Neurol* 2008;65:1669.
182. Brismar J, Brismar G, Coates R et al. Increased Density of the Thalamus on Ct Scans in Patients with Gm2 Gangliosidoses. *AJNR Am J Neuroradiol* 1990;11:125-130.
183. Brinker T, Stopa E, Morrison J et al. A New Look at Cerebrospinal Fluid Circulation. *Fluids Barriers CNS* 2014;11:10.
184. Nathwani AC, Tuddenham EG, Rangarajan S et al. Adenovirus-Associated Virus Vector-Mediated Gene Transfer in Hemophilia B. *N Engl J Med* 2011;365:2357-2365.